Hemodynamics of vascular access for hemodialysis

Hemodynamica in de vaattoegang voor hemodialyse

Ilse Van Tricht

Supervisor: Prof. P. Verdonck
Dissertation submitted to obtain the degree of
Doctor in de Toegepaste Wetenschappen

Civil Engineering Department
Head: Prof. P. Verdonck
Faculty of Engineering
Academic year 2004-2005

UNIVERSITEIT
GENT

The research of Ilse Van Tricht was supported by the Institute for the Promotion of Innovation by Science and Technology in Flanders (IWT-11254).

ISBN 9090196293

Suggested citation: Van Tricht I., Hemodynamics of vascular access for hemodialysis ISBN 9090196293, PhD dissertation, Ghent, Ghent University, 2005.

Supervisor:

Prof. P. Verdonck PhD, MScCivE, MScBME, MBA
Civil Engineering Department (TW15)
Faculty of Engineering
Ghent University
Sint-Pietersnieuwstraat 41
B - 9000 Ghent

Members of the exam committee:

Prof. R. Verhoeven, PhD, MScCivE (Chairman, Faculty of Engineering, UGent)
D. De Wachter, PhD, MScEE, MScBME (Het Federaal Kenniscentrum voor de Gezondheidszorg (KCE), Brussels)
S. Eloot, PhD, MScCivE, MScBME (Faculty of Engineering, UGent)
Prof. P. Segers, PhD, MScCivE (Faculty of Engineering, UGent)
Dr. JHM Tordoir, PhD, MD (Department of Surgery, University Hospital Maastricht)
Prof. F.N. van de Vosse, PhD (Faculty of Biomedical Engineering, Eindhoven University of Technology)
Prof. R. Vanholder, PhD, MD (Faculty of Medicine and Health Sciences, UGent)
Prof. P. Verdonck, PhD, MScCivE, MScBME, MBA (Faculty of Engineering, UGent)
Prof. F. Vermassen, PhD, MD (Faculty of Medicine and Health Sciences, UGent)
Prof. J. Vierendeels, PhD, MScME (Faculty of Engineering, UGent)

"Niets is sterker
Dan de stilte
Niets heeft zoveel kracht
Als het zwijgen van de nacht
Niets is sterker
Dan de stilte
Niets is sterker dan het woord
Dat niemand hoort "
Stef Bos

I would like to thank these people, past and present, for their support, or faith in me, which has influenced me greatly over the years and which I credit my success. All I added was perspiration and imagination.
I dit not list them chronologically, alphabetically or in order of importance.

Adrienne en Christiane Varlez
Lucien en Rolande Van Tricht - Monté
Paul en Elise Timmerman - Van Tricht
Etienne en Christiane Ost - Raveydts
Marcel en Jacqueline Peereman - Deteye
Peter en Mieke Sergeant - Calus
Daniël en Annie Van Hassel - Varlez
Robert Banasiak
Guy Mareels
Manuella De Kerpel
Stefaan Bliki
Remi Hombrouckx
Bart Meyns
Jan Tordoir
Ruben Dammers
Jennifer Van Wetter
Leen Vincke
Jan Vierendeels
Roland Van Dam
Edwin Wijnen
Benedicte Heyndrickx
Juffrouw Monica
Martin Van den Nieuwenhuyzen
Katrien De Pooter
Johan en Annie Jeanne Van Gucht-Faut
Alfons en Marleen Boschman - De Deyn
Dora, Minoe, Krissie, Shesmyl, June, Bertje
Frans en Gaby Raveydts - De Dobbeleer
Nico en Tim Vanderlinden
Maurits en Godelieve Vanderlinden-Van Ongeval
Wouter en Leen Ryckaert - Heirlings
Johan en Aïsha Dereepere - Antonissen
Doreentje Boschman

Pascal Verdonck
Patrick Segers
Stijn Vandenberghe
Sunny Eloot
Fadi Glor
Kathy Courtens
Massanori Nakamura
Ivo Michiel
Marcel Anteunis
Jurgen Deviche
Martin Van Daele
Stijn Eeckhaut
Ihsan Bakir
Frank van der Sande
Koen Van Crombrugghe
Dries Mahieu
Annelies De Corte
Daniel Vanhercke
Cathy Van Acker
Jean Yves Devos
Johny Raveydts
Ginette De Bleecker
Maria Van Damme
Florence Ost
Ronny Verhoeven
Dirk De Wachter
Koen Matthys
Kris Dumont
Sofie Ost
Lieve Lanoye
Sebastian Vermeersch
Liesbet Dedoncker

Nomenclature

Symbols

A_{free}	free lumen area	m^2	
$A_{stenosis}$	stenotic lumen area	m^2	
a_p	particle radius	m	
B	volume or adiabatic bulk modulus of elasticity	N/m^2	
c	wave propagation speed	m/s	
C	compliance	m^3/Pa	$ml/mmHg$
d	diameter	m	
d_p	distance particle - wall	m	
D_{sys}	systolic diameter	m	
D_{dia}	diastolic diameter	m	
D_{mean}	mean diameter	m	
Hct	Hematocrit	%	
I	unit tensor	-	
MAP	mean arterial pressure	Pa	mmHg
n_0	number of particles		
N_d	needle distance	m	
NWRT	near wall residence time	s	
OSI	oscillatory shear index	-	
p	pressure	Pa	mmHg
pp	pulse pressure	Pa	mmHg
$p_{arterial\ line}$	pressure at arterial line dialysis machine	Pa	mmHg
$p_{venous\ line}$	pressure at venous line dialysis machine	Pa	mmHg
$\overline{PG}$	pressure gradient	Pa/m	
Re	Reynolds number	-	
Q_G	Graft (access) flow rate	m^3/s	ml/min
Q_R	Roller pump (artificial kidney) flow rate	m^3/s	ml/min
RBD	red blood cell damage	%	
SS	shear stress	Pa	
$\overline{\overline{SS}}$	stress tensor	Pa	
t	time	s	
T	period	s	
u	velocity in x-direction	m/s	
$\overrightarrow{v}$	velocity vector	m/s	
v_{sys}	systolic velocity	m/s	
v_{dia}	diastolic velocity	m/s	
v_{mean}	mean velocity	m/s	
V	volume	m^3	
V_0	initial volume	m^3	
V_{nw}	cell surface on the wall	m^2	
WSR	wall shear rate	s^{-1}	
WSS	wall shear stress	Pa	
WSSG	wall shear stress gradient	Pa/m	
WSS_{mean}	mean wall shear stress	Pa	
$\overline{WSS}_{ta}$	time averaged wall shear stress	Pa	
$\overline{WSSG}_{ND}$	normalised wall shear stress gradient	-	

Greek symbols

α	Womersley number	-
γ	strain rate	s^{-1}
γ_c	critical strain rate	s^{-1}
γ_r	relative strain rate	-
μ	dynamic viscosity of blood	Pa.s
μ_p	dynamic viscosity of plasma	Pa.s
ρ	density	kg/m^3
ω	pulsation	s^{-1}
τ_p	Poiseuille wall shear stress	Pa

Abbreviations

AA	Arterial anastomosis
AI	Arterial inlet
AN	Arterial needle
AVF	Arteriovenous fistula
AVG	Arteriovenous graft
CD	constant diameter
CFD	Computational fluid dynamics
DOS	Distal outlet segment
DA	Distal artery
DV	Distal vessel
ESRD	End stage renal disease
FEM	Finite element method
IH	Intimal hyperplasia
LDA	Laser Doppler anemometry
PIV	Particle image velocimetry
POS	Proximal outlet segment
PSH	Platelet stimulation history
PTFE	Polytetrafluorethylene
PV	Proximal vessel
RBC	Red blood cell
RI	Resistance index
PR	Pressure ratio
RD	Relative distensibility
RP	Roller pump
Res	Reservoir
TG	Tapered graft
VA	Venous anastomosis
VN	Venous needle
VAM	Vascular access model
VSMC	Vascular smooth muscle cell
WK	Windkessel

Content

Tables

Figures

Preface

This thesis includes five parts.The introduction describes the renal function and the different renal replacement therapies in particular hemodialysis and its according need for a permanent vascular access. The vascular access studied in this work is a polytetrafluorethylene (PTFE) graft in loop configuration. This access is studied in two ways: in experimental and numerical simulations. The measurement techniques necessary to assess the graft in the experimental set-up are explained just like the procedure used to perform the computational fluid dynamics (CFD) simulations.

In a second part, the vascular access is modelled immediately after the surgical intervention. Two graft geometries (a 6 mm and a 4-7 mm graft) are compared. Pressure, velocity and flow rate are measured at different places in the model. One set of the measurement data served as boundary conditions for the CFD model and a second set to validate the CFD model.

Next, the graft access with a venous outflow stenosis is studied. The efficiency of three different parameters, available in literature, to detect access stenoses were tested. In continuation of this experimental study, a clinical new protocol was written and is currently used to evaluate the clinical relevance of the parameter in patients with a graft access.

The fourth part concerns the simulation of a hemodialysis session. The impact of a hemodialysis session on the vascular access is reported, especially the influence of the flow rate of the blood pump and the influence of the access flow rate. The dialysis needles are are assessed in a CFD study. New and old designs were compared.

The last part of the thesis contains the conclusions of the work together with the future prospects.

Part I

Introduction

Chapter 1

The need for a vascular access

In this chapter, the necessity of a vascular access in patients with end stage renal disease is explained. For completeness, the major renal functions and the renal replacement therapies are incorporated. This way, the vascular access is situated within the set of available therapies.

1.1 The renal function

The three major functions that the two kidneys fulfill in the human body are presented. First: they drain the produced waste products. Secondly, they regulate the water, potassium, sodium, calcium, phosphorus and the acid-base balance. A third function is the synthesis of hormones.

The kidneys are two bone shaped organs that are localized in the posterior part of the abdomen, figure 1.1. They have about 11 cm length, 5 cm width and 3 cm thickness and are situated at each side of the spline just below the liver at the right side and below the spleen at the left side. The concave part faces towards the spine and has an opening, the hilus, where the renal artery, renal vein, the ureter and the nerves enter the kidney. The adrenal gland that produces hormones can be found on top of the kidney.

The outer shell of the kidney, is the renal capsule; the internal part consists of the cortex and the renal medulla that is split into renal pyramids. The center of the kidney is the pelvis, figure 1.2.

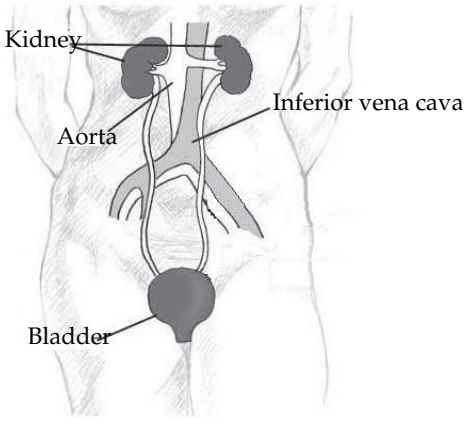

Figure 1.1: The location of the kidneys in the body

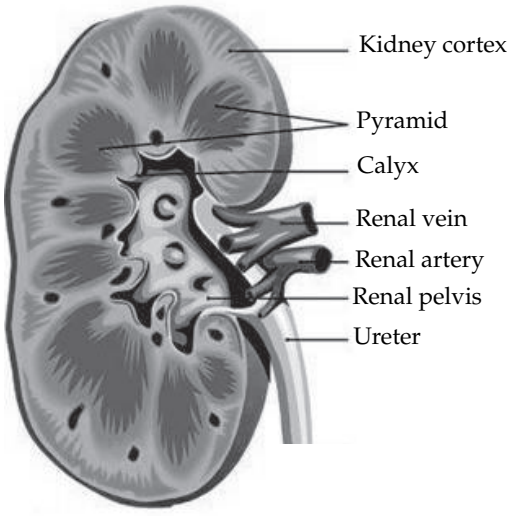

Figure 1.2: A cross section of a kidney [1]

The functional units of the kidney are the nephrons. Each nephron consists of a Bowman's capsule, a tiny proximal and distal tubule, a loop of Henle and a collecting duct. The position of the nephrons in the cortex and pyramids is shown in the left panel of figure 1.3. Each Bowman's capsule surrounds a network of capillaries: the glomerulus. The Bowman's capsule together with the glomerulus forms the Malpighi body and is the filtering unit of the kidney. The Malpighi bodies are positioned in the renal cortex. The twisted proximal tubulus originates in the Bowman's capsule in the renal cortex and straightens in the medulla where it connects onto a loop of Henle. This makes a bend of 180° and connects onto the distal tubulus, a twisted tubule at the altitude of the related Bowman's capsule. The distal tubulus makes contact with the artery that enters the Bowman's capsule. Blood pressure regulating hormones are secreted at the juxtaglomular cells at the contact site. Several nephrons are connected to one collecting duct attached to the pelvis that ends in the ureter and the bladder.

Three processes occur in the nephron: filtration, reabsorption and excretion. Filtration happens in the glomerulus: fluid is transported out of the artery into the cavity of the Bowman's capsule. The filtrate has nearly the same composition as plasma, this is the primary urine, produced at 7.5 liters per hour. The filtering pressure is the blood pressure reduced by the osmotic counter pressure and the pressure

in the Bowman's capsule. It is clear that the efficiency of this transport process is dependent on the blood pressure regulation.
Only 1% of the primary urine will be excreted. The reabsorption process forms concentrated urine. This happens in the proximal tubuli, the loops of Henle and the distal tubuli under osmotic pressure and hormonal and enzymatic pumps. The reabsorption is selective: nutrients return to the blood, the water and salt concentration is regulated just like the acid-base balance. Glucose, amino acids, calcium and magnesium ions return in the blood whereas phosphate ions are secreted systematically. Several hormones regulate the Na^+ and K^+ balance and the fluid concentration of the urine. As a consequence, the blood pressure is regulated. The pH of blood is regulated at a constant value of 7.4.

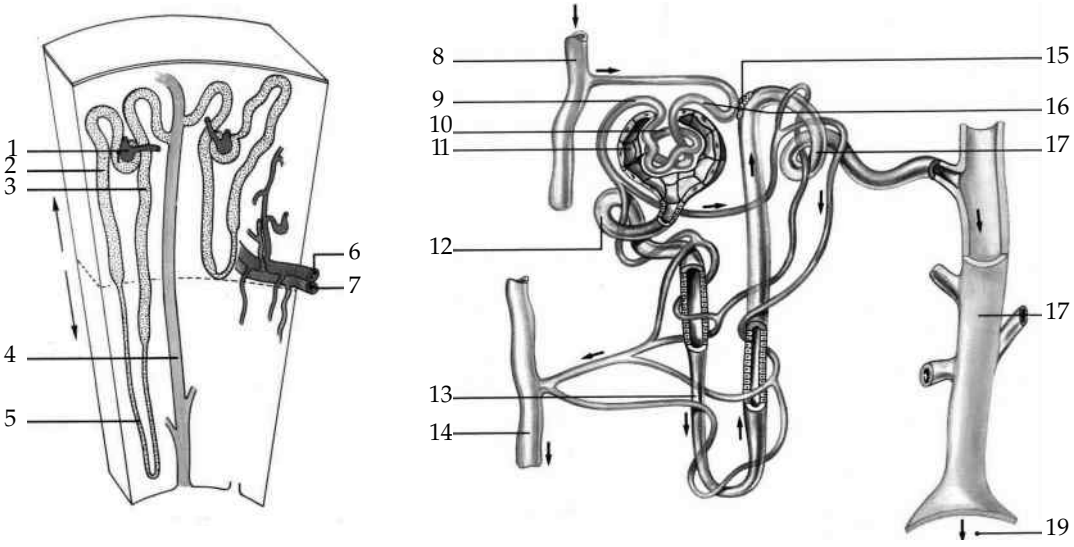

1: the Malphigi body
2: proximal tubulus
3: distal tubulus
4: the collecting duct
5: loop of Henle
6: artery
7: vein
8: artery
9: vas efferens
10: glomerulus
11: Bowman's capsule
12: tubulus contortus I
13: loop of Henle
14: vein
15: juxtaglomular cells
16: vas efferens
17: tubulus contortus II
18: collecting duct
19: renal pelvis

Figure 1.3: The position of the nephron in the cortex and medulla (left panel). The functional parts of the nephron (right panel) [1]

1.2 Renal failure

Renal failure can occur acute, within hours or days, e.g. when the lower limbs are clasped as a consequence of an earthquake resulting in lowered blood flow, release of toxins, and harmful toxins, or when the fluid intake is too less. Renal function can almost always be recovered in case of acute renal failure.

More attention should be drawn to chronic renal failure as there is no chance that the renal function recovers. The major complaints are gout, tired legs, burning feeling in the feet, being thirsty, fatigue and concentration impairment. The kidneys can shrivel or enlarge resulting in lowered filtration in the glomerulus and deterioration of the nephrons. The major reasons of chronic renal failure are diabetes and hypertension.

1.3 Renal replacement therapies

Medical doctors follow up patients with renal failure as soon as the disease is detected. The earlier the patient is followed up, the higher the residual renal function and the more the evolution towards terminal or irreversible renal failure can be delayed. [25] Three commonly used techniques for renal replacement therapies are: hemodialysis, peritoneal dialysis and renal transplantation.

	Transplantation [%]	Peritoneal Dialysis [%]	Hemodialysis [%]
Flanders	6.6	8.87	84.53
Wallonia	4.7	9.05	86.25

Table 1.1: The proportion of patients on the different renal replacement therapies [25]

1.3.1 Renal transplantation

Renal transplantation is the preferred therapy as renal replacement therapy. A donor kidney, from a living or a dead donor, is implanted in the illiaca fossa (figure 1.4) because it is simple, can easily be observed and is easy accessible for biopsies. Donor and acceptor must have genetic resemblance for a successful transplantion. If the surgical procedure was successful, the patient has to take immunosuppressives to avoid rejection of the transplanted kidney.

Patients undergo cardiovascular, gastro-intestinal and lungtests before they can receive a transplant kidney. If the tests confirm that the patient is receptive for a transplant kidney, his name is added to a waiting list. If a suitable donor kidney is available, the kidney is transplanted into the illiaca fossa where arteries, veins, ureters and nerves are connected in the abdomen.
The patient is followed up after transplantation to avoid infections and check for repulsion. The advantages of transplantation are: the water intake is not limited, a less severe diet compared to the dialysis diet, the possibility to go back to work, and the possibility to develop social activities.

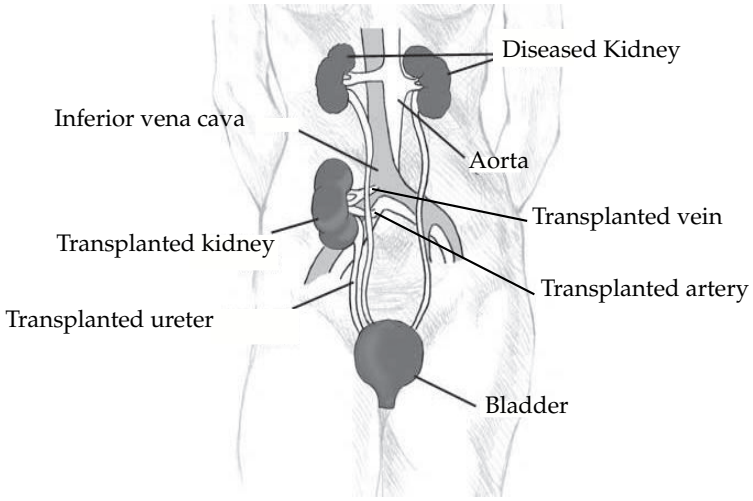

Figure 1.4: The location of the transplanted kidney

1.3.2 Peritoneal dialysis

When peritoneal dialysis (figure 1.5) is the renal replacement therapy, the waste products are transported from the blood to the dialysate via the patient's own peritoneal membrane, a semi-permeable membrane. To do so, the preheated dialysate infusion (37°) is brought into the peritoneal cavity via the peritoneal catheter. There, the waste products are exchanged via diffusive transport through the intercellular gaps of the membrane. When the dialysate infusion is saturated with waste pro-ducts, it is drained from the peritoneal cavity and fresh dialysate is reinfused.
Peritoneal dialysis can be carried out continuously or intermittent (e.g. only during the night). The major advantages of this technique are: the patient is independent

from the hospital, there is no need to add anticoagulation to the blood, hemodynamic stability because the dialysis happens less intermittent than hemodialysis, and the diet is less strict.
On the other hand, there are also disadvantages of this technique: the risk of catheter displacement, exit site and peritoneum infection, uncomfortable feeling due to the catheter, and possibly excessive loss of proteins, and water soluble vitamines.

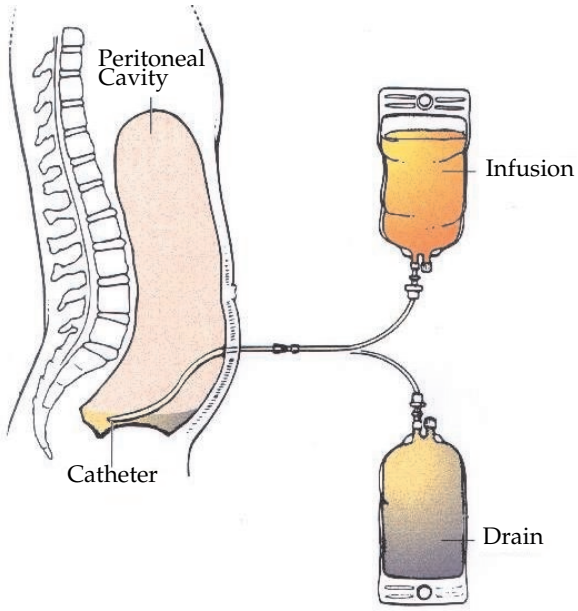

Figure 1.5: The priciple of peritoneal dialysis

1.3.3 Hemodialysis

During a hemodialysis session, see figure 1.6, the patient's blood is pumped into an extracorporeal circuit where it is purified from waste products and the excess of water accumulated in the body. The duration and the frequency of the sessions depend on the patient's needs, and is generally performed trice weekly during 3 to 5 hours. Hemodialysis can be performed in the hospital, at home or in a low-care unit.
To treat the blood extracorporeally, an access to the circulation (vascular access) is necessary. This vascular access is used to aspirate blood out of the patient with a roller pump. The blood flows towards an artificial kidney where the waste ex-

change happens over a membrane between the blood and the dialysate. The best blood clearance is obtained when the dialysate fluid flows counter currently with the blood in the artificial kidney. The purified blood is returned to the patient via the vascular access. Hemodialysis is a therapy that should be applied with caution. First of all, blood clotting inside the artificial kidney has to be avoided. Therefore, anticoagulation is added to the blood. Next, no air bubbles may enter the circulation. To avoid this, air detectors watch the venous return tubes. The most recent dialysis machines are provided with an arterial and venous pressure transducers to monitor the pump function and to detect outflow obstruction respectively.

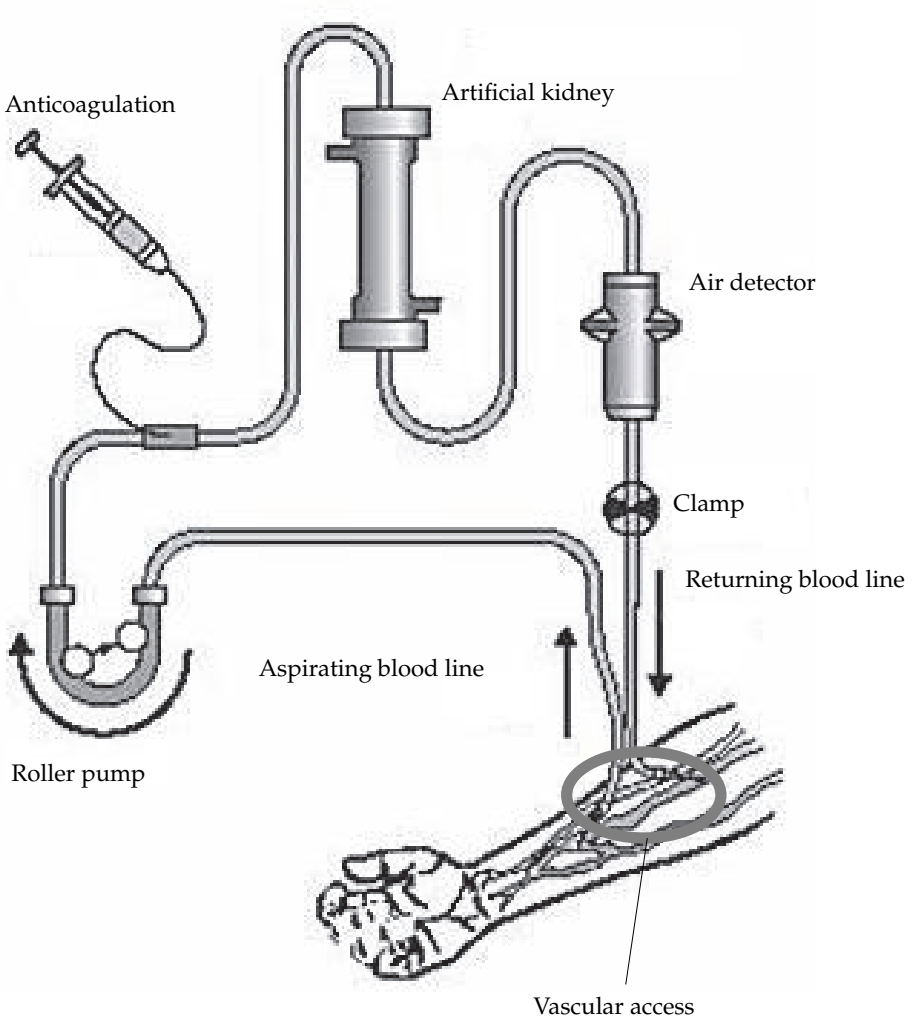

Figure 1.6: Schematic representation of blood purification with hemodialysis

1.4 The vascular access

It became clear from the previous paragraph that an access to the blood circulation is necessary when the chosen blood purification technique is hemodialysis. Different possibilities are available as vascular access. When only native material is used to create a shortcut between the arterial and venous system, an autogenous vascular access is constructed. This access type is only promising if the feeding arteries are still compliant and have diameters above 2 mm. A second possibility is a non-autogenous vascular access. In this case, an autograft vein or synthetic material is used. If the patients have poor vessels and the construction of a fistula is impossible, a catheter or a vascular access port device is utilised.
The different vascular access types, their typical biomechanical behaviour and complications are discussed in depth in the chapter 3.

Chapter 2

Measurement and simulation techniques of hemodynamics

2.1 When one wants to get insight in the hemodynamics ...

Blood pressure and blood flow rate contain important information concerning the condition of the tissue or blood vessels that are of ones interest. Hence the theoretical governing fluid equations in blood vessels will be summarised below. Sometimes it is difficult to estimate correctly the influence of the complicated geometrical changes. Therefore, insight in the hemodynamics can be obtained with the measurement of the blood pressure and velocity in vivo or in vitro. The experimental measurement techniques used in this thesis are techniques that are also applicable in daily clinical practice. These techniques in general offer information about the mean pressure and flow rate of the fluid and are not able to supply the investigator of derived parameters like e.g. wall shear stress. As will be explained further, the wall shear stress is a valuable parameter to detect regions where stenoses, narrowing of the vessel lumen, tend to arise. To search for these sites, computational fluid dynamics is utilised.
This chapter outlines the governing equations and the measurement techniques and computational fluid dynamics used in this thesis.

2.2 Governing equations

Blood is a non-Newtonian, incompressible fluid that obeys the Navier-Stokes equations. The equations that are taken into account in this thesis are the mass (9.1) and momentum (9.2) conservation equations as heat transfer does not occur in the situations studied.

$$\nabla \cdot \ \overrightarrow{v} = 0 \tag{2.1}$$

$$\frac{\delta \overrightarrow{v}}{\delta t} + (v \cdot \nabla)\overrightarrow{v} = \frac{1}{\rho}(-\nabla p + \nabla \cdot \overline{\overline{SS}}) \tag{2.2}$$

with $\overrightarrow{v}$, the velocity vector, $\overrightarrow{v}^T$, the transposed velocity vector; p, the pressure; ρ, the density and $\overline{\overline{SS}}$, the stress tensor.
If the notation for the unit tensor is I and for the molecular dynamic viscosity is μ, the stress tensor (2.3) can more explicitly be described as:

$$\overline{\overline{SS}} = \mu[(\nabla \overrightarrow{v} + \nabla \overrightarrow{v}^T) - \frac{2}{3}\nabla . \overrightarrow{v} I] \tag{2.3}$$

The stress tensor expresses the friction forces inside the blood. The friction forces depend on the velocity gradient and on the dynamic viscosity. The velocity gradient depends on the blood flow rate and the blood vessel geometry whereas the molecular viscosity is a property of blood. It is already mentioned above, blood is a non-Newtonian fluid, the molecular viscosity of blood depends on the strain rate (spatial velocity gradient), the volume fraction of red blood cells (hematocrit) and the plasma viscosity. Non-Newtonian behaviour has extensively been investigated and multiple viscosity models that describe the typical properties are explained in the section below.

It is clear from the mass and continuity equation that all the information necessary to get insight in the hemodynamics, is in the velocity, the pressure and the fluid properties. Consequently, it is obvious that when simulations are performed, pressure and velocity (or flow rate) information is collected. The flow, velocity and pressure measurement techniques and the computational fluid dynamics techniques used in this thesis are explained in the next sections of this chapter.

2.3 The non-Newtonian behaviour of blood

Blood is a non-Newtonian, shear thinning fluid: the blood viscosity depends on the strain rate, the local hematocrit and the plasma viscosity.

This inhomogeneity is not incorporated in the in vitro experiments. Glycerine/water mixtures with a constant viscosity are used in the experimental models. The viscosity of the mixtures used, approach the apparent blood viscosity of hemodialysis patients, which depends on the plasma viscosity and the hematocrit level. The plasma viscosity of dialysis patients varies from 1.35 $\pm$ 0.29 mPa.s to 1.54 $\pm$ 0.38 mPa.s and the hematocrit from 33.6% $\pm$ 5.9% to 41.4% $\pm$ 5.7% during a hemodialysis session. The blood viscosity as a consequence varies from 3.33 $\pm$ 0.77 to 4.36 $\pm$ 1.3 mPa.s [2].
The mixture used in the simulations is a 40/60% glycerin/water mixture. It has a dynamic viscosity of 3.75 mPa.s at a temperature of 25°C.

The non-Newtonian behaviour of blood is included in the computational fluid dynamics models. Different viscosity models are available in literature: the model of Haynes and Whitmore [3], the Casson model [4] [5] [6] and the viscosity model of Quemada [7] [8].
The viscosity model of Haynes and Whitmore expresses the influence of the plasma viscosity and the hematocrit, which can vary considerably in the hemodialysis patients. The major disadvantage of this model is that the influence of the strain rate (the spatial velocity gradient) is not considered.
The influence of the strain rate is integrated in the viscosity model of Casson. However, the influence of plasma viscosity and hematocrit level is not present in the model. An additional drawback is that unrealistic high dynamic viscosities are calculated with the model where low strain rates exist.
Therefore the viscosity model of Quemada is used as this model expresses the influence of the strain rate (γ [1/s]), the plasma viscosity (μ_p [Pa.s]) and the hematocrit level (Hct [%]). The formulas that express the dynamic viscosity (μ) calculated with the Quemada viscosity model are:

$$\mu = \frac{\mu_p}{(1 - 0.5.k.Hct)^2} \tag{2.4}$$

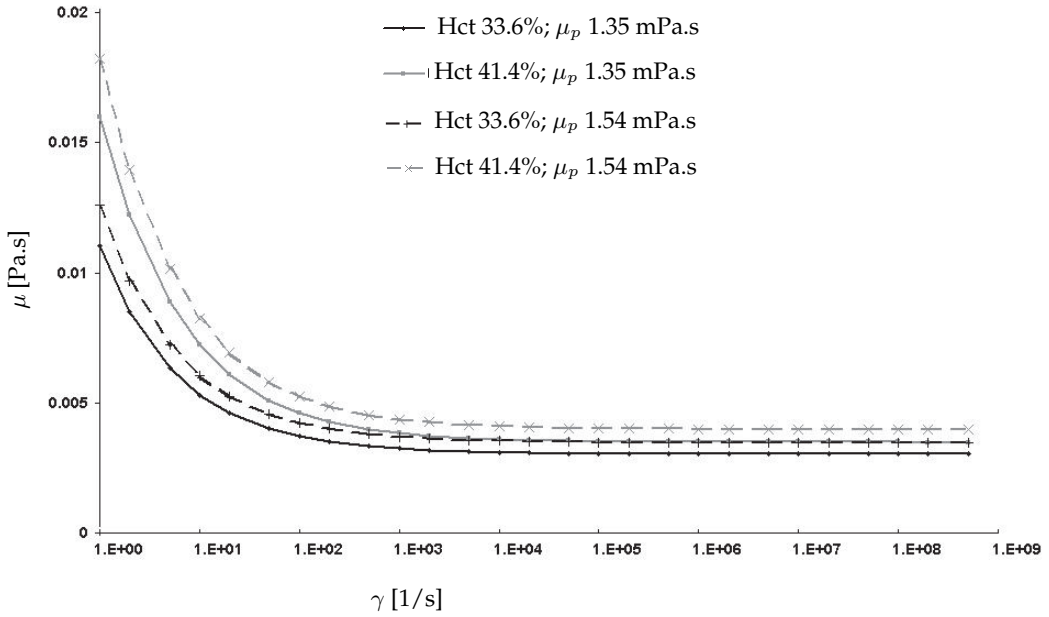

Figure 2.1: The viscosity model of Quemada with plasma dynamic viscosity and hematocrit values observed in hemodialysis patients

$$k = \frac{k_0 + k_\infty \sqrt{\gamma_r}}{1 + \sqrt{\gamma_r}} \quad met \quad \gamma_r = \frac{\gamma}{\gamma_c} \tag{2.5}$$

k_0 [-] is the intrinsic viscosity of the cell suspension at zero strain rate and depends on the hematocrit level:

$$ln(k_0) = 3.874 - 10.410Hct + 13.800Hct^2 - 6.738Hct^3 \tag{2.6}$$

k_∞ [-]is similarly the intrinsic viscosity of the cell suspension at an infinit strain rate and can also be calculated based on the hematocrit level:

$$ln(k_\infty) = 1.3435 - 2.803Hct + 2.711Hct^2 - 0.6479Hct^3 \tag{2.7}$$

γ_c [1/s] is the critical strain rate which also depends on the hematocrit:

$$ln(\gamma_c) = -6.1508 + 27.923Hct - 25.6Hct^2 + 3.697Hct^3 \tag{2.8}$$

Figure 2.1 shows the blood dynamic viscosity values calculated with the Quemada viscosity model as a function of the strain rate. The plasma dynamic viscosity and hematocrit values observed in hemodialysis patients are used to plot the figure.

2.4 Measurement techniques

2.4.1 Transonic flow measurement

Transonic ultrasound probes (Transonic systems Inc ®, Maastricht, The Netherlands) are equipped with two ultrasound transducers at one side of the probe and an acoustic reflector at the opposite side. The ultrasonic plane wave emitted by the downstream transducer, crosses first the bloodline, next the volume flow, next the bloodline again, is subsequently reflected, crosses again the bloodline, the flow and the bloodline and is finally received by the upstream transducer. The received signal at the upstream transducer is converted into electronic signals. The time between emission at the downstream transducer and reception at the upstream transducer is the transit time. Next, the upstream transducer emits a planar ultrasonic wave which is received by the downstream transducer. Again the transit times are recorded.
The transit time of the ultrasonic waves to travel from one transducer to the other depends on the flow rate of the fluid in the bloodline, the fluid properties, and bloodline geometry (diameter, thickness and material). The integral upstream transit time is reduced with the integral downstream transit time which is a measure for the flow rate.
This transducer type has to be calibrated for the tube material, wall thickness, temperature and the fluid density used in the set-up. Different flow probe diameters are available. The flow probes used in the experiments are types H10C and H16C. The corresponding ultrasound frequencies are 3.6 MHz and 0.9 MHz respectively. This flow sensor makes it possible to measure the mean flow rate or the time dependent waveform.

The flow probe types used are a H10C and a H16C flow probe. These probes have a typical eight hour zero stability of ± 10 ml/min and the absolute accuracy is $\pm 2\%$ of the flow reading. The resolution of the flow reading is 5 ml/min.

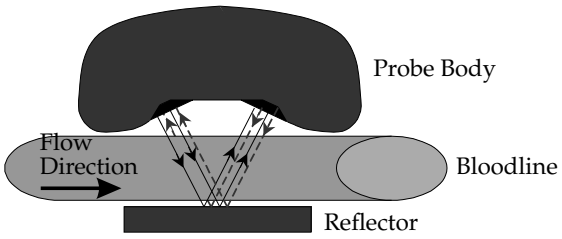

Figure 2.2: Schematic representation of upstream and downstream emitted ultrasound waves with a transonic flow probe

2.4.2 Doppler ultrasound

The physics of diagnostic ultrasound

The probes of diagnostic ultrasound equipment emits longitudinal ultrasonic waves by a vibrating piezoelectric element. This acoustic energy is transferred through the diagnostic medium based on the principle that all materials possess elasticity of volume and allows particle vibrations. If a pressure increase Δp is imposed on a material with initial volume V_0, the volume of the material changes with an amount ΔV. This phenomenon is expressed as:

$$\Delta p = -B\frac{\Delta V}{V_0} \tag{2.9}$$

with B the volume or adiabatic bulk modulus of elasticity. The bulk modulus of elasticity for water equals $2.2\ 10^9 N/m^2$.
The general wave equation for one dimensional ultrasound waves, with propagation speed c, is:

$$\frac{\delta^2 u}{\delta t^2} = c^2\frac{\delta^2 u}{\delta x^2} \tag{2.10}$$

The solution of this differential equation, that neglects dispersion, can be written as:

$$u(x,t) = f_f(x-ct) + f_b(x+ct) \tag{2.11}$$

$f_f(x-ct)$ is the forward going wave and $f_b(x+ct)$ is the backward traveling wave. The wave travels at the propagation speed c. The average speed of sounds in biological tissues with density ρ_0 is estimated at 1540 m/s. The density of biological substances varies depending on the type of tissue considered: the density of fat is e.g. 920 kg/m^3, the density of skin 1100 kg/m^3, the density of blood 1060 kg/m^3

and the density of bone varies between 1700 and 2500 kg/m^3.

$$c = \sqrt{\frac{B}{\rho_0}} \tag{2.12}$$

When equation (2.12) is calculated with the properties of blood, the propagation speed calculates is:

$$c = \sqrt{\frac{2.2\ 10^9 N/m^2}{1060 kg/m^3}} = 1441 m/s$$

An acoustic wave contains kinetic energy that makes the material particles move and potential energy associated with the elastic deformation. It is proven that this energy can be written as:

$$\epsilon = 4\pi\rho_0 f^2 E\ \ cos^2(kx - \omega t) \tag{2.13}$$

E is the maximum particle displacement, k is the wavenumber and ω is the pulsation ($\omega = 2\pi f = k\ c$). The average energy $\langle\epsilon\rangle$ over one cycle is consequently $\langle\epsilon\rangle = 2\pi^2\rho_0 f^2 E^2$. Once the average energy over one cycle is known, the intensity of a wave can be calculated. The intensity of a wave $\langle I\rangle$ is defined as the energy per unit time that flows across a unit area perpendicular to the wave direction. $\langle I\rangle = 2\pi^2 c\rho_0 f^2 E^2$ is the intensity of an infinite one directional plane wave.

A wave that travels through biological tissue encounters different media. The wave will partially be reflected and partially be transmitted at the interface between the media. It should be noted that the higher the difference in speed of sounds between the media, the more the wave will be reflected. That is the reason why it is difficult to visualise bone (66% reflection) and gasses (99% reflection).

The ultrasound waves are up to now described in pure elastic media where the wave can only be transmitted or reflected. However, biological tissues are visco-elastic, which means that the energy emitted can be converted into other forms of energy (like heat) besides kinetic and potential energy. The visco-elastic effect results in a waveform that weakens with the distance. If the wave intensity is I_0 at the source plane, the intensity at a distance x from the source plane becomes:

$$I = I_0 exp[-\nu x] \tag{2.14}$$

ν is the intensity absorption coefficient and is the sum of the absorption and scattering coefficient.

Figure 2.3 shows the parameters of an ultrasound probe. The probe body holds a certain number (N) of piezoelectric ultrasound transducers with an aperture a. r_{max} is the maximum depth at which the probe can measure and depends on the time delay T between two successive pulses. The beamsteer, θ_0, is the maximum angle at which can be measured before it becomes impossible to determine the radial direction in which an echo was generated. θ_0 is about 90°. The range resolution, Δr depends on the bandwidth (B) of the emitted pulse. The angular resolution $\Delta\theta$ depends on center frequency f_c of the transmitted pulse, the aperture a, the beam direction θ_0 and the speed of sound c. The aim of the technique is to capture images sufficiently fast to visualise the events going on in the body. The frame rate FR is the frequency at which the images can be refreshed. The formulas that express the relationship between the different parameters are summarised in table 2.1.

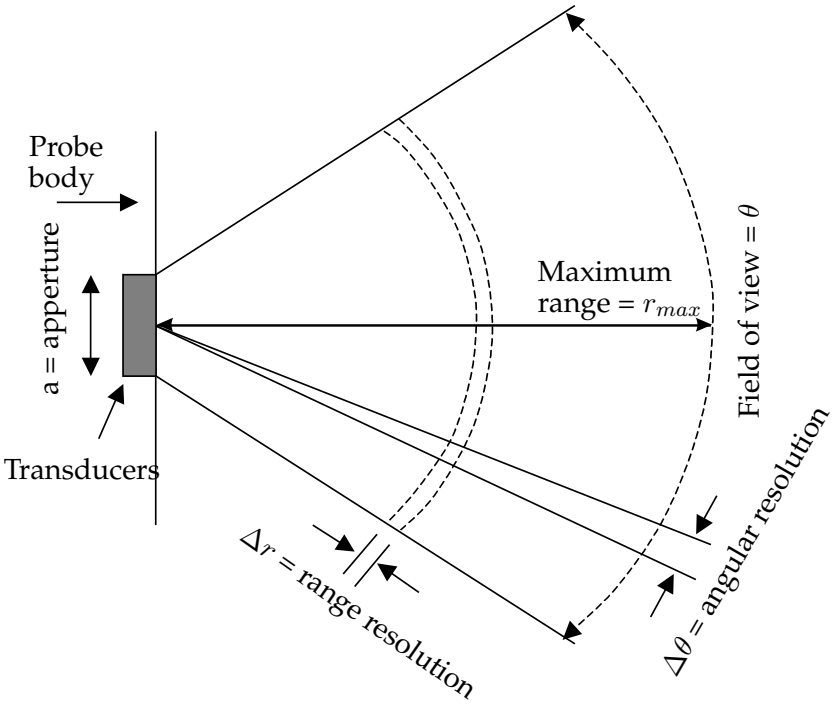

Figure 2.3: Schematic representation of an ultrasound probe

If a transmitter transmits an ultrasound wave with frequency f_s towards a red blood cell with velocity v, it is scattered and can be captured at the receiver. The

maximum range, r_{max}	$r_{max} = \frac{cT}{2}$
bandwidth, B	$B = \frac{2}{\Delta t} = \frac{2c}{\Delta r} < 2f_c$
frame rate, FR	$FR = \frac{c\Delta\theta}{2r_{max}\theta_0}$
beamwidth, $\Delta\theta$	$\Delta\theta = sin^{-1}\left(sin\theta_0 + \frac{c}{af_c}\right) - sin^{-1}\left(sin\theta_0 - \frac{c}{af_c}\right)$
number of elements	$N > \frac{2a}{\lambda}$
beamsteer	$\theta_0 \leq sin^{-1}\left[\frac{N_c}{f_c a} - 1\right]$

Table 2.1: Summary of the design parameters of an ultrasound system. (r_{max}: the maximum measurement depth, c: the sound of speed, T: the time delay between two successive ultrasound pulses, B: the bandwidth, Δr: range resolution, f_c: the center frequency of the transmitted pulse, $\Delta\theta$: the angular resolution, N: the number of piezoelectric elements, θ_0: the beam direction)

transmitter is positioned under an angle θ_t and the receiver under an angle θ_r with regard to the red blood cell velocity vector. The wave captured at the receiver has a slight different frequency f_r when compared to the transmitted frequency f_s. This shift is also known as the Doppler shift f_D. If the assumption can be made that $\theta_r \approx \theta_t \approx \theta$, the Doppler shift becomes:

$$f_D = f_s - f_r = -\frac{2f_s v}{c} cos(\theta) \tag{2.15}$$

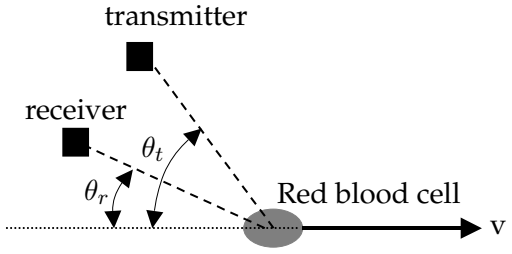

Figure 2.4: The position of the transmitter and receiver under a arbitrary angle according to a red blood cell

Ultrasound Doppler measurement systems send the multiplication of the transmitted and received signal through a lowpass filter to remove the source frequency

and deduce the Doppler frequency. Now, the fluid velocity can be derived as all parameters in equation (2.15) the Doppler frequency is known, the fluid velocity, v, can be calculated.

The continuous wave Doppler system

The continuous wave ultrasound Doppler system consists of two crystals incorporated in one transducer that simultaneously and continuously transmit ultrasound waves. The velocity is measured along the complete beam but without spatial resolution.
The advantages of this method are that the maximal velocity along the beam can be measured and that high-velocity flows easily can be measured.
The disadvantage is that this technique does not allow to localise the velocity along the path.

The pulsed wave Doppler system

In this mode, a range or depth of interrogation can be defined along a line. Pulses are transmitted at a constant rate along the image line: the pulse repetition frequency. One sample of the reflected signal is captured at a fixed time after transmission of the pulse. This technique has an excellent temporal resolution: about 200 - 300 samples per second. However, there is no spatial resolution within the sample volume.

M-mode and B-mode echocardiography

M-mode echocardiography visualises tissue along a selected scanline. If a blood vessel is visualised, the wall movement can be observed during the cardiac cycle. Properties concerning the elasticity of the vessel walls can be derived from these images.
A B mode image is a two dimensional visualisation of the tissue of interest.

The ultrasound system used

The ultrasound system used is the Vingmed CFM800 (Vingmed CFM800, Horten, Norway), color flow mapping system with software version 2.2x.

The 2D images are built up with maximum 128 lines per sector that have 512 samples per line. The temporal resolution of the 2D images is 18ms. The accuracy for measuring distance in 2D mode is 7% for distances between 1 and 10 cm and 5% for distances above 10 cm.
M-mode images contain 400 lines with 256 samples per line. The temporal resolution of the images is 5ms. The Doppler spectrum also contains 400 lines and 256 samples per line and has a temporal resolution of 5ms.
Pulsed mode is used in the in vitro experiments. In this situation, the maximum depth measurable is 17.3 cm and the depth resolution is 0.1 mm. The sample volume size is minimal 0.8 mm and maximal 22.5 mm. The accuracy for the distance measurement is 5-7% and the accuracy for the velocity measurement varies between 5 and 15%. The probe used is a pediatric/neonatal 7.5 MHz probe.

2.4.3 Pressure measurement

Two different pressure transducers were used in the in vitro studies: a Millar Mikro-Tip®(Fysicon Medical Technology, Oss, The Netherlands) and a piezoelectric pressure transducer (Datex-Ohmeda, Gent, Belgium).

Millar catheter:
These catheters are meant for intra-operative pressure measurement with the pressure sensor on the tip of the catheter. The type that was used in the experiments is model MPC-500. It has an operating pressure range from -50 to 300 mmHg, and overpressure is when the sensor is submitted to 4000 mmHg. The temperature error band at zero pressure is 1 mmHg and the linearity and hysteresis error is $\pm$5% of the full scale. An overview of all the specifications of the Millar catheter, model MPC-500, can be found in appendix A.

Piezoelectric pressure transducer:
The sensor uses the piezo resistive principle of semiconducters. Atoms in the crystal structure are shifting if pressure is applied to the material with a change in electric resistance as a consequence.
The transducer consists of a silicon membrane wherein resistance tunnels are integrated and that are placed in a wheatstone bridge. When pressure is applied onto the membrane, the wheatstone bridge is out of equilibrium proportional to the applied pressure.
A fluid filled catheter has to be connected to the pressure transducer to be able to

measure pressure inside a blood vessel.
This sensor has a sensitivity of 5μV/V/mmHg and has a maximum inaccuracy due to non-linearity and histeresis of 2% of the reading or 1 mmHg. It's operating pressure range is between -30 and +300 mmHg. All specifications about the DTX plus disposable transducers (Datex-Ohmeda, Gent, Belgium) can be found in appendix A.

2.5 Computational fluid dynamics (CFD) for the assessment of blood flow

The pressure and velocity in a hydraulic circuit can be either measured or simulated by solving the governing equations in the circuit with computational fluid dynamics (CFD). The advantage of measurements is that one gets fast and easily insight in the general behaviour whereas the results of CFD simulations can provide detailed information of the flow field.

The geometry that has to be investigated is designed in a computer aided design (CAD) program and imported into Gambit 2.0.4 (Fluent, Sheffield, UK), the mesh generation software. A mesh is generated and boundary and continuum types are written to a Fluent mesh file. The mass and momentum conservation equations are discretised and solved in the CFD package Fluent 6.1.18 (Fluent, Sheffield, UK). The postprocessing of the results is executed using the postprocessor of Fluent and in house developed Matlab (The Mathworks inc., Gouda, The Netherlands) utilities. This procedure is visualised in a flowchart in figure 2.5.

2.5.1 Geometry and mesh generation

The geometry is generated in solidworks (SolidWorks Benelux, Alkmaar, The Netherlands) as this is software which allows the user to generate the complicated geometry within an acceptable time span. The geometry is in Solidworks exported as a parasolid file and subsequently imported in Gambit 2.0.4 (Fluent, Sheffeld, UK).
Gambit is the mesh generating software. Different approaches can be chosen to generate the mesh. The user can choose to mesh the edges first, subsequently the faces and next the volume. Either a mesh with a constant size or a mesh gradually increasing in size can be applied to the geometries. Especially useful are boundary

layers and size functions. Both tools make it possible to impose a dense mesh in regions of specific interest that gradually change into a coarser mesh. The mesh can be evaluated in Gambit: the skewness of the cells and the length/width relation can be investigated.
Once an acceptable mesh is generated, the CFD package has to be defined: the boundary and fluidum zones can be indicated then.

2.5.2 Preprocessing

The continuum and boundary conditions, the discretisation schemes, the turbulence model and the solver have to be chosen before the simulations can be executed.
For problems that have time-dependent boundary conditions, the unsteady solver has to be chosen. If the boundary conditions are constant and the solution of the problem is time-independent, a steady solver has to be used. When the time-dependent boundary conditions are imposed, they have to be programmed in a user defined function that has to be compiled and loaded in Fluent.
It is evident that for laminar flow, the laminar solver is relevant and for turbulent flow, the turbulent solver with a turbulence model. All flow simulations performed in this thesis are limited to laminar flow. The Reynolds number $Re = \frac{\rho v d}{\mu}$ (ρ: the fluid density; v: the mean fluid velocity; d: the hydraulic diameter; μ: the dynamic viscosity of the fluid) has to be calculated to know whether we are dealing with laminar or turbulent flow. The maximum Reynolds number observed is 2800, which is transient flow. To calculate this, the unsteady laminar solver is used as the turbulence models included in Fluent are for high Reynolds flow; Re=10^6. The unsteady formulation allows to calculate the transient effects. Pulsatile flow is characterised by the Womersley number (α)

$$\alpha = \frac{d}{2}\sqrt{\frac{\omega\rho}{\mu}} \tag{2.16}$$

ω[rad/s] is the pulsation. α expresses the proportion of inertia forces to viscous forces in pulsatile flow. The higher α, the more flow conditions differ from Poiseuille flow. α equal 1 means that flow is still unsteady, but the velocity profile looks like that of Poiseuille flow. A laminar boundary layer is always present near the wall but the velocity profile is rather flattened in the middle of the blood vessel. α varies between 6,25 and 9,40 in this thesis. α is 4.0 in the brachial artery of a

healthy human and 22.2 in the proximal aorta.
In a next step, the discretisation schemes need to be adjusted. The pressure discretisation scheme was set to ”second order” and the momentum discretisation scheme to ”second order upwind”. The pressure-velocity coupling scheme set is ”SIMPLE”.
In a last step, the velocity has to be initialised. The whole velocity and pressure field can be set to zero or coupled to an initial guess of the velocity and pressure. The latter especially will be chosen when the user can estimate the velocity and pressure profile.
The residuals are calculated every iteration. It is accepted as rule of thumb that the solution is converged when the residuals have decreased three decades. This convergence criterion is sometimes strengthened in the case that the calculated flow field deviates from the one observed in experiments.

2.5.3 The CFD calculation and postprocessing

The user can opt to follow the convergence in text form on the display or the convergence can be visualised in a graph. Fluent checks every iteration the convergence criterion. As soon as it is reached, the iterations stop.
When the simulations are finished, the results can be visualised using the postprosessor of Fluent.

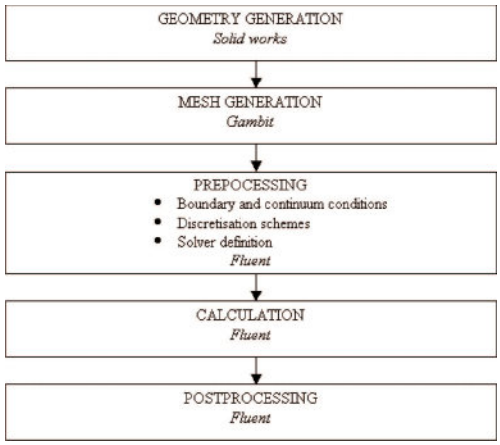

Figure 2.5: A flowchart of the computational fluid dynamics for the assessment of blood flow.

Chapter 3

Hemodynamics and complications encountered with arteriovenous fistulas and grafts as vascular access for hemodialysis: a review

3.1 The different vascular access types and the related hemodynamics complications

3.1.1 Vascular access types

End stage renal disease (ESRD) patients referred to hemodialysis therapy need a vascular access to withdraw blood from the patient at a blood flow rate of approximately 350 ml/min. If renal recovery is presumable, a temporary access is used. Standard temporary accesses are catheters directly inserted in the femoral or

The content of this chapter is published as: Van Tricht I., De Wachter D., Tordoir J., Verdonck P., Hemodynamics and complications encountered with arteriovenous fistulas and grafts as vascular access for hemodialysis: a review , Annals of Biomedical Engineering, Vol. 33, No. 9, September pp. 11421157; 2005

jugular vein. If the patient deals with enduring kidney failure, a permanent vascular access is chosen. The permanent access types available for patients on long term dialysis are autogenous arteriovenous fistulas, non-autogenous arteriovenous fistulas, permanent catheters and vascular port access devices. This review especially focuses on the hemodynamics in autogenous and non-autogenous arteriovenous fistulas.

The vascular accesses have different outcome rates, or patency rates, due to the different susceptibility for complications. The primary patency rate expresses the number of functioning accesses without revision history, compared to the total number created. The secondary patency rate expresses the number of functioning accesses, including the revised accesses, compared to the total number. Table 3.1 summarises primary and secondary patency rates for autogenous arteriovenous fistulas and grafts (non-autogenous fistulas).

	AVF		Graft			
	wrist	elbow	autograft	bovine	sheep	synthetic
Primary Patency 1 year	72-87% [112]	77.5% [113]	89.4 % [22] 70 [119]	n/A	n/A	72-87% [17]
2 year			89.4% [22] 50% [119]			
3 year			71.5% [22]			
Secondary Patency 1 year	74% [27] 85% [114] [115]	74.1% [116]	76% [121] 63% [122]	65% [27] 79% [26]	71% [27]	74% [120] 58% [27]
2 year	80% [114] [115]	86% [117]		69 % [26]		59% [120]
3 year	64% [27]		52% [121]	24% [27] 63% [26]	45% [27]	47% [120] 40% [27]
4 year		61.3% [116] 80% [118]				
7 year	50% [114] [115]					

Table 3.1: Overview of the patency rates in autogenous (AVF) and graft arteriovenous fistulas. (n/A: not available)

Arteriovenous fistulas

The arteriovenous fistulas can be subdivided into two groups: the autogenous and non-autogenous fistulas. If only native material is used, an autogenous fistula is constructed. If the patient has inadequate or unavailable veins to construct an autogenous vascular access, surgeons rely on grafts and consequently a non-autogenous fistula is placed. The construction of a non-autogenous fistula is avoided if possible because of the lower outcome. Fistulas can be placed over the whole body, but by preference in the upper extremity because of the lower complication rates [15] [16]. Surgeons choose the most distal available site to preserve more proximal vessels for possible future accesses in the case the first access fails. When all possibilities in the upper extremities are exhausted and no adequate vessels are available there, a vascular access is installed in the lower extremity.
Autogenous fistulas show the highest patency rates compared to the non-autogenous fistulas. Patency rates vary considerable between studies in different centers. This is of course because of the human factor involved, the surgeons' skills and the patient pool definition. Some studies exclude ligated fistulas, others patients with patent fistulas that switched therapy and others the early failures (in the first month). This uncovers the need of a statistical standard for reporting patency rates of vascular accesses [17].

The minimum flow rate that can be accepted in an autogenous arteriovenous fistula is 500-600 ml/min while the minimum flow rate that can be accepted in the non-autogenous fistula is 650-800 ml/min. When the access flow rate remains above these values, the fistula outcome will not be harmed [59] [19] [20].

Autogenous fistulas An autogenous artery and a vein are surgically connected via the anastomosis and bypass the peripheral capillaries. Four different anastomosis types can be constructed (see figure 3.1): (i) end artery to end vein anastomosis, (ii) end artery to side vein anastomosis, (iii) side artery to end vein anastomosis and (iv) side artery to side vein anastomosis. The most distal end of the vessel is ligated if an "end to -" anastomosis is constructed. The name of the fistula and the vessels used depend on the site where it is constructed. The most common autogenous fistulas are discussed below.

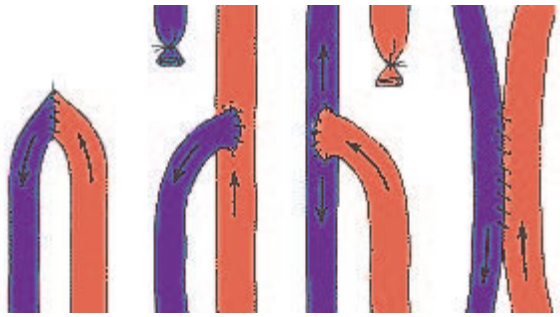

A: End artery to end vein anastomosis

B: Side artery to end vein anastomosis

C: End artery to side vein anastomosis

D: Side artery to side vein anastomosis

Figure 3.1: Four different anastomosis types

The Radial-Cephalic fistula is the most distal access. It is created between the radial artery and cephalic vein at the wrist. This fistula type suffers from many failures during the first month of construction: about 20%. Especially the group of patients above 70 years deal with failures: 40% patency after 1 year [21]. When this type of fistula fails to mature or when the wrist vessels are inadequate, a proximal forearm fistula is created. End cephalic vein is sewn on side radial artery. The elbow fistula (figure 3.2) is the next, more proximal, option. In this fistula, the brachial artery is connected to either a forearm vein or the cephalic vein or the transposed basilic vein. The major disadvantage of this fistula is that the developed flow is high: 1000-2000 ml/min. If even an elbow fistula is impossible to construct an upper arm fistula between brachial artery and either the cephalic vein or the transposed basilic vein is considered. When no large or visible vein is available in the upper arm, the basilic vein is transposed (tunneled through subcutanous tissue). Transposition of basilic vein is an alternative to a prosthetic graft. The previously described fistulas are primary autogenous fistulas.

Secondary autogenous fistulas are constructed using the greater saphenous vein, the basilic or brachial vein as an autograft. The graft is preferably put in in a loop configuration. The primary patency rates amount to 89.4%, 89.4% and 71.5% at 1, 2 and 3 years for the greater saphenous vein autograft and to 70% and 50% at

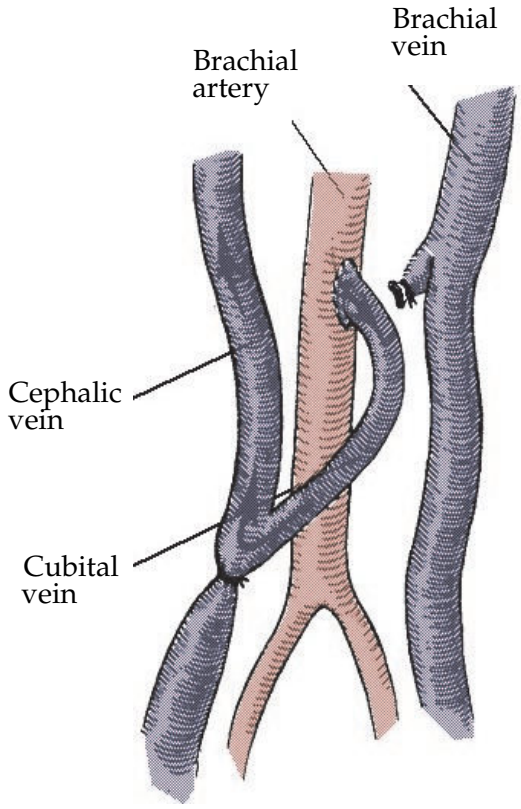

Figure 3.2: A native arteriovenous fistula in the elbow region between artery brachialis and caphalic vein

1 and 2 years for the basilic vein loop graft [22].
If the surgeon decides to construct a fistula in the lower limbs, an autogenous fistula can be constructed between either the femoral or the popliteal artery and the femoral vein, which is transposed to a superficial position.

Non-autogenous fistulas For patients with inadequate superficial veins, an autogenous arteriovenous fistula is not possible and non-autogenous arteriovenous graft is chosen as vascular access. Synthetic materials like polytetrafluorethylene (PTFE), silicone as well as biologic materials like homologous veins and bovine and sheep vessels are used as grafts each with their own benefits and drawbacks.
PTFE is the principal graft material used. Up to 83% of the hemodialysis patients in the USA have PTFE grafts [23] compared to 10% in Europe [24] and only 7% in Belgium [25]. Standard wall, thin and stretch wall PTFE grafts are available. The thin

wall grafts showed disadvantages compared to the standard wall grafts, patency rate was lower and infection rate higher in the thin wall graft. All graft types can be placed in a straight or loop configuration either in the forearm or in the upper arm, patency of the loop graft configuration is higher than for the straight.

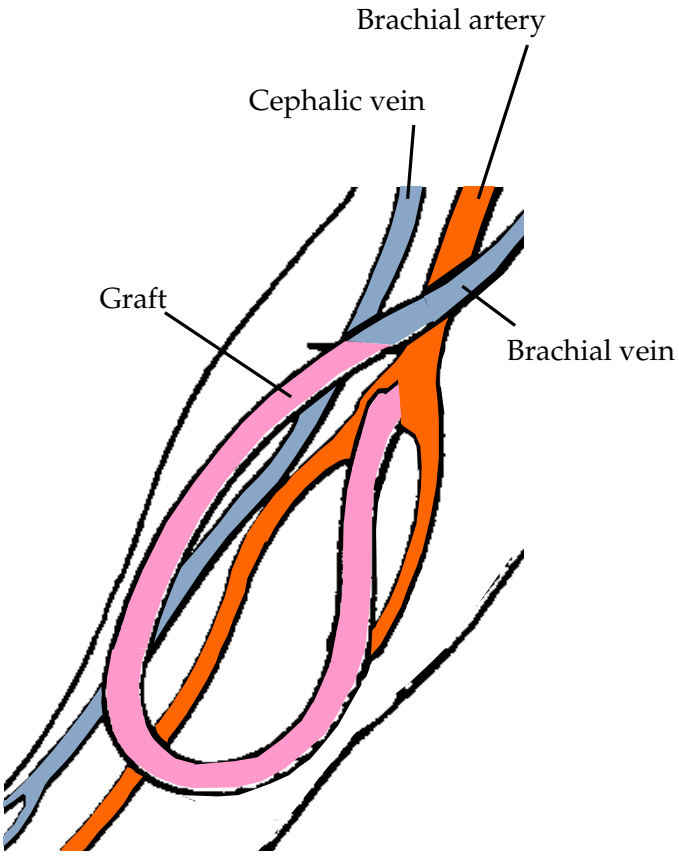

Figure 3.3: A PTFE-graft in loop configuration in the elbow region

If the loop graft configuration (figure 3.3) is applied, attention should be paid to avoid kinking and twisting at placement. The specific complications that make the graft fail are described below (see paragraph 3.1.2). When the complication progresses and graft rescue becomes impossible, the graft must be surgically replaced. When previous grafts have failed, the risk of following graft failure rises significantly; prior failed autogenous arteriovenous fistulas can not be correlated to graft failures. Overall PTFE graft patency varies depending on the consulted source (table 3.1). Patency rates in diabetes are lower compared to non-diabetics. Denatured homologous veins have secondary patency rates comparable to PTFE

grafts. The major complication with this graft type is aneurysm formation. Other homologous grafts are the cryopreserved saphenous vein that is sewed between brachial artery and cephalic vein. Bovine heterografts are comparable to PTFE grafts: complications and secondary patency rates are similar: 79%, 69% and 63% at 1,2 and 3 year [26]. Sheep collagen grafts are another type of heterografts used and have 71% and 45% overall patency rates at 1 and 3 year respectively [27]. Dacron composite and silicone composite grafts are rarely used. Clinical tests have also been performed on multilayered self sealing poly-urethane grafts. These grafts showed similar patencies as PTFE grafts, although 53.9% early cannulations (before 9 days), and they showed a short time to hemostasis [28].

If there are no access sites available in the upper extremity, a non autogenous fistula can be constructed between the common femoral artery and the common femoral vein. Bovine and PTFE can both be used as graft material. Patency rates in the lower extremity are remarkably lower compared to the upper extremity: 47% and 44% at 1 and 2 year respectively [29].

Catheters and vascular port access devices

A catheter (figure 3.4) is a synthetic tubing that is mainly inserted in the femoral and internal jugular vein. Mostly dual lumen catheters are used: one lumen is used to withdraw blood from the patient, a second is used to return purified blood to the patient. The internal jugular vein is frequently used if available because this is the location where the complication rate is least (see 3.1.2).

Dialock®(Biolink Corp., MA, USA) is an implantable titanium chamber connected to two silicone catheters. The device allows the insertion of two needles in the chamber without stagnating blood flow zones. This access offers an alternative to permanent catheters and reduces infection rates [9] [12]. Inter-dialytic periods are bridged with a heparin lock or an adjunctive antibiotic-anticoagulant lock [9] [10] [11].

A second port device is the LifeSite® (Vasca, Inc., Tewksbury, MA, USA) where two titanium ports each are attached to a 12F silicone catheter, connected to the dialysis machine via two 14G fistula needles. The major differences with the Di-

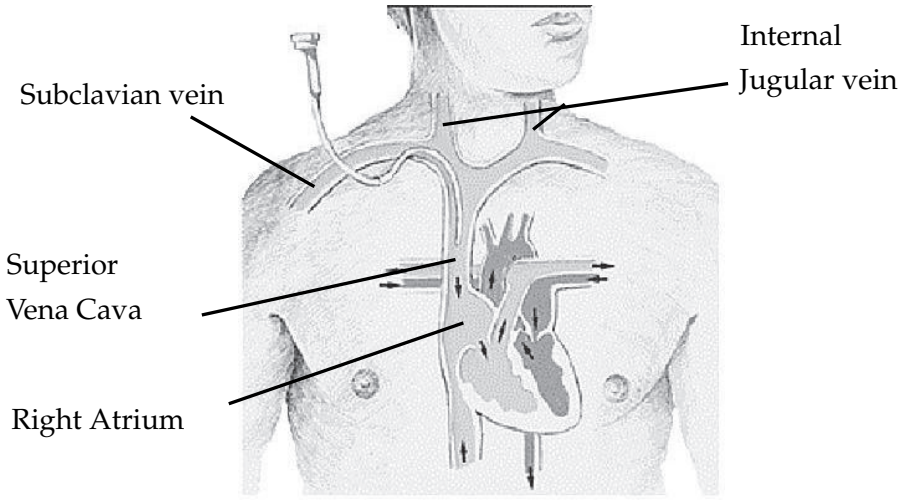

Figure 3.4: A catheter inserted in the subclavian vein

alock® system are the two separated port valves. The LifeSite® system reduces the complications encountered with catheters [11] [13]. It can be easily implanted and used as a bridge to a matured fistula or as an alternative to a permanent catheter [13].

3.1.2 Complications

The hemodynamic complications that can occur in fistulas (AVF) and non-autogenous arteriovenous grafts (AVG) are thrombosis, stenosis, aneurysm formation, ischaemia, steal syndrome and heart failure. Infections are complications of a non-hemodynamic nature that form an important complication, but is out of the scope of this review.

Thrombosis

Thrombosis is the major reason for failure of all types of arteriovenous fistulas, autogenous and non-autogenous. Early thromboses, appearing in the first few months, are due to technical errors, like kinking or twisting of the vessel or graft at placement, or an inadequate in- or outflow of the vascular access. Thrombosis at a later lifetime of the vascular access is mostly preceded by a stenosis (see 3.1.2).

There are four typical sites for thromboses to occur at: (i) at the anastomosis, (ii) in the remodeled vein that is used for cannulation (autogenous fistula), (iii) in the graft (non-autogenous fistula), or (iv) in the draining vein.
The clots can be removed by a thrombectomy: the access is surgically opened and a balloon catheter is passed beyond the bloodclot. A balloon at the tip of the catheter is inflated and the thrombus is removed when the catheter is withdrawn. Another option for thrombus removal is the mechanical thrombectomy: the rotational tip of the catheter breaks the thrombus into small pieces that are aspirated in the catheter. No incision is necessary: the catheter can pass through a small puncture. This technique is more successful in forearm fistulas than in upper arm fistulas and grafts; number of maintenance reinterventions were lower [30]. A last technique to take the blood clot away is pharmological dissolution [31].

Catheters placed in the internal jugular vein are well prevented from thrombosis development. As catheters are susceptible to thrombosis, a heparin lock in the catheter, is an indispensable precaution in the inter-dialytic period.

Stenosis

Stenosis is usually the underlying cause for thrombosis. Stenoses in AVF, develop mainly in the anastomosis and in the draining vein and rarely in the feeding artery. The rationale to understand why the majority of stenosis grow at the anastomosis and the draining vein becomes clear when the flow situation in the vein after vascular access creation is compared to the normal venous flow situation. For the latter, pressure is low (about 20 mmHg), flow is not pulsatile and wall shear stress is below 0.76 Pa [32] [33]. No single property remains the same in the vein near the anastomosis after the access creation: pressure has increased: it varies between 60 and 120 mmHg, flow is pulsatile and wall shear stresses increase above 0.76 Pa [32] [34]. The underlying mechanism of this stenosis formation is intimal hyperplasia (IH).

To understand the IH development, the vein layer structure is presented first. The inner layer, the intima, consists of a monolayer of endothelial cells, the basement membrane and the subendothelial matrix. The latter is composed of glycoproteins and connective tissue elements. The next layer is the tunica media where

the vascular smooth muscle cells (VSMC) are situated just like collagen and elastic fibres. The thick outer layer is the adventitia that consists of longitudinally oriented collagen bundles and scattered fibroblasts.
In the IH process, VSMC migrate from the media to the intima layer. When about 20% of the VSMC have migrated from the media to the intima, have proliferated and deposited extracellular matrix, compromising 60 to 80% of the intimal area, it can be stated that IH is present. IH is initiated by injuries like incisions, handling by forceps and sutures. On the other hand, cyclic stretch, abnormal wall shear stress values, the high venous pressure, elastic property mismatch between the graft and the blood vessels and the angle between the graft (or artery) and the vein also influence the degree of IH development [32].

The stenotic lesions in graft vascular accesses are mainly situated at the venous anastomosis and in the draining vein or at both places [35, 36]. Stenoses in arteriovenous fistulas are situated at the anastomosis or in the draining vein [36]. Sivanesan et al. [37] situated the stenosis sites in arteriovenous fistula between radial artery and cephalic vein more specifically. Stenoses were found in all fistulas and they could be classified in three categories. The first and the second type, i.e. at the anastomosis and at the curved inner wall of the vein, were not progressive. The third type, at the point where the cephalic vein straightens out, was found to be progressive.

Stenoses are complications that arise in all vascular access types. Also the introduction of a catheter in the vascular system can initiate stenosis development. It has been observed that catheters placed in the internal jugular vein develop less stenosis than catheters inserted in the subclavian vein. There is a more implicit advantage coupled to catheters inserted in the internal jugular vein: if a stenosis develops in the jugular vein, the subclavian vein will be preserved from stenosis. This is advantageous if a catheter is a temporary solution and an arteriovenous fistula is to be constructed afterwards because the subclavian vein is the draining vein in this case.

As a stenosis often leads to a thrombosis, it is important to detect stenosis formation at early stage. The risk for thrombosis increases with an increasing stenosis degree. The Kidney Disease Outcomes Quality Initiative (K/DOQI) guidelines define a significant stenosis at 50% lumen diameter reduction, this corresponds to

75% area reduction. [38]. Different approaches are possible to investigate a vascular access where a stenosis is probably present. Each approach has its specific advantages e.g. non-invasive, performed within a minute, cheap and disadvantages e.g. expensive, invasive or not accurate.

Doppler ultrasound is a frequently used non-invasive tool to detect stenosis. Peak systolic velocity of the Doppler spectrum is found to be an accurate parameter for stenosis detection [36]. The flow velocity increases in a stenotic lesion which produces an increase in the velocity of the backscattered signal.
Angiography is a reliable imaging technique to detect a vascular access stenosis. The disadvantage is that it is more expensive compared to Doppler ultrasound and that a contrast medium is used.
Ultrasound dilution technology with reversed hemodialysis lines is a frequently used technique for vascular access blood flow measurements [39]. A monthly decrease of 20 to 25% is considered as a predictor for the presence of a stenosis. However frequently used, access flow is a relatively inaccurate parameter as stenosis predictor. Access flow surveillance incorporates the assumptions that the measurements are reproducible, that stenoses are progressing slowly and that other factors than flow rate do not influence stenosis development. When access flow is measured, the moment in time during the dialysis session should be reproduced; one should be aware of the arising access flow drop of about 20% over the first 90 minutes of a dialysis session [40].
There exist also hemodynamic based parameters for stenosis detection in vascular accesses besides direct flow rate measurement. The first parameter, the resistance index ($RI = \frac{v_{sys}-v_{dia}}{v_{sys}}$) is a tool to characterise the flow by means of the measured velocity waveform using Doppler ultrasound. The maximum velocity in the waveform is the systolic velocity (v_{sys}) and the minimum velocity is the diastolic velocity (v_{dia}). When v_{dia} becomes negative, in the case of a high resistance blood vessel, RI becomes larger than 1 [41].
Kleinekofort et al. detects stenoses by calculating the ratio between pressure at the venous line of the dialysis machine and mean arterial blood pressure (MAP). When this ratio is larger than 0.5 a stenosis is considered present at the venous outflow [42].
Van Tricht et al. [43] have presented a new index, the pressure ratio
($PR = \frac{p_{arterial\ line}-p_{venous\ line}}{p_{arterial\ line}} \times 100\%$; $p_{arterial\ line}$ is the pressure at the arterial line of the dialysis machine when the pump is stopped and $p_{venous\ line}$ is the pressure at

the venous line of the dialysis machine with stopped pump), to detect in prosthetic arteriovenous fistulas a significant stenosis, one that needs intervention, i.e. 75% area stenosis according to the K/DOQI guidelines. When this pressure ratio is below 8%, it indicates that easy outflow of the vascular access is impeded.
The third parameter presented showed reliable results in vitro: all significant and critical stenoses were detected. However, it is recommended to verify the parameter in vivo because of his promising in vitro results.

Once a significant stenosis has developed, the stenosis must be treated to avoid thrombosis development. Stenoses are treated with balloon angioplasty procedures. A catheter with an inflatable balloon on top is passed through the stenosis and is inflated to dilate the stenosis.
If the stenosis cannot be successfully removed by balloon angioplasty, stents are placed in a similar procedure: a stent is put over the balloon and when the balloon is inflated, the stent is opened to the vessel diameter and keeps the vessel open. However, the restenosis rate varies between 15 and 40% in general [44]. The success rate of stenting depends e.g. the stent design and the presence of diabetics. All these factors explain the wide variations in outcome.
If balloon angioplasty or stent placement is impossible, the stenosis has to be treated surgically [44].

Aneurysm

The opposite of a stenosis is aneurysm formation, a pathological enlargement of the vessel diameter. Aneurysms in an autogenous fistula can be found at the anastomosis and at a weakened vein wall which originated in the many venipunctures. A pseudo-aneurysm can arise in a graft because of recurrent needle traumas. Aneurysms also contain a continuous thrombosis danger because of the high residence time of blood and accordingly higher risk of platelet aggregation.
Aneurysms are detected with Doppler ultrasound or CT scanning of the vascular access. The aneurysm can either be removed surgically or an endoluminal stent can be placed.

Ischemia and steal syndrome

The tissue distal to a well functioning fistula can suffer from ischemia and steal syndrome. Ischemia means that the tissue is inanimate because blood supply is inhibited. This results in a blocked oxygen, mineral and nutrient provision to the tissue. Steal syndrome is a generic term for the results of ischemia like a painful limb and necrosis. Possible treatment of ischemia is partial ligation of the graft or feeding artery so that distal perfusion is assured.
The risk for ischemia and steal syndrome is especially high when grafts are implanted in the elbow region or within diabetics, as they typically suffer from peripheral vascular disease. Radial-Cephalic fistula rarely suffer from ischemia or steal syndrome, because the blood flow rate in these fistulas is mostly limited.
To avoid ischemia in non-autogenic arteriovenous fistulas, the tapered, 4-7 mm, graft was invented. This graft has a smaller diameter at the arterial anastomosis than the conventional straight graft: 4 mm instead of 6 mm. The diameter of the tapered graft increases gradually to 7 mm. The original idea was that the tapering at the arterial anastomosis would involve a decrease of the flow through the graft and consequently more flow towards the hand and the digits and accordingly less ischemia. Clinical tests did not show reduced ischemia risk however, but an increased thrombosis risk compared to the conventional graft [45, 46]. The tapered graft involved more secondary procedures compared to the straight graft.

Heart failure

Heart failure is also a common problem in the end stage renal disease (ESRD) population. The fistula flow makes the cardiac output increase and imposes continuous cardiac loading. Besides, ESRD patients suffer from accelerated arteriosclerosis leading to an increased afterload and left ventricular hypertrophy, or even to heart failure [62].

Infection

Finally, besides hemodynamic complications, local and systemic infections of the vascular access are also important complications of vascular accesses. Infections e.g. occur at the needle puncture sites [46]. They can be determined because

of a painful or a swollen access. Infected accesses should be treated with antibiotics or should be removed when antibiotic treatment is unsuccessful. Infections represent about 20% of all access complications.
Permanent catheters are equipped with a cuff as a barrier to infections and they are preferably placed in the internal jugular vein instead of the femoral vein because of the higher infection rate in the femoral vein [31].

Routine fistula and graft management

Several methods are available to check the vascular access performance. Some techniques can be performed every dialysis session, others are scheduled monthly.

The first set of methods is to verify the vascular access performance in every dialysis session. The vascular access is checked before each cannulation by visual inspection for infections, aneurysms and hematoma [47]. Next, regularly palpation of the fistula is advised: in a well functioning access, a strong thrill can be felt. Finally an auscultation can be performed to check patency.
When the patient is subsequently connected to the dialysis machine, the vascular access has to be cannulated. If an abnormally high cannulation resistance is experienced, this can indicate a thrombosis. When this experience is coupled with aspiration of clots, even if the puncture is repeated, the access should be assessed for an impending thrombosis.
In a next step, during the hemodialysis session, the access function can be tested by occluding the access instantaneous in between the two needles. If an inflow problem would be present, arterial pressure would fall; if an outflow problem would be present, venous pressure would rise [48]. A last non-quantitative tool is observation of the bleeding time after the dialysis session. Prolonged bleeding indicates elevated intro-access pressure, which can indicate a venous outflow stenosis or an infection.
Quantitative access management tools which can be observed each dialysis session, are venous and arterial pressures. If dynamic venous pressure repeatedly increases above 150 mmHg at a blood flow rate of 200-225 ml/min, a venous outflow stenosis might have developed [49]. This technique is less valuable in under arm autogenous fistulas than in graft and upper arm autogenous fistulas because the lower arm autogenous fistulas have multiple run off veins.
If the dynamic arterial pressure is below -150/-250 mmHg, the blood pump is not

able anymore to deliver the prescribed blood flow rate [50]. This situation often points out an inflow complication.

The regularly, e.g. monthly, access flow and recirculation measurement is a reliable procedure. Doppler ultrasound [51] and dilution techniques [52] [53] [54] [55] can be used to measure the access flow rate. The blood flow rate is an important indicator for the access performance since access failure risk increases below a flow rate of 500-600 ml/min in native arteriovenous fistulas and below 650-800 ml/min in graft fistulas.
Even more interesting than a onetime flow measurement, is the observation of the access flow trend. To exclude the hemodynamic instability of a patient during the hemodialysis session, the access flow rate should be measured at the beginning of the dialysis session. There is some disagreement in the field about the influence of flow decrease on thrombosis formation. The study of Neyra et al. [56] reports high thrombosis danger at a flow rate decrease of 15 % and a 14-fold thrombosis risk increase at a 35 % flow rate decrease compared to accesses without flow decrease. Wang et al. [57] weakened this proposition: they agreed with the previous thesis as far as the non-autogenous grafts are concerned. Paulson et al. [58] could not confirm the study of Neyra et al.: in their study they reported no relationship between access flow decrease and thrombosis formation. However, it cannot be denied that access flow measurement is the best practical method to evaluate the access function and in the prediction of access failure [59] [60] [56] [61].
Moreover, it is hard to compare the access flow studies since there is no unique standard for access flow follow up. What is more, non-autogenous and autogenous arteriovenous fistulas should be followed up in a separate protocol as they have a different hemodynamic behaviour. What should be considered as standard, are dimensionless parameters based on the static intra-access pressures and the access flow rate.

3.2 Factors initiating intimal hyperplasia development

Several factors potentially initiate IH development: absence of endothelial cells, increased turbulent flow, compliance mismatch between a graft and a native vessel, endothelial injury by high shear forces, vessel damage and growth factor release because of venipunctures, mechanical injury or because of the disruption of the

plaque [65–67].

3.2.1 Surgical intervention

As already mentioned earlier, IH appears in particular at the venous anastomosis and in the draining vein. IH at the anastomosis of grafts originates especially at the suture line, in all grafts. Endothelial injury and surgical trauma certainly contribute to IH development at the suture line.
Surgical trauma, due to clamping and anoxia, influence IH development: the higher the trauma degree, the higher the degree of IH [89].

3.2.2 Compliance mismatch

The elastic properties of the blood vessels and grafts can be expressed with the compliance, the relative distensibility or the area increase. The compliance ($C = \frac{dV}{dp}$) is the ratio of the volume change (dV) over the corresponding pressure change (dp). The relative distensibility ($RD = \frac{D_{sys}-D_{dia}}{D_{sys}} \times 100\%$) gives the fractional diameter increase between diastoly, diastolic diameter D_{dia}, and systole, systolic diameter D_{sys}. Area increase ($Area\ Increase = \frac{\pi(D_{sys}-D_{dia})D_{dia}}{2}$) represents the capacity of the vessel wall to store blood during one heart cycle, see appendix.

In 1994, Hofstra et al. [67] compared area increase in saphenous vein grafts, expanded polytetrafluorethylene (ePTFE) grafts and stretch PTFE (sPTFE) grafts at the artrial inlet segment, the proximal and distal graft and the venous outlet segment. They found a sudden area decrease (a negative area increase) at all arterial anastomoses and a sudden increase at the venous anastomosis of the ePTFE and sPTFE graft. This sudden area increase, which is a measure for the compliance mismatch, was correlated to IH development at the venous anastomosis. The increased IH development at the suture line of the anastomosis of the PTFE graft [90] amplified the supposition that suture line IH originates not only in vascular healing but also in compliance mismatch.
In 1995 however, Hofstra et al. themselves countered the theory that compliance mismatch and IH formation are related [35]. They even observed a better match in elastic properties in the fistulas that developed stenoses compared to non-stenotic fistulas. The peak strain rate however correlated to the sites where stenoses were formed.

Some discord remained and other studies were set up to investigate the relationship between IH development and compliance mismatch. To reduce the compliance mismatch at the anastomoses, vein collars and patches have been introduced in vascular surgery performing bypasses in the lower extremity. For peripheral anterior obstructive diseases, Miller vein collars improved 2 year bypass patency from 19% to 50% [70] and Taylor vein patches improved patency to 58% [71]. Although these patches showed improved patency in arterial bypass grafts, according to Lemson et al. [32], the opposite was true for grafts used as vascular access for hemodialysis [32]. Gagne et al. [72] perceived a similar phenomenon in their study where they put in a Tyrell vein collar at the venous anastomosis of a vascular access graft. The vein pieces to construct the collar are superficial forearm veins or saphenous vein branches. The failures of a patient group with collar are compared to these of a group without collar. In 9 months in the Tyrell vein collar group 86% graft failures were observed compared to only 20% failures in the control group. The failed grafts showed also increased IH development in the venous anastomosis and the first 2 cm of the venous outflow tract.
The studies from Gagne et al. and Lemson et al. close up to the study of Hofstra et al. and make us assume that IH development in vascular accesses for hemodialysis cannot be correlated with compliance mismatch.

More promising than separate cuffs and patches, is the venaflo^{TM} graft: a cuffed PTFE graft for hemodialysis access. Overall patency rates found in a clinical study were 90.9% at one year and 68.2% at two years [66]. The lost grafts were because of outflow obstruction thrombosis and not because of a significant venous outflow stenosis. Other studies have been performed on tissue engineered grafts containing a matrix of human collagen and a monolayer of vascular endothelial cells. The aim is obtaining a graft with similar compliance as the native vessels and reducing the thrombogenecity. The graft has already been submitted to arterial shear stresses in vitro but needs in vivo tests to confirm its advantages [73,74].
The studies above indicate that compliance mismatch is not the major factor that causes intimal hyperplasia development in grafts for hemodialysis.

3.2.3 Wall Shear Stress (WSS) and strain rate

The shear stress, SS, is the friction force per area unit that an infinitesimal fluid element exercises on its neighbour infinitesimal fluid element. If Poiseuille flow exists, the shear stress can be calculated with the formula: $SS = \mu\frac{\delta v}{\delta y}$. μ is the

dynamic viscosity of the fluid and $\frac{\delta v}{\delta y}$ is the strain rate, also called the shear rate in some studies. If the shear stress surpasses 7.5 Pa for 5 minutes, leukocytes get activated and aggregation of leukocytes and platelets is stimulated [75]. When platelets are exposed to 50 Pa, during 1s, serotonin release will happen. Time is an important factor in this process since serotonin release will also happen when platelets are exposed for 0.01s to 400 Pa [76] [77] [78]. If red blood cells are exposed to 200 Pa for 1s or to 400 Pa for 0.01s, hemolysis occurs [78] [79] [80]

The shear stress value near the wall is the wall shear stress (WSS), where IH development is associated with. Normal WSS values are below 0.76 Pa for veins and between 1 and 3 Pa in large arteries and between 2 and 6 Pa in arterioles [33]. Wall shear stress values in arteries below 1 Pa are associated with IH development [81] as well as wall shear stress values above 35 Pa [82]. The endothelium is damaged in the latter case within an hour of exposure. Endothelium damage can easily start the IH development procedure. Consequently, the WSS values above 35 Pa are to be tracked in studies where the wall shear stress is calculated.

So when a vascular access is constructed, flow through the vessels of the access increases. Increased blood flow results in increased WSS for a constant vessel diameter. For arteries it is known that they remodel to maintain WSS at the normal level, about 1.5 Pa [65]. This means that the vessel radius increases when elevated WSS is sensed and vice versa. This remodeling can be accompanied by IH development. A similar process is mentioned in venous bypass grafts. The forces that suddenly act on the vein are arterial forces. Cuffs at both anastomoses of the bypass are used to reduce this phenomenon [70,71,84].
However, the situation is different between bypass grafts and vascular accesses for hemodialysis. When an autogenous fistula is constructed, a sudden increase in mean WSS and artery diameter is seen while peak WSS remained at the same level as preoperative. One year postoperative, the diameter had increased further but the mean WSS level was not returned to the preoperative level [85].

Hofstra et al. [35] correlated an increased peak shear rate to stenosis development. Area increase and relative distensibility were similar in the groups with and without stenosis development. Peak shear rate, in the vein 1 cm proximal to the venous anastomosis, increased in stenotic fistulas: 308/s compared to 212/s. This shear rate corresponds to a WSS of 1.11 and 0.76 Pa, respectively, if the dynamic

viscosity of blood is estimated 3.6 mPa.s. The value in the stenotic fistulas is out of the range of WSS values (0.076-0.76 Pa) observed in normal veins [33]. The corresponding peak velocity in the venous anastomosis is about 3.50 m/s.

It is in different studies observed that the wall shear stress or strain rate level can be correlated to intimal hyperplasia development. Moreover, platelets, leucocytes and red blood cells can be damaged under abnormal wall shear stresses. WSS is a valuable parameter to investigate concerning IH development.

3.2.4 Vessel wall thrill

Fillinger et al. [86] correlated kinetic energy transfer to intimal hyperplasia development. The kinetic energy transfer causes perivascular tissue vibration that can induce chronic vascular injury and subsequent IH development. Perivascular tissue vibration was less in the vein near the heel (see figure 3.5) where the fewest IH development was observed. Loth et al. [87] repeated the experiments of Fillinger et al. [86] by implanting PTFE-grafts in swines. They discovered mitogen-activated protein kinases (MAPK), more specifically: ERK1 and ERK2 in regions of increased vein wall vibrations. The concluding supposition of these studies is that MAPK can act as mediator between hemodynamic forces and the release of growth factors. Both studies prove a correlation between tissue vibration and IH development.

3.2.5 Blood pressure

Venous blood vessels in autogenous vascular accesses are subjected to increased blood pressure (about twice the normal venous blood pressure) and an increased blood flow. This increased blood pressure can result in increased vessel wall thickness to restore wall stress to the normal values [88]. Vein graft fistulas in hemodialysis however are exposed to higher increases: four times or more the normal venous pressure. It is clear that these grafts may respond similar to damaged tissue and induce IH formation.

Many different research methodologies, like patient observations, animal studies, in vitro experiments and computational fluid dynamics analyses, have been performed to examine the correlation between the different factors and IH development. Sites where the wall shear stress, strain rate and vessel wall thrill deviate from the values found in healthy humans are proven to correlate with IH development. It is also observed that the vessel wall responds to increased pressures and to vascular trauma. In the past, it was believed that compliance mismatch induced IH formation but this theory is nowadays rejected.

3.3 Experimental and computational studies

The different anastomosis regions are subdivided in floor, heel, toe, hood, proximal vessel, distal vessel and graft as shown in figure 3.5. This nomenclature simplifies references to the specific regions.

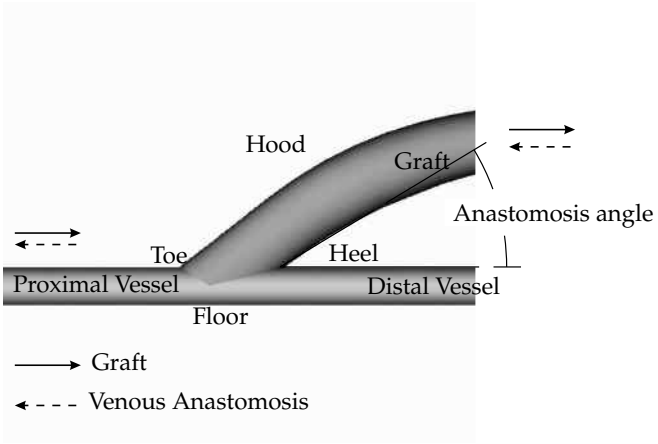

Figure 3.5: The geometry nomenclature used at an anastomosis

3.3.1 Experimental studies

In vitro and in vivo animal studies have been set-up to investigate the influence of the geometry, the flow rate, and the flow division on the hemodynamics and the

IH development.

The geometry strongly influences the hemodynamics. At first, trials with different anastomosis angles showed different pathologies. At a low anastomosis angle of 10°, intimal thickening existed at the anastomotic floor [94]. Also at a little higher angle, 30°, the highest IH development was observed at the floor [92]. In the latter study, it was observed that the locations where mean wall shear rate (WSR) remained below 100/s were responsible for 75% of the IH formation. Similar results have been found in low wall shear stress (WSS) regions: vein patches exposed to low WSS values at implantation (0.007 Pa), show a higher level of cell cycling [93]. When the angle was higher, 45° till 90°, thinning of the vessel wall or even aneurysma formation was observed on the floor [94]. It is clear that different hemodynamics cause a different vessel wall response. The higher the anastomotic angle, the more flow collides with the vessel floor and flow separation arises near the toe in the mid acceleration phase of the flow cycle [95]. Wall shear stress values are also found to vary with a varying anastomotic angle except on the floor in the vicinity of the heel where the WSS is quasi zero at all angles. Influence of the anastomotic angle of arterial bypass grafts is experienced at the toe: wall shear stresses are low (0.5 Pa) at all angles except 20°. This difference is also apparent on the floor opposite the toe: elevated WSS, 3 Pa, occur at 45 and 60° and peak WSS at 20 and 30 ° is only 1.5 Pa [95]. This study proves that IH development near the toe can originate in low WSS values.

Anastomotic geometry is also influenced by the graft diameter in the second place. When patients with poor vessels need a graft vascular access, surgeons often deal with a small artery diameter, about 3 mm, that has to be connected to a graft with 6 mm diameter. This is one of the reasons why the 4-7 mm graft was developed: it has a diameter of 4mm at the arterial anastomosis and the diameter increases the following 50 mm to 7 mm diameter. This 4-7 mm graft is in several studies compared to the 6 mm diameter graft. Both graft types were e.g. implanted in dogs where the outcome was that mild IH development was observed at the toe of the venous anastomosis in the 4-7 mm grafts and moderate IH development at the toe of the venous anastomosis in the 6 mm grafts [86]. Different clinical human studies showed however a similar outcome for both grafts [85] [46] [45]. Van Tricht et al. [96] investigated the hemodynamic differences in a 4-7 mm and a 6 mm graft in an in vitro model of a loop graft. Although the general behaviour of both grafts is similar, the major hemodynamic difference between both grafts is the

high pressure drop after the arterial anastomosis at the 4-7 mm graft followed by pressure recovery in the wide segment. This is opposite to the 6 mm graft where the pressure drops continuously over the arterial anastomosis.

The cuff technique also brings about a modified flow behaviour depending on the cuff dimensions. Flow separation zones that remain during a complete cardiac cycle should be avoided to have a nice particle wash-out. When surgeons create a cuff, the flow pattern changes completely compared to the conventional anastomosis. The cuff is used to obtain a stable flow pattern in the anastomosis. Fisher et al. [97] proved however that the Miller cuff length/height ratio determines whether the flow pattern is stable. When the ratio was 1.18 and 1.63, cohesive vortexes developed and the flow pattern was stable and WSS approximates normal values. A second advantage of a stable vortex is that particle residence is nihil and platelet activation is reduced. When the ratio was increased to 2.25 and 2.6, complex three dimensional vortexes were present and the areas of flow separation were large. Heise et al. [98] observed with particle image velocimetry (PIV) measurements large heel separation zones, which is associated with IH, in a Miller cuff silicastic model and large hood separation zones in a Taylor patch geometry. A novel femoro-crural patch anastomosis develops small toe and heel separation zones that do not persist during the complete cardiac cycle, leading to a better particle wash-out.

Flow visualisation techniques improve the insight in the vortex development and the secondary flow patterns originating at the anastomoses.
Particle image velocimetry (PIV) measurements of anastomotic flow in arterial bypass grafts showed particles skewing to the anastomosis hood and the presence of a downstream moving stagnation point at the floor during acceleration. During deceleration, the stagnation point moves back towards the middle of the anastomosis floor. Secondary flow patterns are observed near the suture line and the lateral walls besides the large vortex near the heel [90]. IH developed at the arterial floor where the flow reattached and low shear zones were observed. This brings up that the anastomosis geometry plays an important role in the sites of IH development as it determines the flow field.
The flow division at the anastomosis influences the location of the stagnation point. Flow at the outlet of arterial bypass grafts can stream out completely through the distal outlet segment (DOS) or partially through the proximal outlet segment (POS).

Increased POS flow results in increased separation at the graft hood and less stagnation point displacement. Low WSS values were found in all cases at the artery floor [99].
Sivanesan et al. [91] have built a realistic model to visualise the flow phenomenons in a native arteriovenous fistula. They observed extreme high and low WSS values within 10 mm from the suture line in autogenous arteriovenous fistula. The maximal WSS value was 40 Pa whereas the minimum value was 1 Pa. The WSS values in the draining vein vary between 5 and 14 Pa, values that are above the WSS values observed in veins (0.076 - 0.76 Pa). High WSS levels can be indicators for stenosis development as it occurs at the sites where stenoses tend to develop [37].

Another determinant for the hemodynamic behaviour is the flow rate. Sivenesan et al. [91] simulated three different flow rates in a wrist arteriovenous fistula and performed laser Doppler anemometry (LDA) measurements in the symmetry plane of the anastomosis. At a Reynolds number of 100, two stable vortexes were observed: the first near the heel and in the distal vein and a second occupying the anastomosis near the distal artery. When the Re number increased to 600, the fluid motion became completely chaotic and no organised flow could be observed. When flow in the model was made pulsatile (mean Reynolds number = 600), mean WSS and oscillatory WSS were calculated. The highest values were found at the outer vein wall and amounted to 57 Pa. Mean WSS values decreased to 9 Pa 70 mm downstream in the run off vein.

The experimental studies clearly show that IH development is influenced by the anastomosis geometry, the flow rate and division and the wall shear stress level.

3.3.2 Computational studies

The advantage of numerical simulations is that they make it possible to investigate parameters that are difficult to measure directly in vivo like the wall shear stress gradient, pressure gradient and oscillatory shear index. The definition of each parameter and the specific meaning is explained in the paragraph below.

The definition of the instantaneous wall shear stress gradient WSSG (5.6) on the

vessel wall is:

$$WSSG = \nabla WSS \tag{3.1}$$

To take the WSSG over the complete period into account and to be able to compare WSSG in different geometries, the dimensionless time averaged and normalised WSSG ($\overline{WSSG}_{ND}$) (5.7)is defined as:

$$\overline{WSSG}_{ND} = \frac{d}{\tau_p T} \int_0^T WSSG \ dt \tag{3.2}$$

d is the vessel diameter and τ_p is the mean Poiseuille wall shear stress at the inlet artery. T is the duration of one cycle. The zones where the highest $\overline{WSSG}_{ND}$ are found are places where the WSS varies considerably over a limited distance.
A high pressure gradient ($\overline{PG}$) value indicates flow towards the wall and not well aligned with the vessel axis. Equation (5.8) defines the time averaged $\overline{PG}$.

$$\overline{PG} = \frac{1}{T} \int_0^T \frac{p(i) - p(0)}{\Delta r} \ dt \tag{3.3}$$

A high $\overline{PG}$ corresponds with a high local load of the vessel wall. $p(0)$ is the pressure on the wall and $p(i)$ is the pressure in the fluid element adjacent to the vessel wall and r is the radial distance.
The oscillatory shear index is defined as:

$$OSI = \frac{1}{2} \left(1 - \frac{|\int_0^T WSS dt|}{\int_0^T |WSS| dt} \right) \tag{3.4}$$

If the OSI equals zero, there is no change in flow direction during the flow cycle, if the OSI equals 0.5, there exists fully oscillatory flow without net forward flow.
The parameters mentioned above are calculated in several numerical studies and investigated under different flow rates and in different geometries.

The Reynolds number and the anastomosis angle strongly influence the flow profile in the outflow anastomosis of a conventional bypass. The higher the Reynolds number and anastomosis angle, the more the flow is skewed towards the anastomosis floor and the higher the observed shear rates [100]. The hemodynamic parameters are also strongly dependent on the graft end design: extreme hemodynamic factors are noticed in grafts when bulges are present [101]. The vessel geometry also influences the WSS values importantly. Ene-Iordache et al [103]

made a patient specific autogenous arteriovenous fistula CFD model and found WSS 35 Pa in the bending zones and discovered secondary flow patterns in the bending and bulbing zones of the fistula.
The impact of the different geometry of a 4-7 mm compared to a 6 mm graft is considerably at the arterial anastomosis (figure 3.6) [34]. The WSS, $\overline{PG}$ and $\overline{WSSG}_{ND}$ values at the arterial anastomosis of the 4-7 mm graft are at least two times the values at the arterial anastomosis of the 6 mm graft. E.g. the maximum WSS in the 4-7 mm graft is 164 Pa around the suture ring. This value approaches 200 Pa which is the hemolysis threshold. At the venous anastomosis is observed that the parameter level (WSS, $\overline{PG}$ and $\overline{WSSG}_{ND}$) could be related to the degree of IH present in the dog study of Fillinger [86].

The numerical studies of Kute et al. [104] confirm that the flow division influences the hemodynamics in the anastomosis. The maximal WSS and WSSG values on the floor in the anastomosis of an arterial bypass graft depend on the flow rate through the proximal outlet segment. The maximal WSS values are found in the anastomotic toe region and the minimum at the floor. High WSSG values are found at the toe and heel with a maximum of 105 Pa/m. The study of Lei et al. [105] supplies in a comparable geometry the oscillatory shear index (OSI). This parameter indicates that the floor, the suture line and the heel are subjected to oscillating wall shear stresses as OSI varies between 0.3 and 0.5 there.

In the Miller cuff geometry, recirculation zones are found on the artery floor opposite the junction and in the cuff wall near the toe. As the recirculation zone periodically enlarges and reduces, the stagnation point on the floor also migrates. However, the migration is most in the conventional anastomosis and reduced in the Miller cuffed anastomosis and when 20% proximal outflow is allowed [106].
Krueger et al. [107] found also less harmful wall shear stresses in the venaflo^{TM}® graft, which has a modified outflow anastomosis, than in a conventional anastomosis. Peak WSS on the vein floor of the venaflo^{TM} graft is only 4.4 Pa compared to 5.9 Pa in the conventional. WSS is diminished about 50% on average in the venaflo^{TM} graft.

The above mentioned computational results are limited to the hemodynamics in a rigid wall structure. However, blood vessels are compliant structures that deform under influence of the blood pressure. This can be modelled with a combined model of CFD and FEM (finite element models), the so called fluid-structure

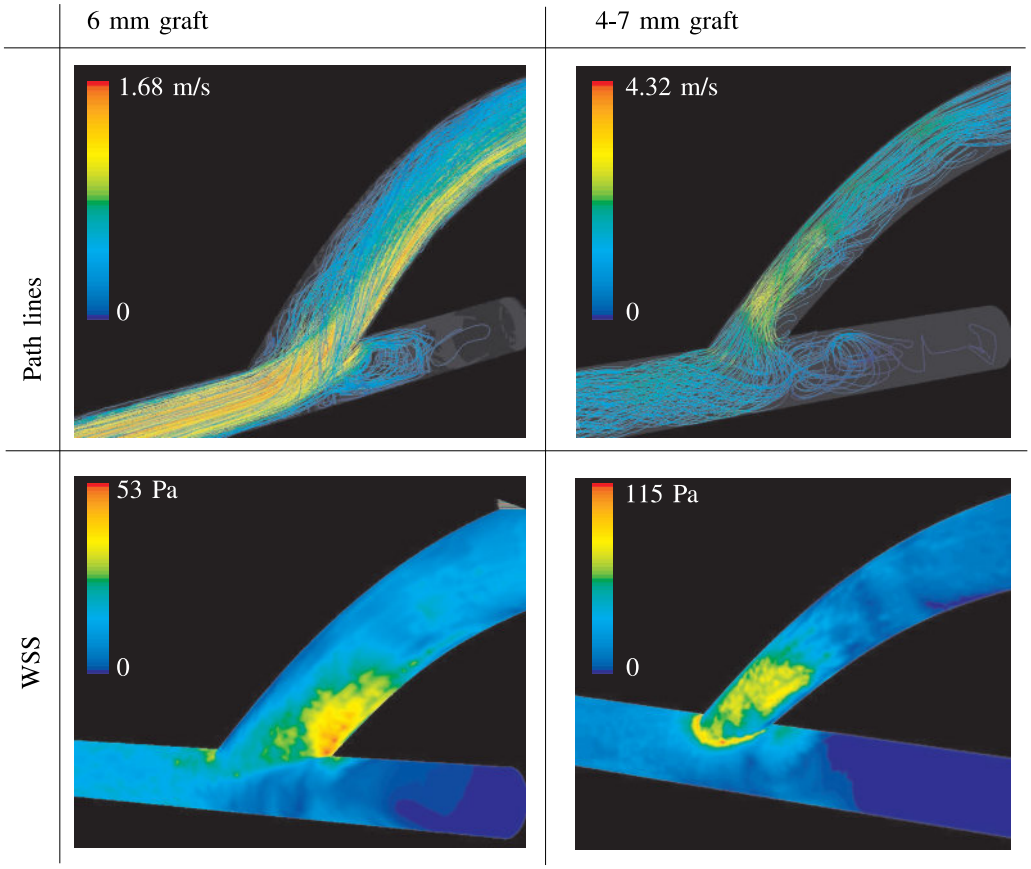

Figure 3.6: The pathlines (left and right top panel) in the arterial anastomosis of a 6 mm (left column) and a 4-7 mm (right column) graft. The pathlines are colored with the velocity magnitude. The left and right bottom panel show the wall shear stress (WSS) values in the 6 mm and 4-7 mm graft. The mean flow rate that corresponds with the panels shown is 1000 ml/min.

interaction models.

The above mentioned techniques like cuff placement and alternative anastomosis design are developed to prevent stenosis as a stenosis influences flow through a blood vessel considerably. Simulations on axisymmetric and asymmetric stenoses confirmed that the flow patterns look completely different in both geometries even with identical stenosis percentages. A first flow separation zone is in all cases situ-

ated just downstream the stenosis and periodically enlarges and reduces in shape. A second zone originates more downstream the stenosis during deceleration and disappears during acceleration in the axisymmetrical model, while it is present during the whole period in the asymmetrical model at 50 and 75% area stenosis. The stenosis geometry influences the separation zone length: the separation zones in the asymmetrical model are larger than these in the symmetric model [108]. The vortices in the recirculation zones are completely three dimensional. The vortex roll up stops during deceleration and a shear layer extends far downstream [109]. The recirculation zones cause critical flow conditions: high WSS values in the stenosis that can cause plaque rupture, platelet activation, and thrombus formation. There exists moreover negative transmural pressures at stenosis percentages above 78%. This negative transmural pressure can cause vessel collapse and consequently plaque rupture [110].

Wall shear stress and compliance mismatch are in the past frequently associated with IH development [32] [101] [107] [104]. Recently, IH development has been associated with blood particle stasis and deposition near the injured dysfunctional endothelium [111] [67]. Longest et al. [111] have introduced a near wall residence time (NWRT) model for platelets that incorporates shear stress induced platelet activation. The near wall residence time in a local near wall volume summed over all particles passing, is calculated as:

$$NWRT = \frac{Q_{av}}{n_0.V_{nw}} \sum_{p=1}^{n} \int_{path,p} \left(\frac{a_p}{h_p}\right)^s \frac{1}{||\overrightarrow{v}||} \mathrm{d}r \tag{3.5}$$

Q_{av} is the average flow rate in the system, n_0 is the total number of particles incorporated and V_{nw} equals the cell surface on the wall multiplied by 50 μm which is the height of the layer of biophysical interaction. $\left(\frac{a_p}{h_p}\right)^s$ is a probability of interaction factor, a_p is the particle radius, h_p is the distance between the center of the particle and the wall and the power s equals 2 to match experiments. $||\overrightarrow{v}||$ is the particle velocity magnitude and $\mathrm{d}r$ is the infinitesimal segment of integration along the particle path and $\frac{1}{||\overrightarrow{v}||}\mathrm{d}r$ consequently is the local particle residence time. The model described above can be extended with the platelet stimulation history (PSH) to include the shear induced platelet stimulation and the surface reactivity (SR) to include the surface proneness for thrombus formation. The PSH is a measure for

the shear stress level that the platelets are exposed to and for the exposure time:

$$PSH = \frac{1}{WSS_{mean}.T}\int_{t_{in}}^{t} WSS(t)\mathrm{d}t \tag{3.6}$$

WSS_{mean} is the mean WSS level in the vessel, T is the period of the input waveform and $WSS(t)$ is the local immediate WSS. The definition of the surface reactivity is:

$$SR = \frac{WSS_{mean}}{WSS_{ta}} \tag{3.7}$$

WSS_{mean} is the mean WSS in the vessel and WSS_{ta} is the local time-averaged WSS in the artery. This factor quantifies the local significance of platelet interaction with intact endothelium.
The maximum value of the product of NWRT, PSH and SR showed very good agreement with sites of IH development in two arterial bypass anastomosis geometries.

For drawing correct conclusions, one has to consider that both, geometry and boundary conditions strongly influence the hemodynamics.

3.4 Conclusion

Clinical studies have localised the spots where intimal hyperplasia tends to develop and promoted the investigation of the biological processes. In vitro studies are subsequently performed to get insight in the general hemodynamic behaviour. These experiments justified the need for in numero studies to visualise the places where high wall shear stresses and gradient parameters occur.
The cooperation of biomedical engineers, scientists and medical doctors is necessary to find the missing link between intimal hyperplasia development and the hemodynamics and the vascular wall biomechanics in a vascular access.

3.5 Appendix

The formula used for area increase in the manuscript: $\frac{\pi}{2}(D_{sys} - D_{dia})D_{dia}$ is a simplification of the general formula: $\frac{\pi}{4}(D_{sys}^2 - D_{dia}^2)$. D_{dia} is the diastolic diameter

and D_{sys} is the systolic diameter in the expressions.

If ΔD is the difference between the diastolic diameter and the systolic diameter: $\Delta D = D_{sys} - D_{dia}$, then the general formula can be rewritten:

$$\begin{aligned} \frac{\pi}{4}(D_{sys}^2 - D_{dia}^2) &= \frac{\pi}{4}((D_{dia} + \Delta D)^2 - D_{dia}^2) \\ &= \frac{\pi}{4}(D_{dia}^2 + 2.D_{dia}\Delta D + \Delta D^2 - D_{dia}^2) \\ &= \frac{\pi}{4}(2.D_{dia}\Delta D + \Delta D^2) \end{aligned}$$

If ΔD^2 can be neglected, one becomes the formula cited in the article $\frac{\pi}{2}(D_{sys} - D_{dia})D_{dia}$.

If the blood vessels have a relative distensibility of 4%, thus the systolic diameter equals 1.04 times the diastolic diameter, the simplified formula underestimates the real area increase with 2%.

Part II

Modelling of the hemodynamics in the vascular access graft immediately after the surgical intervention

Chapter 4

Hemodynamics in a compliant hydraulic in-vitro model of straight versus tapered PTFE arteriovenous graft

4.1 Introduction

End stage renal disease (ESRD) patients need a renal replacement therapy such as hemodialysis. Waste products and the excess of water are drained into an extracorporeal artificial kidney. To obtain a sufficient dialysis performance, blood must be circulated at a flow rate of about 300 ml/min in the extracorporeal system. In Europe, the commonly used vascular accesses like central venous catheters (10% of the cases), arterio-venous fistula (AVF) (60%) and access grafts (30%) are used to deliver this flow rate [15]. Preferred sites for the vascular access are in the upper extremity, because the infection rate, ischemia and steal syndrome are less frequent in the arms than at other sites [16]. Despite the lower primary patency rate for the AVF (20 - 30% early failures), AVF have a higher secondary patency rate (50-78% after 3 year) than PTFE-grafts (40-59% after 3 year) [31]. The main reason for

The content of this chapter is adapted from: Van Tricht I., De Wachter D., Tordoir J., Verdonck P. Hemodynamics in a compliant In Vitro model of a Straight versus Tapered PTFE Arteriovenous Graft., J. Surg. Res., 116/2: 297-304 J. Surg. Res.

PTFE-graft failure is stenosis development at the venous anastomosis leading to thrombosis [32] [123] [124].

Intimal hyperplasia and thrombosis are the result of several abnormal biological processes (abnormal for the considered blood vessel) introduced by unphysiological high flow events as summarised by Longest and Kleinstreuer [101]. Flow separation and reattachment, low oscillatory wall shear stresses, vortical flows, stagnation point flows, high shear stress regions, high pressure flows and long particle residence time are known as unphysiological pathological flow events in the extremities. These events cause endothelial cell dysfunction, endothelium injury, enhanced wall permeability, aggregation and deposition of platelets and fibrin and smooth muscle cell proliferation. Pressure and velocity measurements, shear stress calculations and shear stress gradient calculations are indicators, which can be used to minimise the risk and set up recommendations for favorable graft designs. The aim of this study is the assessment of vascular hemodynamics in an experimental setup simulating flow through a PTFE loop graft between brachial artery and vein respecting the geometry and physiologic pressure, flow and relative distensibility (RD) ranges. This work was a first step to obtain boundary conditions and validation data to perform numerical simulations with. Wall shear stress will be investigated more in detail in the latter as a second step. The last step in our work will be the tracing of any correlation between wall shear stress and intimal hyperplasia.

4.2 Materials and Methods

4.2.1 The vascular access model: anatomy and physiology

One PTFE-graft (Gore-Tex®) and one compliant silicon artery and vein are used to create the vascular access model (figure 4.1). Mean internal artery diameter is 4.25 mm at 100 mm Hg and mean vein diameter is 6.3 mm at 40 mm Hg. The PTFE-graft is sutured to the artery and the vein (end graft to side artery and vein) by a vascular surgeon. Two graft types are studied: a straight and a tapered one. The straight graft is the conventional graft whereas the tapered graft was introduced to (i) limit the difference in diameter between the artery and the graft and to (ii) limit the flow rate through the vascular access [102]. The straight, 6mm PTFE-graft, has

a constant internal diameter (d) of 5 mm. The internal diameter of the tapered, 4-7 mm PTFE-graft increases from 3 mm at the arterial anastomosis to 5.5 mm about 50 mm distal of the anastomosis and from this point, the diameter remains constant. The inner diameter of the graft is calculated by measuring the outer circumference and wall thickness of it. Assuming a circular cross-section and constant wall thickness, the inner diameter can easily be calculated. The length of both grafts is 340 mm. The arteries and veins are manufactured with silicon to simulate patient blood vessel distensibility in the experimental model. Silicon is painted on stainless steel molds, and is hardened in the oven for 90 min at 150°C. 8 layers are painted for an artery, 6 for a vein. Blood vessel properties are examined using the wall track method (Pie Medical - Maastricht - The Netherlands). Relative distensibility (RD) is determined and only silicon arteries and veins with 4% relative distensibility in the operating pressure range (vein: 20 - 50 mm Hg; artery: 70 - 130 mm Hg) are used in the experimental model.

$$RD = \frac{D_{sys} - D_{dia}}{D_{dia}} \times 100\% \tag{4.1}$$

D_{sys} is the systolic diameter and D_{dia} is the diastolic diameter. Relative distensibility is expressed as a percentage.

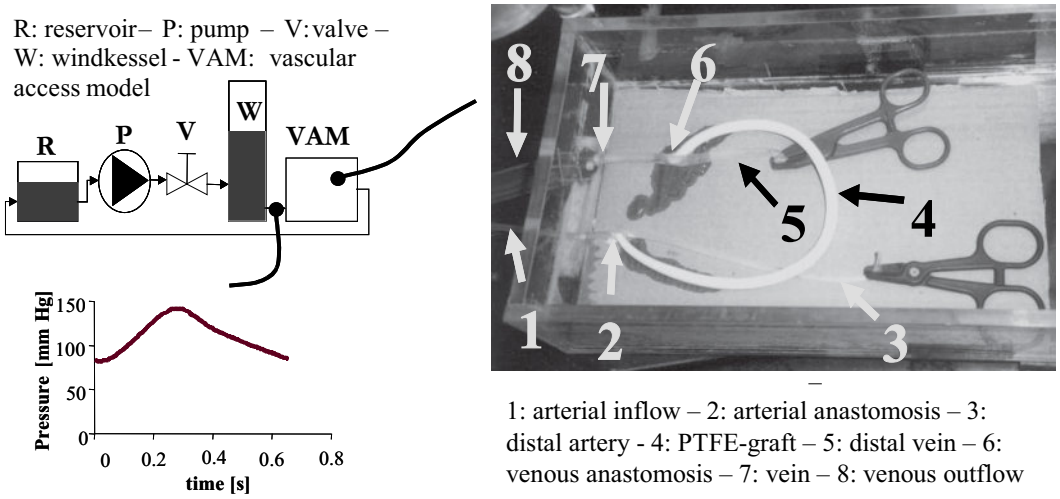

Figure 4.1: scheme of the hydraulic setup (left top panel), detail of the vascular access model (right panel) and the generated pressure wave at the arterial inlet of the vascular access model under the normal pressure conditions (left bottom panel)

4.2.2 Measurement Protocol

The hemodynamics of both graft types are investigated in the vascular access model. A mixture of 40% glycerin and 60% water circulates in the system as a Newtonian blood analogon [63] [64]. Density (ρ) of the fluid is 1103 kg/m^3 and dynamic viscosity (μ) is 3.75 mPa.s at 25°C. A cardiac simulator (Harvard apparatus, pulsatile pump 1421, Model 55-3339) pumps the fluid from a reservoir (R) through a valve (V) into the windkessel (W, figure 4.1 - left top panel), simulating resistance and compliance respectively. The fluid flows from the windkessel into the arterial inflow of the vascular access model (VAM), next through the artery, the arterial anastomosis, the PTFE-graft, the venous anastomosis, the vein and via the venous outflow back in the reservoir (figure 4.1 - right panel). The distal artery and vein are clamped off in the setup. Flow rate is varied between 500 and 1500 ml/min. Two conditions are considered in the experiments. (i) Control condition: mean pressure at the arterial inlet is held constant at 100 mm Hg and pulse pressure (the difference between maximum and minimum pressure) is 60 mm Hg. (ii) Low resistance condition: mean pressure at the venous outlet is held constant at 20 mm Hg and pulse pressure is held constant 60 mm Hg at the arterial inlet. The latter condition simulates the situation of an arterial stenosis, in the proximal artery brachialis or axilaris, before the vascular access. This is at the extremity of our model. An example of the generated cardiac cycle at the arterial inlet in the control condition can be seen in figure 4.1. Heart rate is 90 beats per minute (BPM). Considering all these parameters the highest Reynolds number (Re) is 2800 in the artery at a flow rate of 1500 ml/min. The Womersley (α) number varies between 6.25 (at 500 ml/min) and 9.40 (at 1500 ml/min) (see appendix). They indicate that the flow is transient between laminar and turbulent flow. These relatively high Reynolds and Womersley numbers express that the inertial forces dominate over the viscous forces and that viscous flow in an arteriovenous loop graft strongly differs from Poiseuille flow conditions. Measurements have been performed in twice independently.

Mean flow is measured volumetrically at the outlet of the VAM. Pressure along the experimental vascular graft is measured using a fluid filled catheter connected to a piezo electric pressure transducer (Datex-Ohmeda, Gent, Belgium). Pressure signals are amplified and sampled with a data-acquisition PC-card (NI, Texas, USA) Flow velocity (v) is measured with Doppler ultrasound (Vingmed CFM800, Horten, Norway).

4.3 Results

4.3.1 Pressure data

Tapered versus straight graft

Mean and pulse pressure measured at a flow rate of 1000 ml/min under the control conditions, for straight and tapered graft are shown in figure 4.2. A high mean pressure drop of 28.7 mm Hg is present at the arterial anastomosis of the tapered graft comparing to only 10 mm Hg pressure drop in the straight graft. Mean pressure loss along the graft is similar for both geometries: 31.4 mm Hg for the tapered graft and 27.2 mm Hg for the straight graft. Because of the differences in pressure drop at the arterial anastomoses, a difference in pressure level exists between the two graft types: mean pressure in the arterial anastomosis of the tapered graft is 91 mm Hg while it is 79 mm Hg in the straight graft. Pulse pressure is high ($\pm$ 60 mm Hg) in the artery and drops to $\pm$ 30 mm Hg in the graft. This level is maintained in the vein of the tapered graft model, where pulse pressure gradually decreases to less than 20 mm Hg in the straight graft model.

Control versus low resistance conditions

The differences between the control and the low resistance condition mainly appear in the vein and graft near the venous anastomosis. The same effects appear in both models at different flow rates. Mean pressure and pulse pressure along the graft model are shown in figure 4.3 for the straight graft at a flow rate of 1000 ml/min. The artery and the graft behave similar under both conditions. Mean pressure is 61% and pulse pressure is 19% lower at the venous outlet in the low resistance condition compared to the control condition. Quasi steady flow is obtained in the vein under low resistance condition.

4.3.2 Velocity data

Doppler ultrasound measured velocity images in the straight graft at different flow rates and in both conditions, are shown in figure 4.4. Velocity values are summarised in table 4.1. Δv is the difference between maximum and minimum velocity, v_{mean} is the mean velocity.

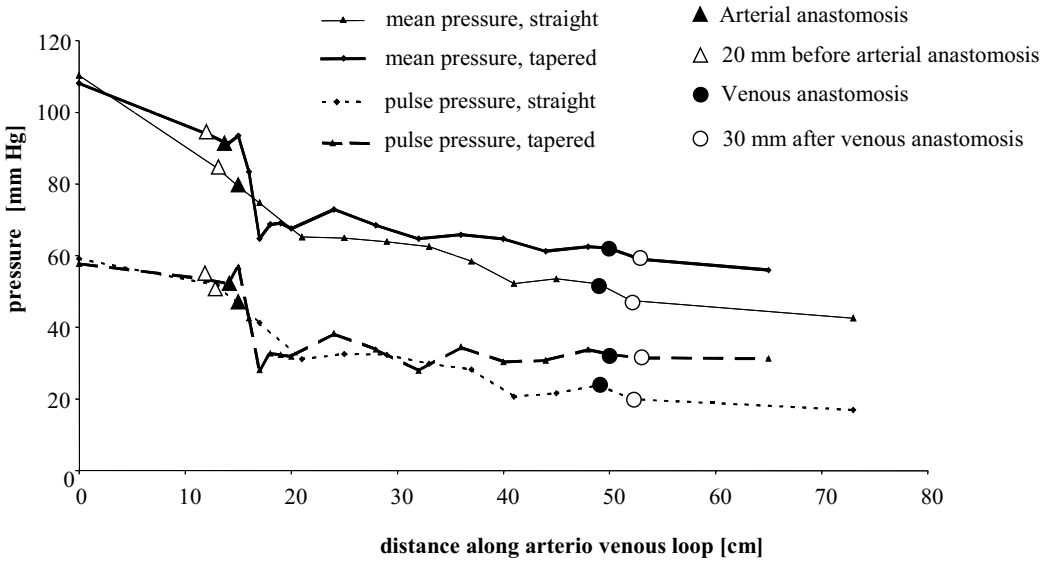

Figure 4.2: Comparing pressure distribution (mean and pulse pressure) over two graft geometries in the control condition, straight and tapered graft at a flow rate of 1000 ml/min.

Summary of the Velocity Data

	1500 mL/min				1000 mL/min				500 mL/min			
	Control		Low Resistance		Control		Low Resistance		Control		Low Resistance	
	V_{mean}	ΔV	V_{mean}	ΔV	V_{mean}	ΔV	V_{mean}	ΔV	V_{mean}	ΔV	V_{mean}	ΔV
Artery	1.7	0.7	1.65	0.7	1.3	1.25	1.3	1.2	0.7	1.5	0.7	1.5
Vein	0.85	0.4	0.8	0.4	0.55	0.4	0.5	0.35	0.3	0.65	0.3	0.4

Table 4.1: Summary of the velocity data. All velocities are presented in m/s.

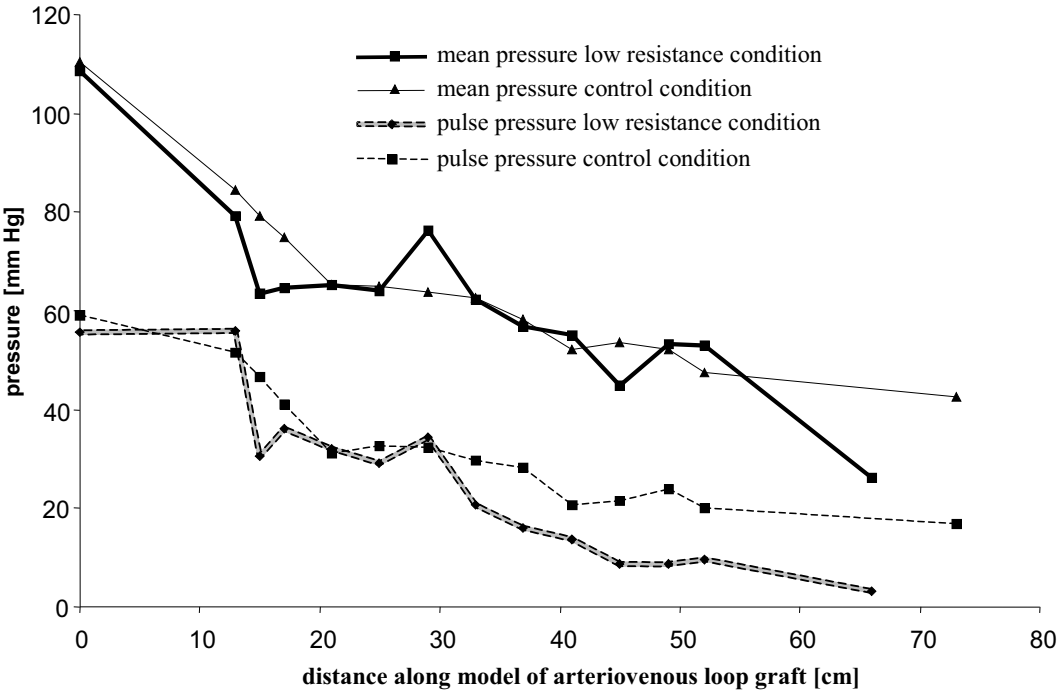

Figure 4.3: Comparing pressure distribution (mean and pulse) in the straight graft at a flow rate of 1000 ml/min for two different conditions: control and low resistance.

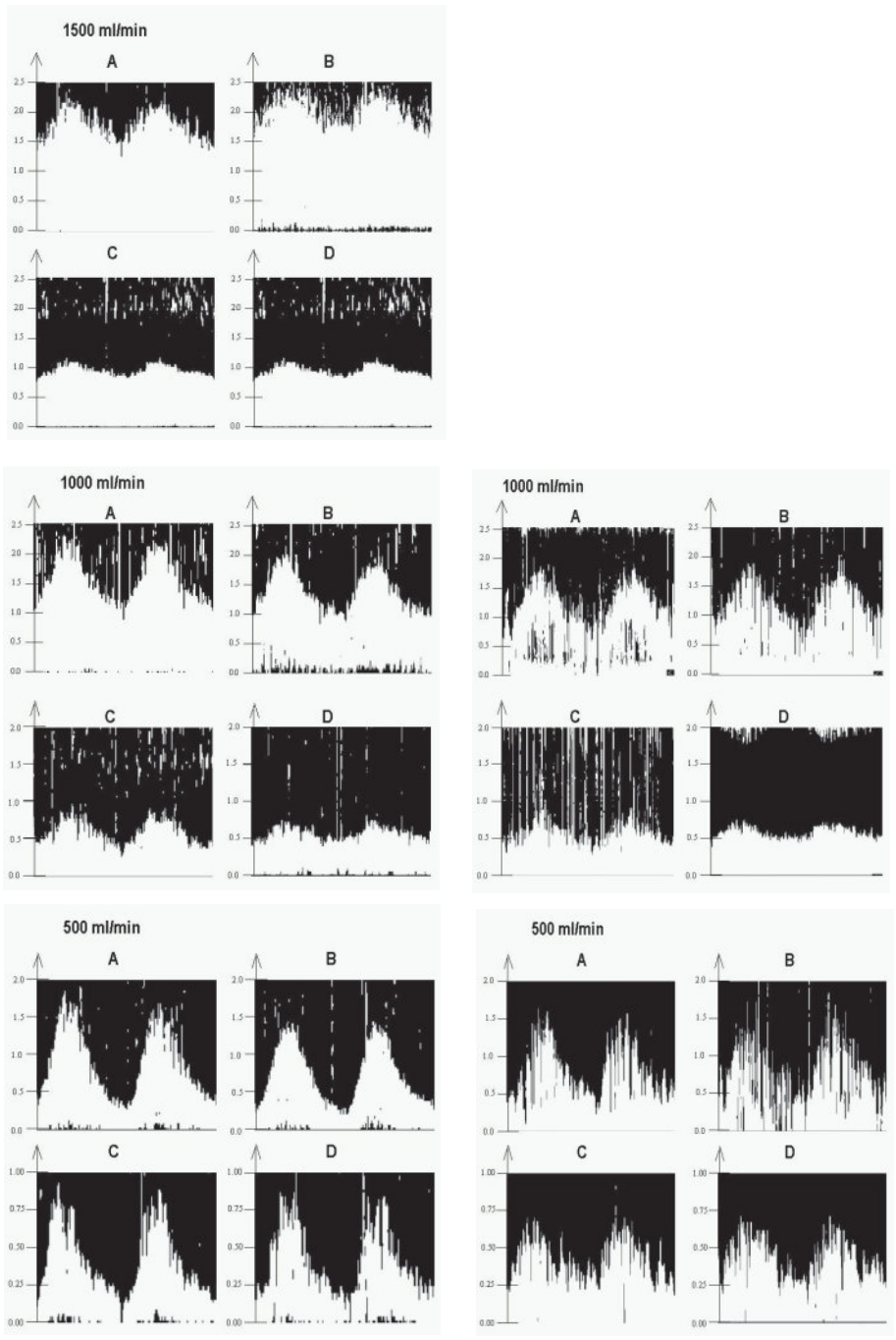

Figure 4.4: Ultrasound images for the straight graft, images of the control condition in the left column, of the low resistance condition in the right column. (A: at the arterial inlet; B: 2 cm before the arterial anastomosis; C: 3 cm after the venous anastomosis; D: at the venous outlet for different flow rates: range 500 - 1500 ml/min.

4.4 Discussion

The major finding in our study is that the main difference in the hemodynamics of both graft types is the high pressure drop at the arterial anastomosis of the tapered graft, while mean pressure drop over the grafts is almost identical. Comparing the normal and low resistance condition learns that mean and pulse pressure and flow velocity approach the normal venous conditions 15 cm distal to the venous anastomosis in the low resistance condition. In contrast, in the control condition, mean and pulse pressure remain higher and flow is still pulsatile at the venous outflow.

The blood vessels in our model are a relevant approximation of reality. The properties are based on the findings of Hofstra et al. and Kosch et al. In humans with PTFE-graft vascular accesses, Hofstra et al. [67] measured a brachial artery diameter between 4.1 and 6.7 mm with relative distensibility (RD) between 1.8 and 6.0 % and a venous diameter between 2.7 and 8 mm with a RD between 0.9 and 9.5 %. Kosch et al. [62] measured similar brachial artery diameters: 4.5 ± 0.4 mm and found RD of 5.1 ± 0.9 %. Both our straight 6 mm and tapered 4-7 mm models are a realistic approximation of in vivo wall mechanics as they have similar diameters and relative distensibilities. Also the setup parameters are chosen to be consistent with in vivo studies. Kosch et al. [62] included arterial (brachial) pressure and heart rate measurements in their study; systolic blood pressure: 127- 142 mm Hg, diastolic blood pressure: 70-75 mm Hg and heart rate varied between 80 and 98 beats per minute (BPM). In order to achieve adequate blood flow rate for hemodialysis, flow rate in the graft access should be between 500-800 ml/min although flow rates exceeding 1000 ml/min are often measured [15]. In our hydraulic model, pressure under the control condition is adjusted such that mean pressure is 100 mm Hg at the arterial inlet and with a pulse pressure of 60 mm Hg. Heart rate is 90 BPM and flow is varied between 500 and 1500 ml/min, consistent with Koch's hemodynamic observations.

An important innovation in our model is the use of compliant, silicone rubber models for the artery and vein. Doing so, our model vessels are able to buffer fluid during systole and release it during diastole (the so called windkessel concept [125]). Another consequence is that their diameter increases at increased pressure. A higher diameter for a given flow rate involves a lower mean pressure

drop as pressure drop is proportional to the inverse of the fourth power of the diameter. A drawback of our model is that our silicon blood vessels become weaker at elevated pressures where it is the opposite in vivo. In the pressure range applied in the experiments, however, this effect is negligible. Another drawback is that vasoconstriction of blood vessels is possible in vivo. This is of course not the case in our experimental setup.

Mean pressure drop over the two different grafts in the same conditions and at comparable flow rates are almost equal, but pressure drop distribution over the graft is different for the two geometries. Pressure loss over the arterial anastomosis of the straight graft is 37% of the total pressure loss over the straight graft, where it is 90% for the tapered graft. Such a high pressure loss in the latter case is caused by a sudden variation in flow direction and complex geometry. We suppose that vortices also play an important role in flow deviation at the anastomosis as previously mentioned in literature [101] [100]. Mean pressure level in the graft and vein differs in both graft types for the same conditions and flow rates because of different pressure drops in the artery (tapered: 15 mm Hg; straight: 27 mm Hg). The silicon arteries in the different models have identical material and geometrical properties though. If the arteries were identical stiff tubes, pressure drop over the artery would have been identical for a given flow rate because pressure loss in a straight tube depends purely on wall friction. In our model, pressure loss is not only determined by friction, but also by deformation of the vessel. We observed that deformation of the artery nearby the arterial anastomosis is greater in the tapered than in the straight graft. Resistance at the arterial anastomosis is highest in the tapered graft. The artery buffers temporary more fluid leading to a lower mean pressure level in the tapered graft.

As mentioned before, we considered two different conditions in our experiments: : (i) the control condition and (ii) the low resistance condition. Differences between hemodynamic conditions show up at lower flow rates in the velocity patterns. Δv increases at lower flow rates in the control condition. Comparing velocity profiles of the different grafts and of the different measurement series do not show significant differences. Mean pressure drop over the graft is almost equal in both grafts but mean pressure level differs according to conditions applied. Resistance in the control condition is high at the venous outlet resulting in an increase in diameter of the vein. This results in a smaller pressure drop in the normal compared

to the low resistance condition. Flow in the low resistance condition simulates the situation of an arterial stenosis proximal to the vascular access. In this condition, flow in the vein becomes less pulsatile in that case, resulting in less cyclic vessel venous wall stretching with possibly subsequently less chronic vessel wall injury. This, however, requires further detailed study and analysis, both in vitro and in vivo.

The hemodynamics depend on both the graft characteristics and the compliance of the blood vessels. Stiff arteries probably would have shown almost equal pressure drops. Although we were not able to measure the velocity profile through a cross section of a blood vessel, our experiments clearly show that flow in a loop graft vascular access is completely different from Poiseuille flow. Flow in the vein of a healthy person is constant in contrast with the pulsatile flow in our measurements. Mean pressure level and pulse pressure level are higher than expected. Δv in the vein differs from zero, which means that the possibly damaged vessel wall is subjected to flow disturbances, oscillating wall shear stresses, and cyclic stretching. This last item is also suspected to introduce intimal thickening in the near environment of the venous anastomosis [126].

Fillinger et al. [86] reported a strong relationship between the Reynolds number (flow disturbances) and intimal medial thickening for in vivo canine arteriovenous loop grafts (femoral artery-femoral vein). Another result of their study was that the flow disturbances cause high frequency thrill and energy transfer through the vessel wall causing perivascular tissue vibration, which can introduce chronic vessel wall injury. Fillinger et al. also included mean pressure measurements in their study. They found little difference in pressure drop over the graft (tapered: 60 mm Hg; straight 48 mm Hg), but they found a similar distribution of the pressure drop (77 % at the arterial anastomosis of the tapered graft and 54 % for the straight). Pressure drop over the canine artery is greater in the taperd graft (17 mm Hg) than in the straight (9 mm Hg). This differs from our results. Blood vessels in vivo are embedded in tissue and are not allowed to expand free. Moreover, our blood vessels become weaker under elevated pressures where it is the opposite in vivo. This means that the diameter of the artery is more constant in vivo, because of the vasoconstriction, where diameter easily increases in vitro.

The site where progressive stenosis leading to thrombosis tends to develop is

at the venous anastomosis [67] [35] [127] [66]. Our measurements on a compliant wall model indicate flow disturbance at the venous anastomosis which is in accordance with literature [101] [106] [109] [100] [131]. Further detailed analysis of the flow field, using numerical simulation techniques, are the subject of future research.

As all phenomena (disturbed flow at the anastomoses and pulsatile flow in the vein) appear in both graft geometries, one should conclude that hemodynamics-related intimal hyperplasia appears in both geometries which is also noted by Dammers et al. [128] Significantly different hemodynamics only result from different operating conditions, as e.g. the control and low resistance conditions in our experiments.

4.5 Appendix

The Reynolds number is defined as

$$Re = \frac{\rho v d}{\mu} \tag{4.2}$$

where ρ [kg/m^3] is the fluid density, v [m/s] is the mean velocity of the fluid, d [m] is the internal diameter of the tube and μ [Pa.s] is the dynamic viscosity of the fluid. The Reynolds number expresses the ratio between inertial and viscous forces in the fluid. The higher Re is, the more ascendancy inertia forces have. If Re is smaller than 2300 in a stiff tube with steady flow, viscous forces are dominant and flow is laminar. The highest Reynolds number in our experiments is 2800, which means that in that case there is transition to turbulent flow. The Womersley number (α)

$$\alpha = \frac{d}{2}\sqrt{\frac{\omega\rho}{\mu}} \tag{4.3}$$

characterises pulsatile flow. ω[rad/s] is the pulsation. α expresses the proportion of inertia forces to viscous forces in pulsating flow. The higher α, the more flow conditions differ from Poiseuille flow. α equal 1 means that flow is still unsteady, but the velocity profile looks like that of Poiseuille flow. A laminar boundary layer is always present near the wall but the velocity profile is rather flattened in the middle of the blood vessel. α varies between 6,25 and 9,40 in our study. α is 4.0 in the brachial artery of a healthy human and 22.2 in the proximal aorta.

Chapter 5

Comparison of the hemodynamics in 6 mm and 4-7 mm hemodialysis grafts by means of CFD

5.1 Introduction

Patients with insufficient kidney function need a renal replacement therapy such as hemodialysis. Waste products are purified from blood in an extracorporeal artificial kidney. Blood flow through the artificial kidney is about 350 ml/min to obtain efficient hemodialysis. As blood flow in blood vessels in the limbs doesn't reach 350 ml/min, the construction of a vascular access is necessary. In patients with poor blood vessels such as diabetics and elderly, a polytetrafluorethylene (PTFE) graft is often the access of choice because the blood vessels of these patients don't allow to create a native arteriovenous fistula [15] [16] [31].

The major complications appearing with grafts is the development of intimal hyperplasia (IH) near the anastomoses. IH leads to stenosis and finally results in a

The content of this chapter is adapted from: Van Tricht I., De Wachter D., Tordoir J., Verdonck P., Comparison of the hemodynamics in straight and tapered hemodialysis grafts by means of CFD , J. Biomech., In press.

thrombosis [32]. Only 22% of the PTFE-grafts remain patent without complications 3 years after placement [15] [31]. This indicates that graft upkeep imposes an important cost on health care. Several investigators suspect that these complications originate from disturbed hemodynamics which is definitely the case at the anastomoses. The anastomotic geometry influences the hemodynamics. The more the angle between the blood vessel and the graft approaches 90° the higher the local wall shear stress and the larger the vortices in the anastomotic region. Wall shear stress (WSS) has been found to lie within the pathologic range in both anastomotic regions. Therefore the cuff technique was introduced to reduce these anastomotic complications. Contradictory results are found [67] [135] [132] [86] [134]. Regions of extreme high and low WSS and high particle residence time, seem to show good correlation with IH development. Also compliance mismatch [62] [93] [69] [67] and vessel wall thrill [133] are possibly responsible for IH formation.

As the anastomosis geometry influences the hemodynamics directly, WSS and other derived hemodynamic parameters vary with different anastomotic geometries [131], we have compared the hemodynamics in two commercially available PTFE-grafts: a 4 to 7 mm and a 6 mm graft (GORE-TEX® Stretch Vascular Graft, Arizona, USA). Clinical results did not show better outcome for the 4-7 mm graft [128] [46] [45]. A validated three dimensional numerical model of a looped PTFE-graft between brachial artery and a suitable vein in the elbow region is considered in our study. The hypothesis tested is: "Does the use of the 4-7 mm graft have an advantage like beneficial WSS values and derived hemodynamic parameters compared to the 6 mm graft?"

5.2 Methods

The three dimensional geometry of a loop graft vascular access in the forearm is drawn in Solid Works (SolidWorks Benelux, Alkmaar, The Netherlands) where it is exported as a parasolid file to import it in Gambit 2.0.4 (Fluent, Sheffield, UK), the mesh generation software. A mesh is generated and boundary and continuum types are written to a Fluent mesh file. The Navier-Stokes equations are solved for an isothermal case and an incompressible fluid in Fluent 6.1.18 (Fluent, Sheffield, UK). The postprocessing of the results is executed using the postprocessor of Fluent

and in house developed Matlab (The Mathworks inc., Gouda, The Netherlands) utilities.

5.2.1 Geometry, governing equations and hemodynamic parameters

Two different graft geometries are studied: a straight, 6 mm, graft (internal diameter 5 mm) and a tapered, 4 to 7 mm, graft (internal 3 mm diameter at the arterial anastomosis increasing to 5.5 mm 50 mm distal from the anastomosis and from this point on, the diameter remains constant). The artery diameter is 4.25 mm and the vein diameter is 6.3 mm. Both simulated grafts have a length of 340 mm. Figure 5.1 shows the complete geometry and the two different arterial anastomotic geometries in detail. The angle between the blood vessel and the graft at the anastomosis is 45° at both anastomoses. Figure 5.2 shows the anastomosis nomenclature. The full line arrows on that figure indicate the flow direction at the venous anastomosis, the dotted line arrows at the arterial anastomosis. When venous anastomosis flow is supposed, the hood region is the area where the fluid coming from the graft bumps into the graft; the floor region is where the fluid that just left the graft bumps into the vein wall. The toe region is the part around the proximal half of the suture ring; the heel region is the area around the distal half of the suture ring. The distal vessel is closed and the proximal vessel allows drainage.

The inlet and outlet boundary conditions are shown in figure 5.1 in the right top and bottom panel, respectively. The inlet boundary condition is a time-dependent velocity waveform which is reconstructed with the fast fourier transform (FFT) of a velocity waveform obtained from in vitro measurements [96]. The outlet boundary condition is a time-dependent pressure waveform also obtained using the fast fourier transform of a measured pressure waveform. The period of one cycle is 0.63s (heart rate is 95 beats per minute). The mean flow rate considered is 1000 ml/min. The highest Reynolds number that appears is 1593. This occurs in the artery. As the unsteady character of the flow stabilises flow, we accept laminar flow in the computational model.

Fluid flows from the arterial inlet (Figure 5.1 (1)) through the arterial anastomosis (2), through the graft (4), the venous anastomosis (6) into the venous outlet (7). Flow towards the hand via the distal artery (3) and from the hand via the

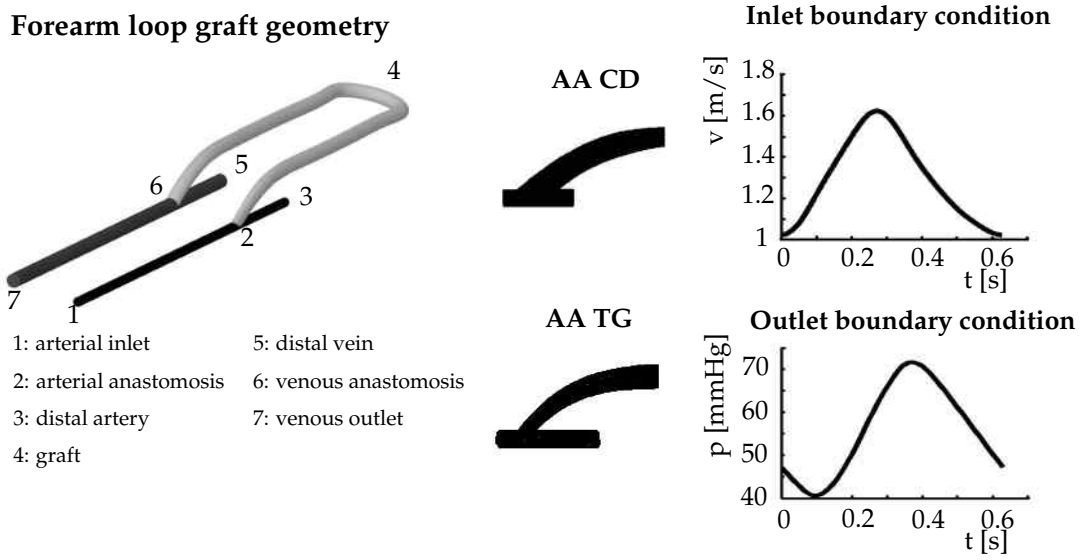

Figure 5.1: Geometry and boundary conditions. Left panel: geometry and nomenclature. Middle panel: detail of the arterial anastomosis (AA) of the 6 mm (CD) and 4-7 mm graft (TG). Right panel: in and outlet boundary condition (p = pressure; v = velocity; t = time)

distal vein (5) is impeded. At the arterial, venous and graft wall a no-slip boundary condition is set.

The dynamic viscosity and the density, the continuum conditions, are set to 3.75 mPa.s and 1090 kg/m^3, respectively. These values correspond to the properties of the glycerine-water mixture used in the experiments [96].

The governing equations for the isothermal incompressible unsteady flow are

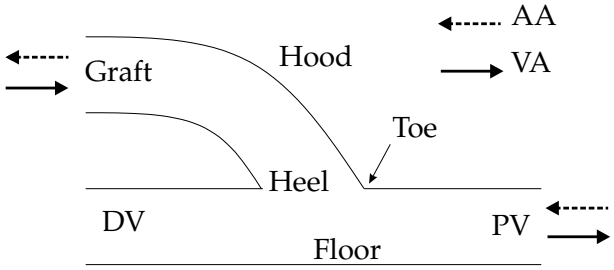

Figure 5.2: The nomenclature used for specific regions at the anastomosis. PV is the proximal vessel segment and DV is the distal vessel segment

the mass (9.1) and momentum (9.2) conservation equations.

$$\nabla \cdot \ \overrightarrow{v} = 0 \tag{5.1}$$

$$\frac{\delta \overrightarrow{v}}{\delta t} + (v \cdot \nabla)\overrightarrow{v} = \frac{1}{\rho}(-\nabla p + \nabla \cdot \overline{\overline{\tau}}) \tag{5.2}$$

$\overrightarrow{v}$ is the velocity vector, p is the pressure, ρ is the density and $\overline{\overline{\tau}}$ is the stress tensor. Velocity and pressure are known after solving the Navier-Stokes equations and derived hemodynamic parameters can be computed using the solution of the fluid field. Kleinstreuer et al. [129] summarised the relationship between disturbed flow interacting with the vessel wall and wall shear stress (WSS), wall shear stress gradient (WSSG) and pressure gradient (PG).
For incompressible fluids, the shear stress tensor is proportional to the rate-of-deformation tensor ($\overline{\overline{D}}$):

$$\overline{\overline{\tau}} = \mu \overline{\overline{D}} \tag{5.3}$$

The shear stress value that can be calculated from the shear stress tensor is:

$$SS = \mu \sqrt{\frac{1}{2} \overline{\overline{D}} : \overline{\overline{D}}} \tag{5.4}$$

μ is the dynamic viscosity of the fluid. The wall shear stress value (WSS) is the shear stress value in the fluidum that is in contact with the vessel wall.
Extreme high ($>$ 3 Pa) and low ($<$ 0.5 Pa) WSS values have been correlated to intimal hyperplasia development leading to stenosis [137] [103] [93].
The shear stress gradient (SSG) expresses the spatial variation of the shear stress. The definition of the instantaneous SSG (5.6) on the vessel wall is:

$$SSG = \nabla SS \tag{5.5}$$

The wall shear stress gradient (WSSG) expresses the spatial variation of the wall shear stress:

$$WSSG = \nabla WSS \tag{5.6}$$

To take the WSSG over the complete period into account and to be able to compare WSSG in different geometries, the time averaged and normalised WSSG ($\overline{WSSG}_{ND}$) (5.7)is defined as:

$$\overline{WSSG}_{ND} = \frac{d}{\tau_p T} \int_0^T WSSG \ dt \tag{5.7}$$

d is the vessel diameter and τ_p is the mean poiseuille wall shear stress at the inlet artery. T is the duration of one cycle.
A high $\overline{PG}$ value indicates flow towards the wall and not well aligned with the vessel axis. Equation (5.8) defines the time averaged $\overline{PG}$.

$$\overline{PG} = \frac{1}{T}\int_0^T \frac{p(i) - p(0)}{\Delta r}\ dt \tag{5.8}$$

A high $\overline{PG}$ corresponds with a high local load of the vessel wall.

5.2.2 Numerical method and model validation

The grid used in the simulations is generated with Gambit 2.0 (Sheffield, UK). The flow field is calculated using the finite volume package Fluent 6.1 (Sheffield, UK).
The mesh applied in the graft and the proximal artery and vein is a cooper mesh. The source face has a triangular mesh, size 1, and the spacing is set to 1mm. The anastomoses are meshed with the tet/hybrid scheme. This means that the mesh is composed primarily of tetrahedral elements but may include hexahedral, pyramidal, and wedge elements where appropriate. The initial mesh size is set to 0.75. A first steady simulation is executed with this rather coarse mesh. When the solution had converged, the gradient adaption tool was used to look up the nodes with high gradients of strain rate. Nodes with high strain rate gradients were detected and marked. The grid was refined in this region. This procedure was repeated until the strain rate solution became mesh independent.
Once the solution was grid independent, the solver was switched to unsteady time formulation. Compiled user defined functions were written in C to apply the velocity and pressure waveforms at the inlet and outlet boundary, respectively.
The solver used is a segregated solver with implicit formulation which was second order accurate time stepping. The pressure and momentum discretization schemes are also second order accurate. The time step size is set to 1% of the period of one cycle and a total of 300 time steps are executed. Three heart cycles are simulated this way. The convergence criterion for the residuals of the continuity and momentum equation are set to 10^{-6}. The number of iterations per time step are set sufficiently high that the residuals convergence criterion is the condition to continue to the next time step.

5.3 Results

5.3.1 Flow pattern

Velocity distribution, in the acceleration phase of the period, in the arterial anastomosis of the grafts is shown in figure 5.3. Figure 5.3.A shows a velocity magnitude contour plot of a longitudinal cut on the centerline of the 6 mm graft arterial anastomosis. Flow comes from the proximal artery (pa) and flows into the graft, no flow is possible through the distal artery (da). Flow is aligned with the vessel in the proximal artery and the flow profile is parabolic. Flow direction suddenly changes in the anastomosis and the development of a vortex is observed in the distal artery. Flow bumps into the graft wall at the heel and forms a recirculation zone at the hood. Flow becomes more aligned with the graft further. Figure 5.3.B shows four cross-sections in the environment of the arterial anastomosis of the 6 mm graft . The vectors shown are the in plane velocity components. Flow in the positive z direction, downstream, is represented in the dark gray zones and in the opposite way in the light gray zones, upstream. The first cut is 10 mm before the arterial anastomosis (AA) and shows no in plane velocity. The second cut is in the AA where three dimensional vortices exist. The third cut, 5 mm downstream the AA, shows that the vortex still exists, but reversed flow in the z direction has disappeared. The last cut, 25 mm downstream the AA, shows flow which is better aligned with the graft, but vortices are still present.

Analogous flow visualisation is presented for the tapered graft, 5.3.C and 5.3.D. The longitudinal cut also shows flow which bumps into the graft wall at the anastomosis and a vortex that develops at the floor of the artery. Mainly similar results as for the 6 mm graft come out of the cross sections. Three dimensional vortices appear at the floor of the anastomosis while flow is not vortical at the hood of the anastomosis.

Figure 5.4 shows velocity distribution at different points of time: acceleration (t=0.16s), deceleration (t=0.32) and minimum inlet velocity (t=0.63s). It is clear that the floor vortex changes in time. The floor recirculation zone enlarges at minimum inlet velocity and a second vortex appears at the graft hood.

The bend in the loop graft also introduces vortices in the flow. The flow pattern

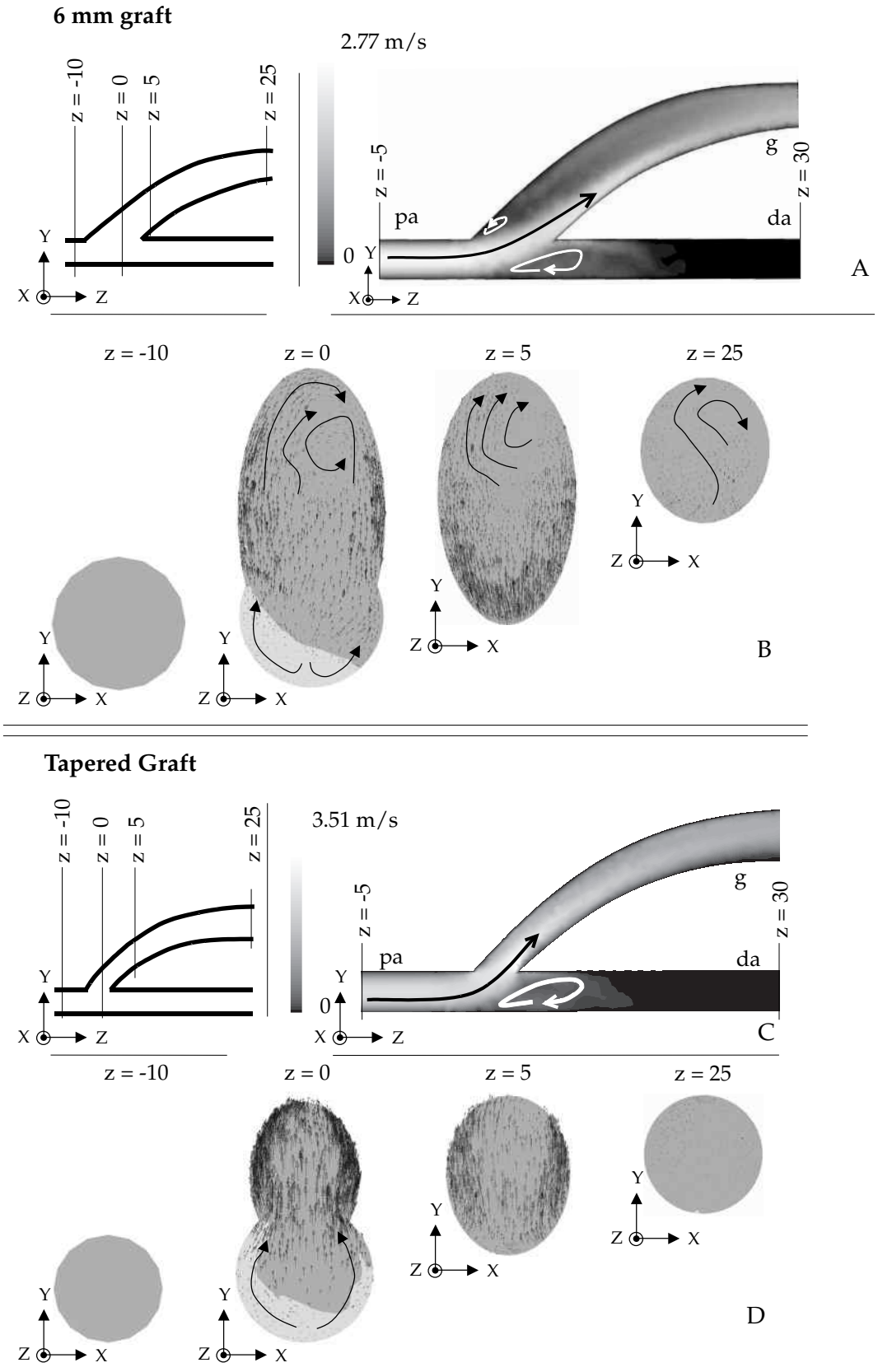

Figure 5.3: Velocity distribution at arterial anastomosis A: Longitudinal cut, 6 mm graft ; B: Cross sections, 6 mm graft ; C: Longitudinal cut, 4-7 mm graft ; D: Cross sections, 4-7 mm graft

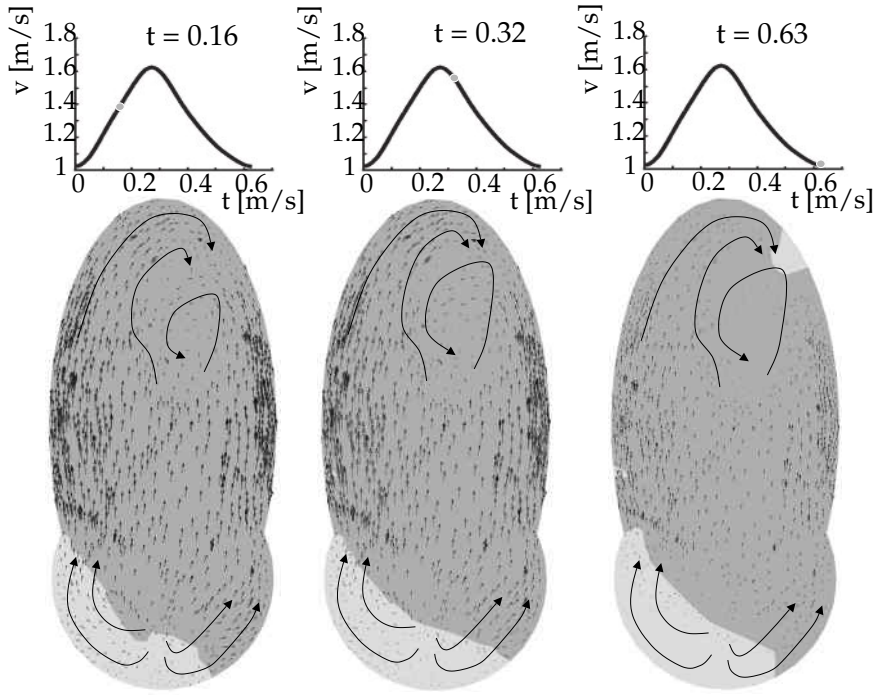

Figure 5.4: Vortex development at different points in time in the arterial anastomosis of the 6 mm graft

is shown in figure 5.5. The maximum in plane velocity components are listed in table 5.1. The highest values appear in the middle of the bend, values are halved at the end of the bend and 60 mm further in plane values are only 13.8% (CD) and 11.8% (TG) of the maximum in plane velocity in the middle of the bend.

Flow pattern at the venous anastomosis of both grafts is represented in figure 5.6. In the longitudinal cuts (5.6A and B) it can be observed that flow collides first with the graft wall at the hood and secondly with the vein floor at the venous

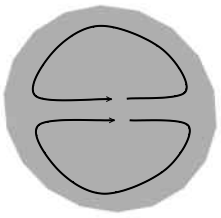

Figure 5.5: In plane velocity components in the graft bend

	Straight	**Tapered**
Middle of bend	0.252	0.221
End of bend	0.132	0.136
60 mm after bend	0.035	0.026

Table 5.1: maximum in plane velocity [m/s] values in the bend of the graft

anastomosis. A first vortex develops in the distal vein and a second in the proximal vein in both grafts. Flow pattern is completely three dimensional as can be noticed in the four cross sections near the venous anastomoses, figure 5.6 C and D. Flow in the light gray zones is in the negative z direction (downstream) and in the opposite way in the dark gray zones (upstream). Flow in the negative z-direction corresponds with flow leaving the graft and going towards the venous outlet. Flow separation at the vein floor and near the toe can be noticed in the cross sections z = 0 and z = -5, respectively. Flow is still a little bit vortical 25 mm after the venous anastomosis, the maximum in plane velocity equals 0.1 m/s.

5.3.2 Derived hemodynamic parameters

As mentioned above, flow separation zones appear at the anastomoses, where the highest fluctuations of the hemodynamic parameters show up.
The hemodynamic parameters at the AA of the 6 mm graft are visualised in figure 5.7, left column. The maximal WSS values appear on the heel side of the suture ring and amount to 80 Pa. On the artery, at the toe, the WSS is in the range 39-55 Pa. The minimal WSS values, 0.006-0.5 Pa are observed on the graft at the toe and in the graft hood region. The $\overline{WSSG}_{ND}$ and $\overline{PG}$ distribution is analogous to the WSS distribution, the maxima are noticed on the heel side of the suture ring ($\overline{WSSG}_{ND}$ = 383, $\overline{PG}$ = 2000 kPa/m) and the zero values are remarked on the graft at the toe and in the graft hood region.
The right column in figure 5.7 visualises the hemodynamic parameters in the AA of the 4-7 mm graft. The maximum WSS of 164 Pa is observed on the complete suture ring. The values at the lateral sides of the graft are between 79 and 112 Pa. The minimum WSS (0 Pa) is found at the graft hood. The $\overline{WSSG}_{ND}$ and $\overline{PG}$ distribution is analogous to the WSS distribution, the maximum values are observed at the suture ring ($\overline{WSSG}_{ND}$ = 1150, $\overline{PG}$ = 5132 kPa/m) and the zero values at the graft hood.

The hemodynamic parameters at the VA are visualised in figure 5.8. The maximum WSS value appears on the graft at the toe side of the suture ring (TG: 45PA; CD: 56Pa). The wall shear stresses on the hood and floor are in the range 18 - 32Pa for the TG and in the range 29-40Pa in the CD. The minimum of 0Pa is present in the vein near the toe and in the graft near the hood. The $\overline{PG}$ and $\overline{WSSG}_{ND}$ distribution is similar to the distribution of the WSS: the maximum occurs in the graft near the toe (TG: $\overline{WSSG}_{ND}$ = 230, $\overline{PG}$ = 945 kPa/m; RG: $\overline{WSSG}_{ND}$ = 307,

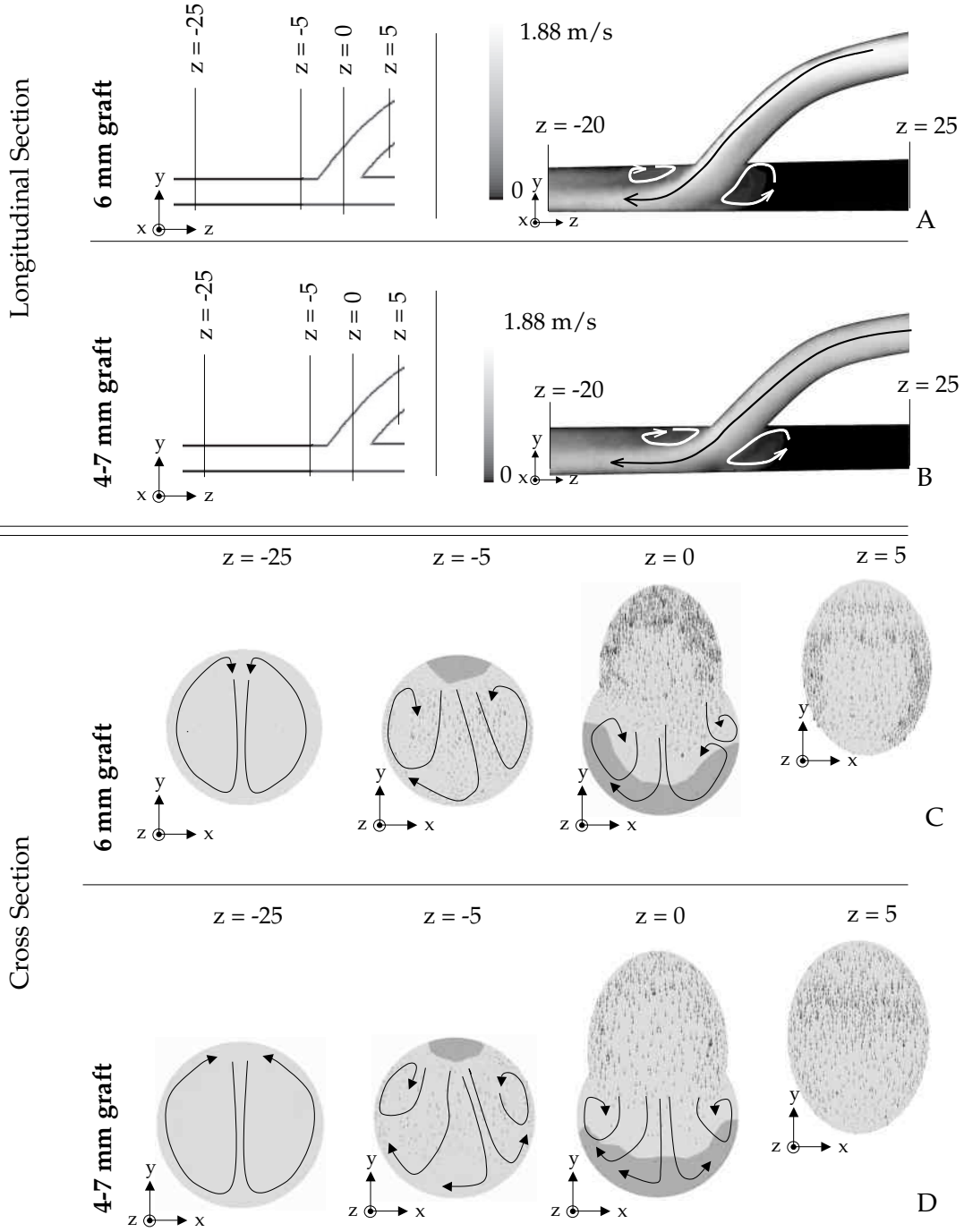

Figure 5.6: Velocity distribution at venous anastomosis
A: Longitudinal cut, 6 mm graft; B: Longitudinal cut, 4-7 mm graft; C: Cross sections, 6 mm graft; D: Cross sections, 4-7 mm graft

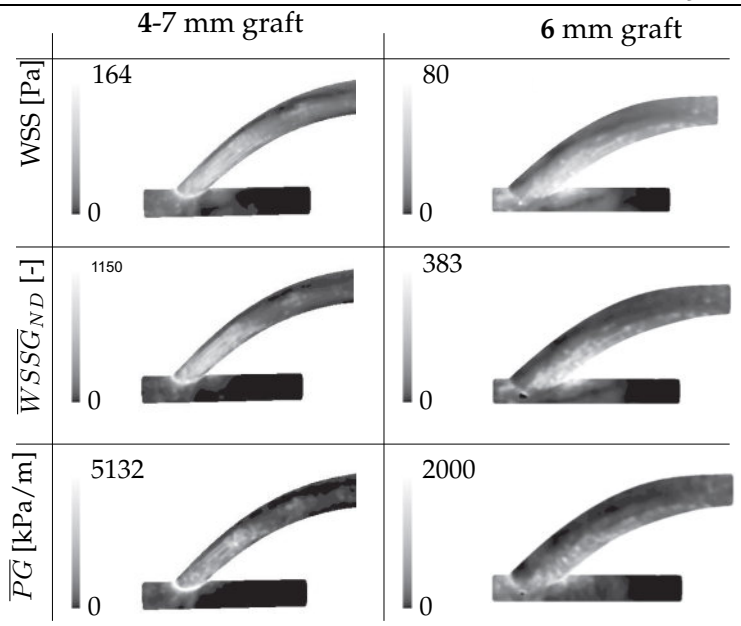

Figure 5.7: WSS, $\overline{WSSG}_{ND}$ and $\overline{PG}$ values at the arterial anastomosis of the 6 mm and 4-7 mm graft

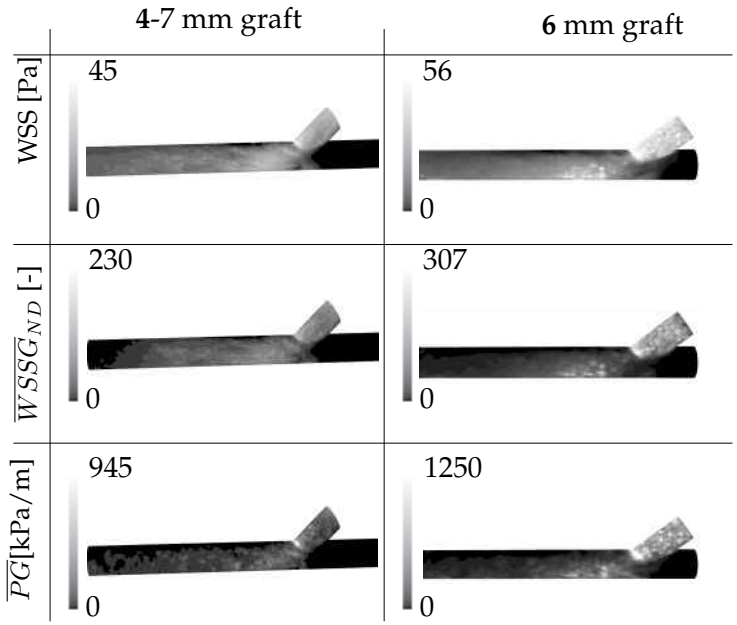

Figure 5.8: WSS, $\overline{WSSG}_{ND}$ and $\overline{PG}$ values at the venous anastomosis of the 6 mm and 4-7 mm graft

$\overline{PG}$ = 1250 kPa/m).The zero values occur at the toe side of the vein and at the graft near the heel.

5.3.3 Model validation

The computational model is validated with measurements on an in vitro model of a loop graft fore arm vascular access, figure 5.9 [96]. The figure shows mean pressure drop along the flow path of the access. The arterial inlet is situated at '0 cm', the arterial anastomosis at '15 cm', the venous anastomosis at '49 cm' and the venous outlet at '69 cm'. The figure shows some deviation between the in vitro and CFD results.

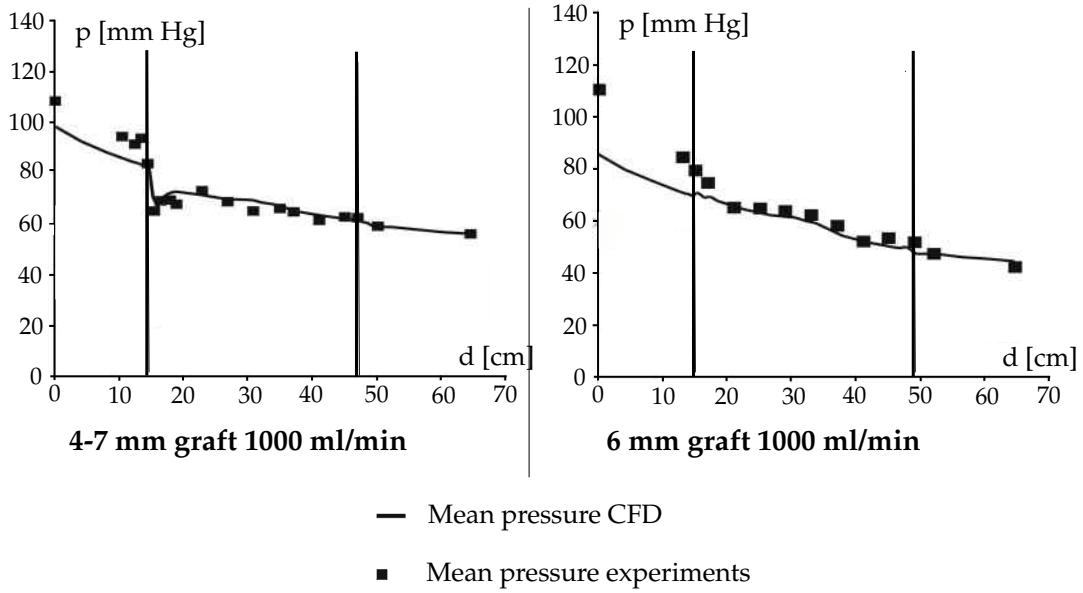

Figure 5.9: Mean pressure drop along the graft

5.4 Discussion

The aim of our study was to investigate whether there is any hemodynamic advantage like beneficial WSS values and derived parameters in using a 4-7 mm graft as hemodialysis vascular access. The 4-7 mm graft is designed to have a limited access flow rate compared to the 6mm graft. However, no statistically

significant decrease in graft flow rate was observed in vivo [128] [86]. This justifies our choice of the same mean graft flow rate of 1000 ml/min in both graft geometries. Other clinical follow-up studies do not show statistically difference in patency rate [128] [46]. Dammers et al. [128] even found similar outcome for thrombosis and stenosis development. Shaffer et al. [45] experienced an increased thrombosis risk in 4-7 mm grafts in diabetic patients. The major clinical benefit for 4-7 mm grafts reported is reduced ischemia by Sabanayagam et al. [46]
To compare the hemodynamics in a 4-7 mm graft to these in a 6 mm graft, we have implemented a three dimensional numerical model of a complete vascular access: artery, graft, and vein. Artery, graft, and vein diameters are chosen consistent with in vivo measurements [67] [62] [136]. The anastomosis angle is 45°, which is the measured angle on an in vivo model sutured by a vascular surgeon. The velocity and pressure waveforms at the boundaries are obtained by in vitro measurements [96]. Mean pressure results from the simulations and the experiments are compared to validate the numerical model. Figure 5.9 shows a good agreement between experiments and the computational results in the graft and vein. The computational results in the artery differ from the experimental results for 10 mmHg in the TG and for 20 mmHg in the 6 mm graft . This difference occurs because the pressure measurements in the experiments are performed with a fluid filled catheter that is placed inside the model. This causes an extra pressure loss compared to the CFD model. Also the special losses at the arterial anastomoses are underestimated in the CFD model compared to the in vitro model. The mean pressure level is consequently higher in the compliant wall model. The rigid wall is a good approximation for the graft because the commercial gore-tex grafts (GORE-TEX® Stretch Vascular Graft, Arizona, USA) used in the experiments has a limited compliance. Moreover, the difference between a compliant model and a rigid wall model is limited. Leuprecht et al. [130] found only 5% difference in the wall shear stress observed in a rigid wall model of an anastomosis compared to a compliant wall model (6% relative distensibility).

The advantage of computational fluid dynamics is that we can have a look in detail on the flow field at both anastomoses. Figure 5.3.A and 5.3.C shows a velocity contour plot of a longitudinal cut at the arterial anastomosis of the straight and 4-7 mm graft, respectively. Flow bumps into the heel and a vortex is formed on the distal arterial floor in both geometries. Maximum velocity in the arterial anastomosis of the 4-7 mm graft increases up to 3.51 m/s compared to 2.77 m/s

in the 6 mm graft. Another important difference is that only one vortex, at the distal artery floor, develops in the 4-7 mm graft whereas a second vortex appears at the graft hood near the toe of the 6 mm graft. The cross sections (figure 5.3.B and 5.3.D) show that flow entering the graft is more vortical in the 6 mm graft but the recirculation region is more enlarged in the artery of the tapered graft. The vortex geometry also depends on the moment that the cross section is considered. The vortex patterns enlarges during deceleration, even a second vortex can be noticed at the graft hood, figure 5.4. The vortices are not symmetrically distributed in the anastomosis while the AA geometry is symmetric. That is the reason why a completely three dimensional model is required.

When flow leaves the arterial anastomosis, it streams through the bend and the venous anastomosis (VA). Little vorticity is introduced in the bend. However, the in plane velocity is only 4% of the mean velocity 60 mm after the bend in both graft types. Flow pattern in both geometries is also identical, which means that the hemodynamics at this point are independent of the upstream arterial anastomotic geometry.

Flow in a longitudinal section of the venous anastomosis is shown in figure 5.6.A and 5.6.B. Flow bumps into the graft hood and vein floor in both geometries. A first longitudinal vortex develops in the distal vein and a second in the proximal vein near the toe. The cross sections show that flow is completely three dimensional and that assuming symmetry in the flow pattern because of geometrical symmetry [129] does not represent reality in detail. Flow splits asymmetrically in the middle of the VA (z=0) but the longitudinal vortex is asymmetric over there. Flow in the cross section is asymmetric 5 mm further, but the longitudinal vortex is symmetric there. This is plausible because a swirling flow develops in the closed distal vein.

The highest hemodynamic parameters at the AA are found in the direct environment of the suture line and at the graft inlet for the TG and at the heel side of the graft and in the artery near the heel for the 6 mm graft. The highest values at the venous anastomosis are found at the graft side of the toe and on the floor of the anastomosis. A comparison of the results for both grafts shows that the major difference between both graft types is located at the arterial anastomosis. The hemodynamic parameter values of the 4-7 mm graft are at least twice the

values of the 6 mm graft. The higher the values, the higher the predisposition for IH development [129] [105], initiating stenosis. The values in the CD are already far above the maximum values found in healthy people. Besides of IH development, grafts fail because of thrombosis formation, therefore it is worth to notice that leukocytes get activated at 7.5 Pa [75]. This value is exceeded at both anastomoses in both graft geometries (figures 5.7 and 5.8). Moreover, if the WSS value oversteps 10Pa, platelets get activated [77] [76]. This threshold is again surpassed at both anastomoses in both graft geometries. Out of this, we can conclude that leukocytes and platelets get activated at both anastomoses. What is more, there are vortexes present at both anastomoses. Activated leukocytes or platelets can easily be dragged into a vortex at the toe of the anastomosis, stay in it and possibly initiate thrombosis formation. Care should be taken to avoid clotting as it is the major cause of access failure [15] [16]. If the WSS value reaches 200 Pa, the hemolysis process may start [80] [79]. Our simulations show that the VA is completely free of hemolysis danger, just like the AA of the CD, but, the WSS on the suture ring of the AA of the TG reaches 164 Pa. Little flow increase or sharp edges because of the sutures can make the WSS increase up to 200 Pa and initiate hemolysis. This is a disadvantage of the 4-7 mm graft compared to the 6 mm graft. Considering the WSS, there is no benefit for the use of tapered grafts as vascular access.

Hemodynamic parameter values at the venous anastomosis are between 24 and 33.5 % higher in the VA of the CD than in the VA of the TG. The highest values appear at the toe and the floor of the anastomosis, sites where IH and stenosis development are expected [32] [69]. Fillinger et al. [86] subdivided the VA in 5 regions like shown in figure 5.10 and reported IH formation after three months in dogs in 4-7 mm and 6 mm grafts. In cross sections 4 and 5, he reported no or mild IH, sites where in our simulations no extreme parameters are observed. In the cross sections 2 and 3 he noticed mild IH in the 4-7 mm graft and moderate IH in the 6 mm graft. At site 1, no IH was observed in the TG and moderate IH in the 6 mm graft. When we compare this with our results, we remark maximum parameter values at the toe and moderate values on the lateral graft side and the floor. The parameter values are higher in the CD compared to the TG. The comparison with the animal study makes us assume that the parameter level is proportional to the severity of IH developed. Additional effect is the presence of very low, < 0.5 Pa, WSS values exist in the VA. Besides high WSS values, low WSS values are found to initiate IH [93] [92]. It is more than probable that extreme high and low WSS

values initiate IH development at the venous anastomosis of both grafts. Although the level of the parameter values in this CFD study can be correlated with the IH formation in dogs [86] under similar hemodynamic conditions the correlation between the hemodynamic parameters and IH formation in arteriovenous grafts in humans has to be investigated in further research.

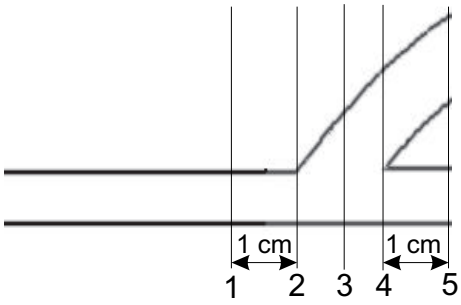

Figure 5.10: The subdivision of the venous anastomosis as presented by Fillinger et al. [86]

5.5 Conclusion

We have performed computational flow simulations in a three dimensional model of a looped hemodialysis vascular access in the elbow region by means of a PTFE graft. The aim was to compare the hemodynamics in a 4-7 mm (tapered) and a 6 mm (straight) graft. The parameters at the venous anastomosis of the 6 mm graft were 24 till 33.5% higher compared to the parameters at the venous anastomosis of the 4-7 mm graft. Unhealthy high and low hemodynamic parameters are established at the floor of the venous anastomosis of both geometries.
According to the wall shear stress levels reached in the arterial anastomosis of both geometries, leukocytes and platelets are activated at the arterial anastomosis. Extreme high hemodynamic parameter values appear in the 4-7 mm graft arterial anastomosis, exposing the blood nearly to hemolysis.
The tapered arterial anastomosis geometry only shows hemodynamic disadvantages compared to the straight arterial anastomosis. Our computational fluid dynamics study confirmes clinical data, which expresses no benefit in the use of 4-7 mm grafts compared to 6mm grafts.

Part III

Modelling of the hemodynamics in the vascular access with a venous outflow stenosis

Chapter 6

Assessment of stenosis in vascular access grafts

6.1 Introduction

Patients with insufficient kidney function need a renal replacement therapy such as hemodialysis. Waste products are purified from blood in an extracorporeal artificial kidney. Blood flow through the artificial kidney requires about 350 ml/min to obtain efficient hemodialysis. As blood flow through blood vessels in the limbs does not reach 350 ml/min, a vascular access is needed. In patients with stiff blood vessels such as diabetics and elderly, a polytetrafluorethylene (PTFE) graft is often the access of choice because the blood vessels of these patients do not allow to create a native arteriovenous fistula [15, 16, 31].
The major complication observed in grafts is the development of intimal hyperplasia (IH) near the anastomoses. IH leads to stenosis and finally results in a thrombosis [32]. Only 22% of the PTFE-grafts remain patent without complications 3 years after placement [15] [31]. Stenoses are frequently observed in the proximal and mid-graft, at the venous anastomosis and in the draining vein [138–140]. The kidney disease outcomes quality initiative (K/DOQI) guidelines define a significant stenosis at 50% diameter reduction (75% area reduction), this is often accompanied by elevated pressure at the venous line of the dialysis machine, decreased access

The content of this chapter is adapted from: I. Van Tricht, D. De Wachter, J. Tordoir, and P. Verdonck. Assessment of stenosis in vascular access grafts. International journal of artificial organs, 28(7):617-622, 2004.

flow and abnormal physical findings. Stenoses are suspected when the flow diminishes by 25% within one month [15]. Other authors detect stenoses by measuring systolic velocity along the access. For a systolic velocity above 4 m/s, stenosis is assumed [138]. Another opinion is that the ratio between pressure at the needle of the venous line of the dialysis machine and mean arterial pressure (MAP) may not exceed 0.5. If it is above 0.5, stenosis can be expected at the venous outflow [42].

In this experimental study, we have made a compliant in vitro model of a PTFE loop graft for hemodialysis, between the brachial artery and a suitable vein, with a venous outflow stenosis 1 cm downstream the venous anastomosis. In this hydraulic model, we respected the pressure, flow, relative distensibility (RD) ranges and geometry of in vivo measurements in hemodialysis patients [96].

The aim of this study is the evaluation of three parameters to detect stenosis: resistance index, the ratio between pressure at the venous line of the dialysis machine and mean arterial pressure and the newly introduced pressure ratio.

6.2 Methods

6.2.1 Parameter definitions

The measurements are performed on a realistic 1:1 scale model with a compliant silicone artery and vein. The relative distensibility (RD) in our model of artery and vein is about 4% in their operating pressure ranges.

$$RD = \frac{D_{sys} - D_{dia}}{D_{dia}} \times 100\% \tag{6.1}$$

D_{sys} is the diameter at systolic pressure and D_{dia} is the diameter at diastolic pressure. The diameter of the silicone artery at 100 mmHg is 4.25 mm and 6.3 mm at 40 mmHg for the vein [96]. The internal diameter of the PTFE-graft is 5 mm.
Flow generated in the system is pulsatile. The maxima of pressure and velocity waveform are called systolic pressure (p_{sys}) and systolic velocity (v_{sys}); the minima are denoted the diastolic pressure (p_{dia}) and velocity (v_{dia}) and the time averaged pressure and velocity values during one heart cycle are mean pressure (p_{mean}) and

velocity (v_{mean}). The difference between p_{sys} and p_{dia} is the pulse pressure (pp).
In this experimental study we investigate the hemodynamic behaviour in vascular access grafts with venous outflow stenosis. Stenosis percentage is defined as:

$$Stenosis\ percentage = \frac{A_{free} - A_{stenosis}}{A_{free}} \times 100\% \tag{6.2}$$

A_{free} is the free lumen area before the stenosis and $A_{stenosis}$ is the lumen area in the stenosis.
The resistance index (RI) is a tool to characterise the flow by means of the measured velocity waveform.

$$RI = \frac{v_{sys} - v_{dia}}{v_{sys}} \tag{6.3}$$

When v_{dia} becomes negative, in the case of a high resistance blood vessel, RI becomes larger than 1.
Kleinekofort et al. detects stenoses by calculating the ratio between pressure at the venous line of the dialysis machine and mean arterial blood pressure (MAP). When this ratio is larger than 0.5 a stenosis is present at the venous outflow [42].
We present a new index, the pressure ratio (PR), to detect a stenosis that needs intervention, i.e. 75% area stenosis according to the DOQI guidelines, as:

$$PR = \frac{p_{arterial\ line} - p_{venous\ line}}{p_{arterial\ line}} \times 100\% \tag{6.4}$$

When this ratio is below 8%, it indicates that easy outflow of the vascular access is impeded.

6.2.2 The setup with the compliant vascular access model

The hemodynamic measurements are performed on an in vitro model with a compliant silicon artery and vein (4% RD) and a 6 mm graft (GORE-TEX® Stretch Vascular Graft, Arizona, USA). The graft is sewn onto artery and vein with an end to side anastomosis (figure 6.1). Measurements are performed on a loop graft configuration. The newtonian blood analogue that circulates, is a glycerine-water mixture (40/60%) with density 1103 kg/m^3 and dynamic viscosity 3.75 mPa.s at 25 °C. This fluid is pumped out of a reservoir by a cardiac simulator (Harvard apparatus, pulsatile pump 1423) into a windkessel. The arterial inlet (figure 6.1) is the

outlet of the windkessel where a physiologic relevant pressure wave is generated: mean pressure is about 100 mmHg and pulse pressure is about 60 mmHg. The fluid flows from the arterial inlet (1) through the compliant artery (2) towards the arterial anastomosis (3). It continues through the graft (4) , the venous anastomosis (9), the stenosis (10), the vein part after the stenosis (11) and the resistance (12). The distal artery (6) and vein (7) are ligated. The potential puncture sites for the arterial (5) and venous needle (8) are indicated.

1: Arterial Inlet (AI): 0 cm
2: Silicone artery
3: Arterial Anastomosis (AA): 17 cm
4: PTFE graft
5: Puncture site arterial needle: 25 cm
6: Distal Artery, ligated (DA)
7: Distal Vein, ligated (DV)
8: Puncture site venous needle: 37 cm
9: Venous Anastomosis (VA): 46 cm
10: Stenosis: 47 cm
11: Downstream Stenosis (AS): 48 cm
12: Resistor: 49 cm

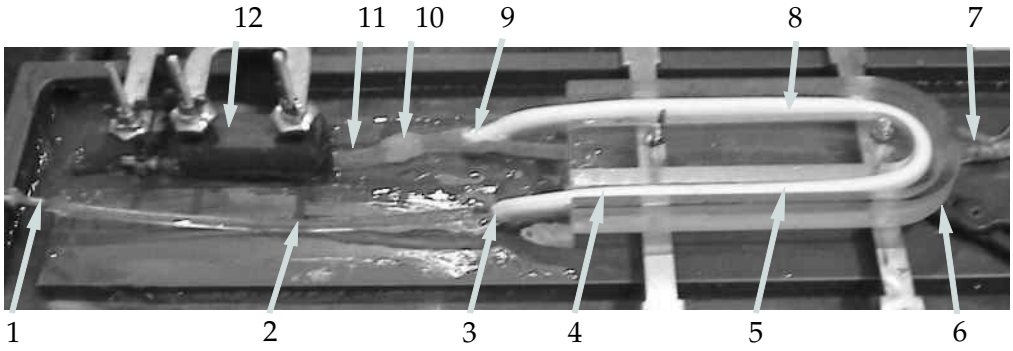

Figure 6.1: The setup

Four different stenoses sizes were introduced in the model: 50%, 65%, 80% and 90% stenosis. All stenoses have a circular lumen and have a length of 1 cm [139]. When the 50 and 60% stenoses are introduced, three different flow rates are adjusted on the cardiac simulator: 500, 1000 and 1500 ml/min. When the 80% stenosis was introduced only 500 and 1000 ml/min could be adjusted. For the 90% stenosis, flow was set to 500 and 750 ml/min. No higher flow rates were set in two latter cases due to model limitations. Heart rate was set to about 90 beats per minute in all cases.

Mean flow rate is measured volumetrically. The velocity waveforms are measured with doppler ultrasound (7.5MHz probe, Vingmed CFM800, Horten, Norway). Cornflower simulates the red blood cells necessary for doppler reflection. The pressure waveforms are measured with a fluid filled epidural catheter connected to a piezo electric pressure transducer (Datex-Ohmeda, Gent, Belgium). These signals

are amplified and sampled with a data acquisition PC card (National Instruments, Texas, USA).

6.3 Results

The dotted line in figure 6.2 shows the velocity wave at the arterial inlet, the full line the velocity wave at the venous anastomosis and the gray line 1 cm downstream the stenosis. Only one cardiac cycle is shown in the figure. The results shown for 50, 65 and 80% stenosis are at a flow rate of 1000 ml/min, flow rate is 750 ml/min for 90% stenosis. A periodic signal is seen at the arterial inlet in all situations. The signals at the venous anastomosis and 1 cm downstream the stenosis do not show a periodic signal any more. Both signals oscillate with high frequencies around a constant level.

Figure 6.3 shows mean and pulse pressure along the flow path. The arterial inlet is situated at x=0 cm, the arterial anastomosis at x=17 cm, the venous anastomosis at x=46 cm, the stenosis at x=47 cm and x=49 cm corresponds to 2 cm downstream the stenosis. Mean arterial pressure (=MAP) at the arterial inlet is 106 mmHg with 50 and 65% stenosis, but rises up to 127 mmHg at 80% stenosis and 132 mmHg at 90% stenosis. Mean pressure drop over the stenosis increases with increasing stenosis percentage: 15, 18, 84 and 112 mmHg at 50, 65, 80 and 90 % stenosis, respectively. Mean pressure in the vein upstream the stenosis also increases with increasing stenosis degree: from 62 (50%) to 113 (90%) mmHg.

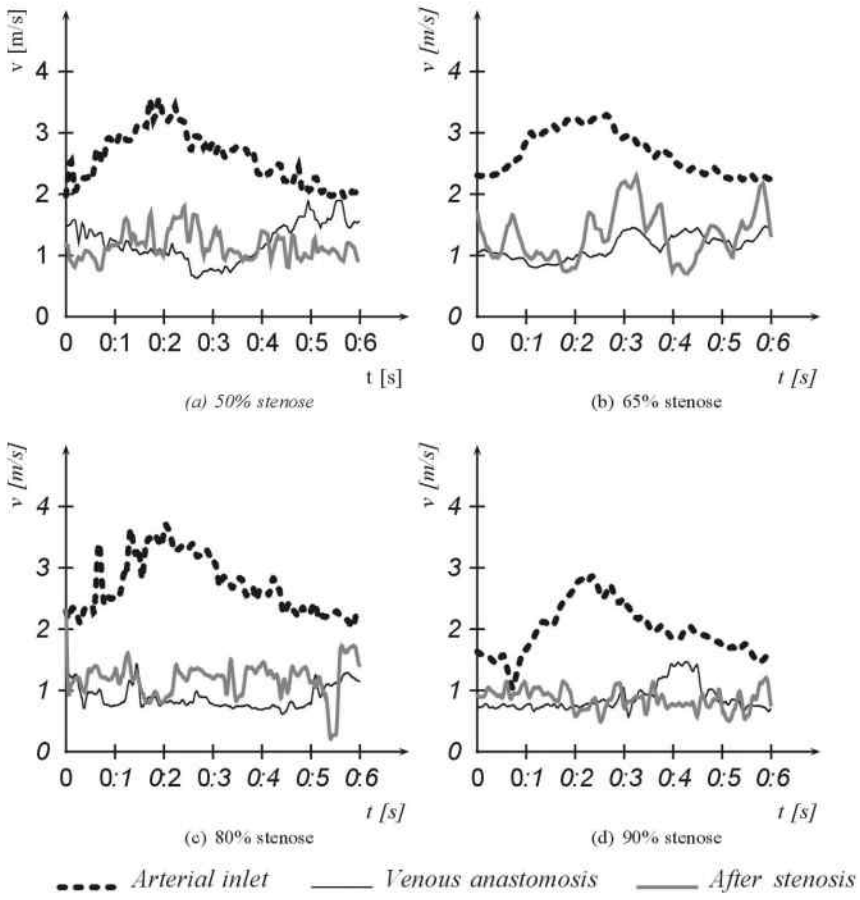

Figure 6.2: One period of the velocity waves at the arterial inlet, the venous anastomosis and after the stenosis at flow rate 1000 ml/min for 50, 65 and 80 % stenosis, and 750 ml/min for 90% stenosis

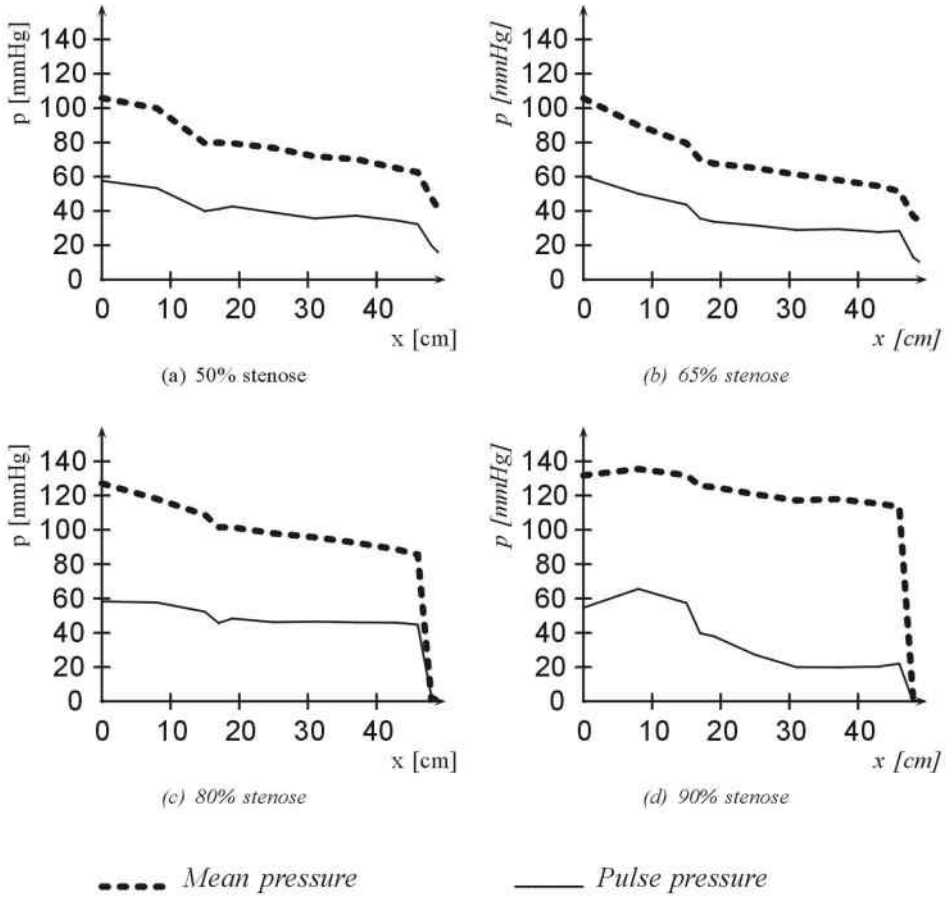

Figure 6.3: Mean and pulse pressure at flow rate 1000 ml/min for 50, 65 and 80 % stenosis, and 750 ml/min for 90% stenosis

Flow rate [ml/min]	500					1000				750	1500		
Stenosis percentage[%]	0	50	65	80	90	0	50	65	80	90	0	50	65
$v_{mean,arterial}$ [m/s]	0.66	0.66	0.66	0.66	0.66	1.32	1.32	1.32	1.32	0.99	1.99	1.99	1.99
$v_{mean,venous}[m/s]$	0.29	0.29	0.29	0.29	0.29	0.59	0.59	0.59	0.59	0.44	0.88	0.88	0.88
RI_{AI} [-]	0.75	0.63	0.90	0.57	**1.08**	0.41	0.46	0.33	0.45	0.37	0.43	0.30	0.33
RI_{VA} [-]	0.78	0.67	0.33	0.37	**1.74**	0.5	0.65	0.48	0.52	0.55	0.35	0.41	0.23
RI_{AS} [-]	N/A	0.82	0.65	0.66	0.72	N/A	0.52	0.69	0.90	0.58	N/A	0.62	0.31
MAP [mmHg]	94	99	102	102	122	110	106	106	127	132	102	129	109
$p_{arterial\ line}$ [mmHg]	73	88	87	90	114	65	77	65	98	121	40	55	59
$p_{venous\ line}$ [mmHg]	65	86	84	89	110	58	70	58	93	118	25	43	48
p_{AS} [mmHg]	N/A	72	12	57	46	N/A	48	37	1	2	N/a	7	6
$p_{venous\ line}$/MAP [-]	**0.69**	**0.86**	**0.83**	**0.87**	**0.9**	**0.52**	**0.66**	**0.55**	**0.73**	**0.89**	0.25	0.34	0.44
PR [%]	11.2	**2.43**	**2.74**	**1.67**	**3.32**	10	8.59	10.79	**5.58**	**2.39**	37.3	21.24	18.64

Table 6.1: Mean velocity in artery and vein; Resistance Index at the arterial inlet (RI_{AI}), the venous anastomosis (RI_{VA}) and after stenosis (RI_{AS}); Mean Arterial Pressure (MAP); pressure at the arterial and venous line of the dialysis machine with pressure heightcorrection [42]; pressure after stenosis (p_{AS}); the ratio between pressure at the venous line and MAP; and Pressure Ratio (PR). The 0% stenosis data result from a previous study [96] The dectected stenoses are indicated in bold.

Table 6.1 summarises the non-invasive measured hemodynamic parameters and indices like mean arterial and venous velocities, the resistance index at the arterial inlet (RI_{AI}), at the venous anastomosis (RI_{VA}) and downstream the stenosis (RI_{AS}) and mean arterial pressure (MAP) for three different flow rates: 500, 1000 and 1500 ml/min. The table summarises next the pressure derived parameters and indices that only can be obtained invasively: mean pressure at the arterial ($p_{arterial\ line}$) and venous line ($p_{venous\ line}$), mean pressure downstream the stenosis (p_{AS}), the ratio between ($p_{venous\ line}$) and MAP and the PR. Only RI_{AI} and RI_{VA} at 90% stenosis and 500 ml/min are above 1, pointing out a stenosis. $p_{venous\ line}$/MAP detects all the stenoses at 500 and stenoses at 500 and 1000 ml/min but even a 0 % stenosis leads to a value above 0.5 (0.69 and 0.52 respectively). PR detects all the stenoses at 500 ml/min and the stenoses of 80% and 90% at 1000 ml/min. Both parameters detect no single stenosis at a flow rate of 1500 ml/min.

6.4 Discussion

The vascular access model is built to be a realistic approximation of the hemodynamics in a loop graft vascular access by means of a PTFE graft. The material and parameters are therefore adjusted to correspond with clinical values [96]. The silicone blood vessels utilised, have diameters and relative distensibility that are observed in clinical practice [62] [67]. Mean pressure at the arterial inlet of the model is adjusted to 106 mmHg (50 and 60% stenosis), to 127 mmHg (80%) and 132 mmHg (90%). Heart rate is adjusted to about 90 beats per minute. These values are in the range of values published in literature on venous outflow stenosis [42] [62] [140] [141]. The four stenosis percentages (50, 65, 80 and 90%) are introduced when flow rate was 500 ml/min. At 1000 ml/min, only 50, 65 and 80% were introduced. It was not possible to introduce 90% stenosis in the model at this flow rate, because an inflating aneurysma originated at the venous anastomosis. Therefore the flow rate was reduced to 750 ml/min. For the same reasons, only 50 and 65% stenosis could be introduced at a flow rate of 1500 ml/min.

The advantage of our hydraulic model in comparison to in vivo measurements is that we have simultaneously access to non-invasive (velocity - ultrasound) and invasive (pressure - catheter) measurement data on a realistic vascular access model and we are able to test new indices in a setup prior to a time consuming clinical study.

From the ultrasound velocity measurements it was shown that at the arterial inlet, a periodic wave is observed. The velocity wave at the venous anastomosis is periodic when 50 and 60% stenosis are inserted in the model, but for 80% and 90% stenosis a high frequency signal oscillating around a constant level is observed. Downstream the stenosis, a periodic wave could never be seen. The absence of a periodic velocity signal indicates a disturbed flow pattern and suggests the presence of stenosis. When such a velocity pattern is observed, the vascular access should be taken under surveillance. Systolic and diastolic velocity can be read on the measured curves and RI_{AI}, RI_{VA} and RI_{AS} calculated. Only two RI values indicated a stenosis (>1): RI_{AI} and RI_{VA} at a flow rate of 500 ml/min and 90% stenosis. Only the highest stenosis degree is detected with the RI parameter. Resistance index is not the recommended parameter to determine whether a stenosis is significant because it detects only very severe stenoses. No trend from low value at low stenosis percentage to high value at high stenosis percentage is present. This is due to the way the index is calculated: the maximum and minimum of the velocity signal in one period are used, two instantaneous recordings. Moreover, when significant stenosis is present, the periodic waveform disappears.

The measured pressure data along the model (invasive) showed that the higher the stenosis degree becomes, the higher the pressure drops over the stenosis. An elevated stenosis degree causes an increased model resistance and consequently a high mean pressure level in the artery and the graft. Pulse pressure is set to 60 mmHg at the arterial inlet and shows a steep drop at the stenosis. The vessel wall is subjected to cyclic stretch upstream the stenosis, as pulse pressure is high there. High cyclic stretch is correlated with vascular smooth muscle cell (VSMC) proliferation and migration [142–144], initiating stenosis. The stenosis initiates a pulse pressure drop, resulting in less cyclic stretch in the distal vein. This supports the hypothesis that stenosis formation is a biological reaction against disturbed hemodynamics.

$p_{venous\ line}$/MAP and PR are parameters derived from invasive pressure data. The values are easy to access, they can be read directly from the hemodialysis machine. Although one should take care when reading the values from the dialysis machine: the pumps must stop while the sensors are read and correction must be made for height difference between the sensor and the vascular access as explained

by Kleinekofort et al. [42]. The $p_{venous\ line}$/MAP and PR values are summarised in table 6.1. All the values and parameters of a previous study on the model without stenoses [96] are included in the table 6.1. The ratio between the pressure at the venous line and MAP detects all stenoses at flow rate 500 and 1000 ml/min, but also includes the normal functioning graft (0% stenosis). $p_{venous\ line}$/MAP has a low specificity. If the threshold would be set to 0.7, instead of the 0.5 proposed by Kleinekofort [42], the parameter would detect the grafts needing intervention. The reason for intervention is not the high stenosis degree when the flow rate through the graft is 500 ml/min and the stenosis percentage is 50 or 60%, but the thrombosis danger at that low flow rate [15]. PR indicates only the grafts needing intervention. The advantage of $p_{venous\ line}$/MAP and PR in comparison to RI is that it uses mean pressure values that are less sensitive to noise than an instantaneous value. Another advantage of the PR parameter is that it uses only pressure at the arterial and venous line of the dialysis machine. Both values are read from the dialysis machine when the patient undergoes the hemodialysis therapy while MAP is measured with the cuff on the opposite arm and $p_{venous\ line}$ at the dialysis machine. The advantage of PR is that a relative pressure gradient is used. The higher the flow rate, the higher the difference in the numerator and consequently the higher PR. This is positive as the presence of stenosis is decreasing the flow rate. $p_{venous\ line}$/MAP only contains pressure information. Another strength of the parameter is that it was calculated to detect stenosis and it does so. When no stenosis is present in the model, the parameter value stays above the threshold. The limitation of our model is that only venous outflow stenosis are tested. Experiments should be performed with a midgraft stenosis. The author expects that PR will have high values, because when a midgraft stenosis is present, $p_{arterial\ line} - p_{venous\ line}$ will be high compared to $p_{arterial\ line}$. The expectancy is that PR will be above a certain threshold indicating a midgraft stenosis. PR is a promising parameter when we look at our in vitro results and is worthwhile for clinical testing.

A limitation of the study is that the parameters are only tested in PTFE grafts. A model for a native arterio venous fistula should be built to investigate whether the parameters behave similar under the typical flow conditions of a native arterio venous fistula. A second limitation is that the diameter of the grafts in the experiments is constant. Tissue ingrowth occurs in grafts of patients, which means that the access lumen is lowered compared to the lumen in the in vitro model. This influence has to be investigated in vivo.

6.5 Conclusion

In conclusion we can state that the pressure ratio and $p_{venous\ line}$/MAP can predict significant venous outflow stenosis and/or grafts needing intervention. However, resistance index is not a reliable index to intercept grafts that need intervention. When no periodic velocity signal is measured in the graft, flow is assumed disturbed due to a stenosis. The newly introduced pressure ratio parameter needs clinical confirmation before it can be used widely to detect stenosis.

Chapter 7

In vivo validation of the Pressure Ratio parameter for stenosis detection in vascular access grafts

7.1 Introduction

Stenoses occur frequently (80% after 1 year) in polytetrafluorethylene (PTFE) graft fistulas. A first classification can be made depending on the site where the stenosis arises. The first stenoses types are the stenoses in the feeding artery or at the arterial anastomosis: the arterial inflow stenoses. The second type is the midgraft stenosis. The last category is the outflow stenosis: stenoses at the venous anastomosis and in the draining vein.

A second method to make a classification in stenoses, is the intervention need. A stenosis is significant when the vessel lumen is reduced with more than 75%. These stenoses imply treatment as thrombosis is likely to occur. A second situation where thrombosis danger exists, is when a stenosis develops at a low graft flow rate independent of the lumen reduction. Both problematic stenoses should be detected as soon as possible and treated immediately.

Non-invasive or minimally invasive techniques to discover the stenoses are essential for clinicians especially if the technique can be performed easily and fast. Performing in vitro experiments, Van Tricht et al. [43] compared three clinical parameters to detect stenoses: the resistance index, the ratio between the pressure at

the venous line of the dialysis machine and mean arterial pressure (MAP) and a newly introduced parameter, the pressure ratio (PR). The major result of the study pointed out that only the PR was selective and successful in the determination of significant stenoses.

The aim of the present study is to investigate whether the pressure ratio is also in vivo the optimal parameter to select significant or problematic stenoses in PTFE graft fistulas.

7.2 Methods

The pressure ratio is defined as:

$$PR = \frac{p_{arterial\ line} - p_{venous\ line}}{p_{arterial\ line}} \times 100\% \tag{7.1}$$

$p_{arterial\ line}$ and $p_{venous\ line}$ are the pressures at the arterial and venous line, respectively, of the hemodialysis machine when the pump has stopped. This parameter will be compared to the ratio between the pressure at the venous line $p_{venous\ line}$ and mean arterial pressure (MAP).

Nine patients with a graft vascular access are included in the follow-up program. Different patient items were stored in a database: the patient name; the date; the time after connection to the dialysis machine; the distance between the needles measured along the flow path; the access flow rate; the blood flow rate through the artificial kidney; the dynamic arterial and venous pressure; the arterial and venous pressure with the pumps stopped; the systolic, diastolic and mean arterial pressure. All items in the database have their specific reason. The date is noted to be able to investigate the evolution in time of the parameters. The time after connection to the dialysis machine is registered since hemodialysis patients are in general hemodynamically stable the first hour after cannulation. In later stages of the dialysis session, patients start to suffer from hypotension. The distance between the needles measured along the flow path is measured to the best of the clinicians knowledge with a flexible ruler. The access flow rate is measured monthly with the ultrasound dilution technique [39] as this is at present included in the clinical protocol for vascular access follow-up. If an access flow decrease of

20% is observed, the patients undergo an angiography for graft inspection. The blood flow through the artificial kidney is read directly from the hemodialysis machine (Fresenius 4008, Fresenius Medical Care, Bad Homburg, Germany). The dynamic venous and arterial pressures are included as venous pressures above 250 mmHg or arterial pressures below 200 mmHg can indicate blood aspiration or return problems like needle misplacement or a blood clot that obstructs the in- or outflow. On the other hand an increased dynamic venous pressure can indicate a venous outflow stenosis. The arterial and venous pressure with the pumps stopped are measured to calculate the PR and $p_{venous\ line}$/MAP. The arterial and venous pressures are collected with an in-house written Labview (Labview 6.1, National Instruments Netherlands BV, Woerden, The Netherlands) program that captures the pressure data via the serial port of the dialysis machine. MAP, the systolic and diastolic pressure are measured with a sphygmanometer.

7.3 Results

The in vivo measurements in the first month of follow-up are presented in table 7.1. The first nine measurements were routine measurements. The last two measurements were performed on the same patient, once before angioplasty at the venous anastomosis and once after. The angioplasty procedure was performed since a significant stenosis was detected at the venous anastomosis.

Name	Date	measurement type	Nd [cm]	Q_a (ml/min)	Q_b (ml/min)	V_p (Q_b=0)	A_p (Q_b=0)	PR (%)	V_p / MAP	PRD(%)
1	1/04/2005	routine	13	583	350	21	42	50.0	0.25	54.17
2	1/04/2005	routine	8	983	353	18	42	57.1	0.26	38.10
3	4/04/2005	routine	10	530	354	32	57	43.9	0.56	36.55
4	4/04/2005	routine	12	1060	351	5	67	92.5	0.06	92.54
5	4/04/2005	routine	9	660	348	12	30	60.0	0.19	45.00
2	7/04/2005	routine	14	1577	355	26	64	59.4	0.27	69.27
6	7/04/2005	routine	10	917	353	33	78	57.7	0.41	48.08
7	8/04/2005	routine	7	1163	346	59	85	30.6	0.46	17.84
8	8/04/2005	routine	10	1200	360	45	100	55.0	0.38	45.83
9	22/04/2005	flow decrease	6	455	356	35	56	37.5	0.42	18.75
9	27/04/2005	post pta VA	7	503	352	17	50	66.0	0.23	38.50

Table 7.1: The data after one month follow-up in vivo. Nd = needle distance; Q_a = access flow rate; Q_b = blood flow rate through the artificial kidney; V_p = pressure at the venous line of the dialysis machine; A_p = pressure at the arterial line of the dialysis machine; PR = pressure ratio; PRD = pressure ratio corrected for the distance between the needles

In these measurements, an extreme high PR was observed for patient 4 and no single PR value below 8% was observed.

7.4 Discussion

It can be remarked from table 7.1 that the PR shows a wide range of values. It should be stressed however that those values are patient dependent and should be corrected before drawing hard conclusions. First, because there is a huge variation in the needle distance between the different patients, the pressure ratio has to be corrected for it. The pressure ratio corrected for the needle distance (PRD) becomes: PR.ND/12, see table 7.1, last column. This was not necessary in our in vitro study because the needles were located at fixed positions in the graft. [43]
Secondly a correction for the in vivo lumen diameter should be made. The lumen in vivo is smaller compared to the lumen used in the in vitro experiments. Moreover, the lumen diameter is patient specific and should therefore be measured in the ultrasound or angiography department. Though, this correction will not be performed since it is not feasible to refer the patients weekly to the ultrasound or angiography department. It would cause the nullification of the ease and cheapness of calculation of the PR.

Because of the different settings (lumen, needles) in vivo versus in vitro, the threshold will be different in vivo compared to in vitro.
When the PRD of patient 7 is compared to the PRD of patient 9 before intervention, it is noticed that the PRD of patient 7 is 17.84 and the PRD of patien 9 is 18.75. Patient 7 has the lowest PRD observed, but has a well functioning vascular access. Patient 9 contrary has a venous outflow stenosis. It might be that it is impossible to formulate an exact absolute threshold as the graft is in vivo not a smooth cylindrical tube because of the tissue ingrowth and the repetitive punctures. The follow-up study has to point out whether it would be interesting to observe the evolution of the PR in time as it is a parameter that is very easy to measure and consequently to follow-up. It is expected that a PR decrease of 30% points out a significant stenosis. Patient 9 confirms this hypothesis. This patient suffered from a significant stenosis at the venous anastomosis. Furthermore, the PRD was doubled after the surgical intervention.

The only stenosis tested in vitro was a venous outflow stenosis. Patients can

also suffer from midgraft stenoses, just like patient 4. The stenosis of patient 4 is not treated at the moment as it limits the graft flow to 1060 ml/min. Nevertheless, this stenosis is detected by the PRD; the PRD has an extremely high value, which is expected for a midgraft stenosis: there exists a considerable pressure difference over that stenosis.

A specific feature of the PR parameter is its potential to be integrated in the hemodialysis machines in the near future. This is perfectly possible since the arterial and venous pressure are available online inside in the dialysis machine. Moreover, as the modern dialysis machines dispose of displays or pressure monitoring, the PRD can be communicated this way. The adaptations described above cost little effort for the hemodialysis machine manufacturers and would help the dialysis staff enormously with the vascular access follow-up.
The next step could be, once the PR has proven its relevance, to add a button to the machine that starts the PR measurement. When this button is pushed, the pump should stop automatically, the arterial and venous pressure should be recorded during e.g. 30 seconds and subsequently time-averaged. Next, the PR has to be calculated. This automatization step can force the line clamps to stay open even with a stopped pump as this pump stop will be forced by an intervention of the medical staff and not because of an error.

7.5 Conclusion

The results of the in vitro experiments concerning the pressure ratio are preliminarily confirmed in vivo. Advises for the hemodialysis machine manufacturers are formulated. This way, the newly introduced pressure ratio parameter can be registered with one button push and offer a cheap parameter to the dialysis staff that is easy to register and follow-up. Significant and problematic outflow and midgraft stenoses can probably be early detected in future so that the vascular access can be cured in time. This step contributes to the patients benefit since his hemodialysis sessions can continue efficiently and extra complications like thromboses are prevented.

Part IV

Modelling of the hemodynamics in the vascular access during a hemodialysis session

Chapter 8

Experimental analysis of Punctured Vascular Access Grafts

8.1 Introduction

End stage renal disease patients need a renal replacement therapy such as hemodialysis. The required blood flow through the artificial kidney is about 350 ml/min to obtain efficient hemodialysis. As the mean blood flow through blood vessels in the limbs does not reach 350 ml/min, a vascular access is constructed. In patients with small or poor blood vessels such as diabetics and elderly, a polytetrafluorethylene (PTFE) graft is often the access of choice when the blood vessels of these patients do not allow to create an adequate native arteriovenous fistula [15, 16, 31].

Patients on hemodialysis are usually three times a week referred to the dialysis unit; the exact duration of a hemodialysis session depends on the personal need of the patient [145]. During the session, waste products are purified from the blood and the excess of water in the body is drained through an extracorporeal artificial

The content of this chapter is adapted from: I. Van Tricht, D. De Wachter, J. Tordoir, and P. Verdonck. Experimental analysis of Punctured Vascular Access Grafts, ASAIO journal (In Press)

kidney. Therefore blood circulates in an extracorporeal system as described below. A rollerpump sucks blood out of the patient via the punctured vascular access, forces it through the artificial kidney and subsequently the blood is returned to the patient. The arterial needle (AN) sucks continuously dirty blood out of the patient and the venous needle (VN) returns continuously purified blood.

It is obvious that the hemodynamics in the graft during a hemodialysis session (intra dialytic) deviate from the hemodynamics in between the sessions (inter dialytic). Blood flow in the graft is first split by the AN into the extracorporeal flow and the continuing graft flow. Secondly, the VN flow is merged with the remaining graft flow. Quantification of the impact of the needle flow on the hemodynamics in the VA is the aim of this in vitro experiment. To do so, a realistic in vitro vascular access model (VAM) with a punctured 6 mm PTFE graft is constructed and connected to a two needle hemodialysis system. We have altered two parameters in our model: the access flow rate (Q_G) and the blood flow rate through the artificial kidney (Q_R). Knowledge of the hemodynamics (intra access pressures and velocities) under different combinations of Q_G and Q_R will provide information on recirculation probability, vessel wall load and complication probability. The benefit of an experimental model is that we can vary one flow rate at the time. This is not possible in clinic as a patient's graft develops a certain flow rate and the blood flow rate towards the artificial kidney depends on the patients need and the physician's choice.

8.2 Methods

8.2.1 Simulation of a hemodialysis session using the compliant vascular access model

A scheme of the setup used to simulate experimentally a hemodialysis session using a compliant vascular access model is shown in figure 8.1. Two interacting loops can be distinguished. The first loop simulates the vascular access of the patient. In that loop, the circulating fluid is pumped out of the reservoir (Res) and next into the windkessel (WK) towards the arterial inlet (AI) of the silicone vascular access model (VAM) [96], that will be described in detail below. From the outlet of the VAM, the fluid flows through the resistor (R) back to the reservoir. The pump (HP) (Harvard apparatus, pulsatile pump 1423) generates pulsatile flow to obtain pres-

sure and flow waveforms in the VAM that approximate the waveforms observed in vivo [62].

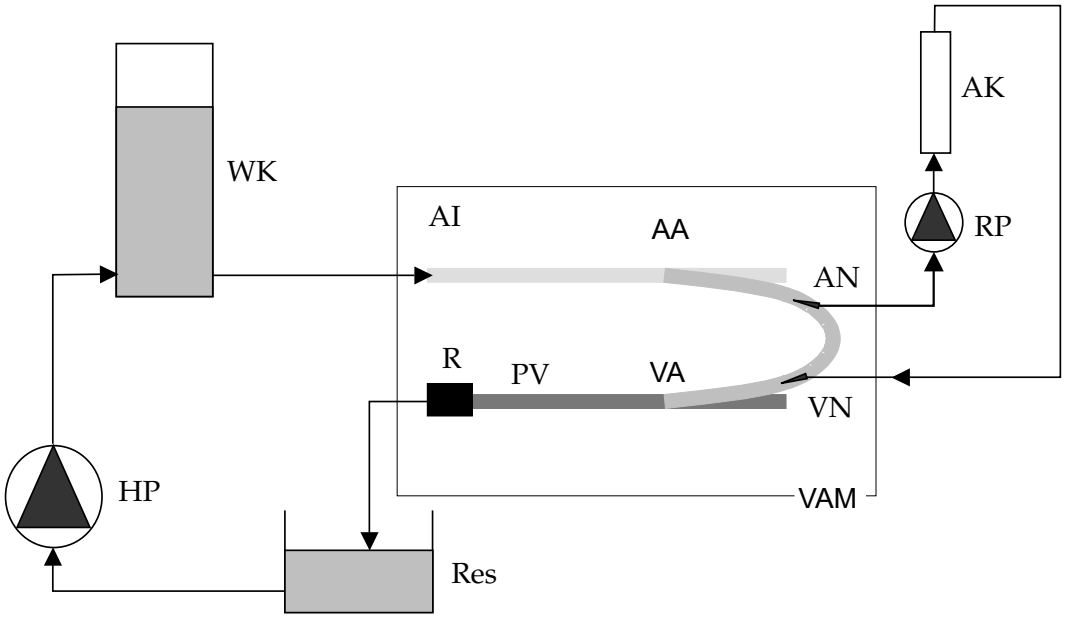

Figure 8.1: Scheme of the setup: A glycerine/water mixture (40/60%) is withdrawn from the reservoir (Res) and pumped (HP) into the windkessel (WK) that is connected to the arterial inlet (AI) of the vascular access model (VAM). The proximal vein (PV) of the silicone VAM is connected to a resistor (R) and to the reservoir. The extracorporeal hemodialysis circuit consists of the arterial needle (AN), the rollerpump (RP), the artificial kidney (AK) and the venous needle (VN). The distal ends of artery and vein are ligated.

Figure 8.2 shows a typical pressure and velocity waveform during one heart cycle as imposed at the arterial inlet. The maximum pressure and velocity are respectively the systolic pressure (p_{sys}) and systolic velocity (v_{sys}); the minimum values are the diastolic pressure (p_{dia}) and diastolic velocity (v_{dia}). At the arterial inlet, mean pressure (p_{mean}) is adjusted to 100 mm Hg and the difference between p_{sys} and p_{dia}, the pulse pressure (pp), is fixed to 60 mmHg. The mean pressure is regulated by tuning the resistor, the pulse pressure by adjusting the volume of air in the windkessel. The simulated heart rate is 90 beats per minute. The mean velocity (v_{mean}) depends on the simulated access flow rate (Q_G). Three different Q_G values are simulated. The first is 500 ml/min, a low graft flow rate where the graft is continuously in thrombosis danger [15] [129]. The patients with $Q_{G,500}$ simulated, are patients with a central vein stenosis or with an inadequate graft inflow. They have in common that the mean arterial pressure is about 100 mmHg. It is clear that patients with an arterial stenosis are not part of the simulations

performed. The second is 1000 ml/min which is generally described as the flow rate of a well functioning vascular access [15]. The last Q_G is 1500 ml/min and simulates an access where ischemia, steal syndrome and heart load are potential complications. [15] [31] [16]

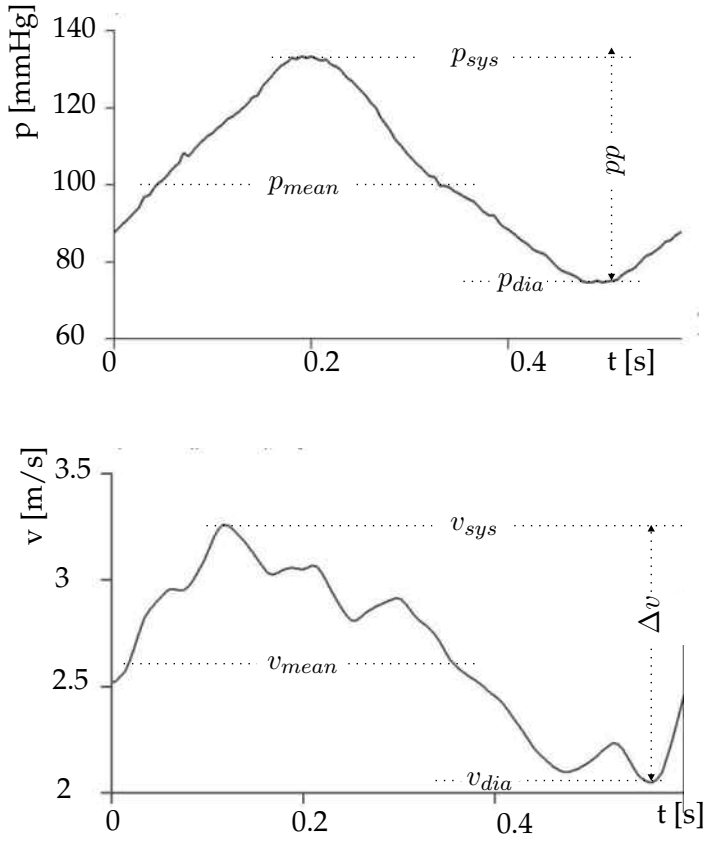

Figure 8.2: The pressure (top panel) and velocity (bottom panel) wave at the arterial inlet for a graft flow rate 1000 ml/min and a roller pump flow rate of 0 ml/min, the interhemodialytic period.

In the second loop, the blood circuit of the dialysis machine, fluid is sucked out of the VAM through the arterial needle (AN) by the roller pump (RP). The roller pump forces the fluid further through the artificial kidney (AK) (F60, Fresenius Medical Care AG,Homburg, Germany) and through the venous needle (VN) back into the VAM. Regular arterial and venous lines (Baxter S.A., Lessen, Belgium) are used in the extracorporeal system. The dialysate compartment of the artificial kidney is filled with water and closed. For each Q_G, five different flow rates are adjusted with the rollerpump Q_R: 0, 200, 300, 400 and 500 ml/min, simulating the blood flow rate through the artificial kidney. Each time Q_R is varied, it is cal-

ibrated volumetrically [153]. In Europe, roller pump flow rates between 200 and 400 ml/min are typically used; in the USA, Q_R rather varies between 300 and 500 ml/min.

A 40/60% glycerine-water mixture circulates in the entire system. It is a newtonian blood analogue with density 1090 kg/m^3 and dynamic viscosity 3.75 mPa.s. Figure 8.3 shows a photograph of the VAM. The artery is at the proximal extend - the arterial inlet (AI) - connected to the windkessel and clamped off at the distal end. A 6 mm PTFE graft (GORE-TEX® Stretch Vascular Graft, Arizona, USA) is sutured end graft to side artery 70 mm distal to the arterial inlet, creating the arterial anastomosis (AA). The second end of the graft is sutured end graft to side vein at the venous anastomosis (VA). The proximal vein (PV) is connected to the resistor (R) and the distal vein is clamped off. The length of the vein segment between the venous anastomosis and the resistor is 50 mm. The length of the graft, placed in loop graft configuration, is 310 mm. The graft is punctured with the arterial needle 100 mm downstream the arterial anastomosis and with the venous needle 120 mm upstream the venous anastomosis. The distance between the needles is 90 mm. Both needles are identical 15G needles (Dispomed® Geinhausen, Germany).

The VAM is a realistic 1:1 scale model. The compliant artery has an inner diameter of 4.25 mm at 100 mmHg and the compliant vein has an inner diameter of 6.3 mm at 40 mm Hg. Both artery and vein are made from silicone rubber and have a relative distensibility (RD) of about 4% in their operating pressure ranges as shown before [96]. The relative distensibility can be calculated with the formula below when the inner vessel diameter at systolic pressure (D_{sys}) and at diastolic pressure (D_{dia}) are known [96].

$$RD = \frac{D_{sys} - D_{dia}}{D_{dia}} \times 100\% \tag{8.1}$$

8.2.2 The measurements and postprocessing

The measurements are performed twice independently by the same operator to test the reproducibility. Pressure in the VAM is measured with a fluid filled catheter connected to a piezo-electric pressure transducer (Datex-Ohmeda, Gent, Belgium). The pressure is recorded during 10 seconds such that 16 cycles are captured. The catheter tip is moved from the arterial inlet through the arterial

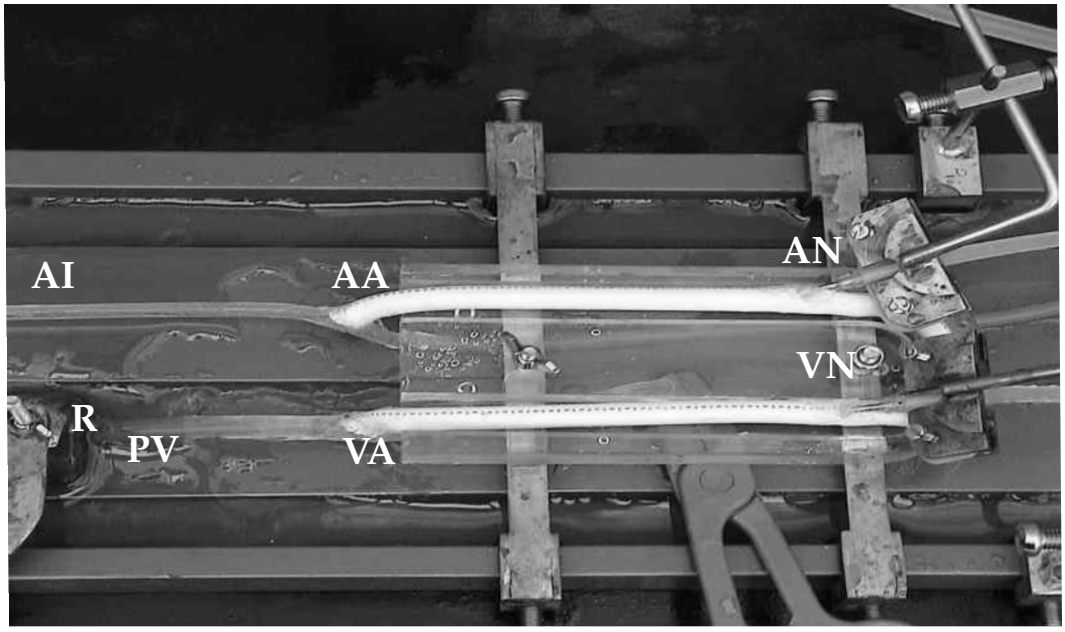

Figure 8.3: The punctured compliant vascular access model. The fluid circulates from the arterial inlet (AI) through the arterial anastomosis (AA), the vascular access graft, the venous anastomosis (VA), the proximal vein (PV) and the resistor (R). The fluid is partially withdrawn from the graft through the arterial needle (AN). The fluid that passed the artificial kidney is returned through the venous needle (VN).

anastomosis, through the graft, the venous anastomosis until the venous outlet. Table 8.1 lists the sites where the catheter is held to measure pressure and its displacement (Δx) measured along the flow path from the arterial inlet. The values for p_{sys}, p_{mean} and p_{dia} reported, are the systolic, diastolic and mean pressure of the averaged heart cycle. The systolic, mean and diastolic pressure drop in between the needles is calculated as the difference between the pressure at the AN and the VN. The pressure drop after the VN is calculated as the difference between the pressure at the VN and 6 cm distal to the VN. The pressure drop over the graft represents the difference between the pressure at the AA and the pressure at the VA. Pressure drops are always calculated as the difference between the pressure upstream and downstream location such that a negative pressure drop corresponds with a pressure rise.

The velocity pattern is measured on the centerline of the blood vessel at the arterial inlet, the arterial anastomosis, the venous anastomosis and the venous outlet with Doppler ultrasound (7.5 MHz probe, Vingmed CFM800, Horten, Norway). The ultrasound doppler image is generated using pulsed wave doppler with angle

No.	Location	Δx [cm]
1	Arterial inlet	0
2	2 cm proximal to the arterial anastomosis	5
3	Arterial anastomosis	7
4	2 cm distal to the arterial anastomosis	9
5	5 cm distal to the arterial anastomosis	12
6	2 cm proximal to the arterial needle	15
7	Arterial needle	17
8	2 cm distal to the arterial needle	19
9	4.5 cm distal to the arterial needle	21.5
10	2 cm proximal to the venous needle	24
11	Venous needle	26
12	2 cm distal to the venous needle	28
13	6 cm distal to the venous needle	32
14	2 cm proximal to the venous anastomosis	36
15	venous anastomosis	38
16	2 cm distal to the venous anastomosis	40
17	Proximal vein	43

Table 8.1: The distance Δx, in cm, measured from the arterial inlet to every pressure measurement location.

correction at a sample frequency (SF) of 200 Hz and is recorded over 4s. The velocity signal is captured from the images by the use of in house developed Matlab code (Matlab 6.5 release 13, The Mathworks Inc., Gouda, The Netherlands). Mean, systolic and diastolic velocity are derived from the average waveform.

8.3 Results

8.3.1 The pressure distribution over the graft

Diastolic, mean and systolic pressure of the mean cycle are determined at the measurement points listed in table 8.1. When the measured mean and pulse pressure are plotted against the distance from the arterial inlet, the curves shown in figure 8.4 are obtained. The curves are grouped per graft flow rate to be able to investigate the influence of Q_R. For $Q_{G,500}$, there is only a small pressure difference between the pressure at the arterial inlet of the model and the venous outlet. The difference decreases with increasing Q_R. For $Q_{G,1000}$, the pressure decreases from the inlet towards the outlet. The same trend is present as for $Q_{G,500}$: the higher Q_R, the lower the decrease along the flow path. For $Q_{G,1500}$, the pressure at the venous

outlet is higher if the roller pump is switched on compared to zero roller pump flow. The pressure level is no longer proportional to the roller pump flow rate. The flow direction is altered at the two anastomoses (AA: 7cm, VA: 38cm) and at the AN (17 cm) and the VN (26 cm). The relative influence of the disturbance of the needles increases with decreasing Q_G.

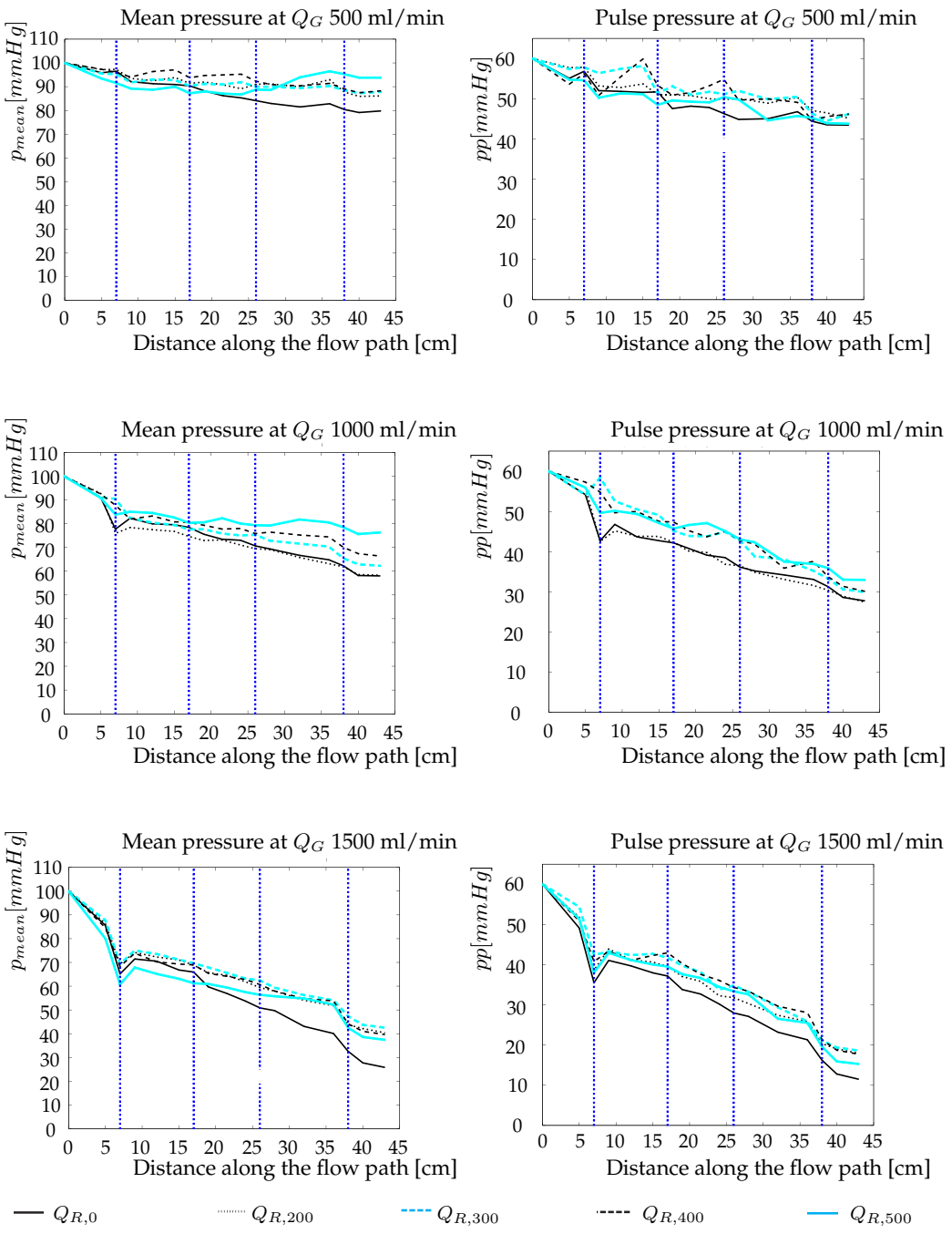

Figure 8.4: The mean pressure (p_{mean}) and pulse pressure (pp) along the vascular access model grouped per graft flow rate (Q_G). The arterial anastomosis is located at 7 cm, the arterial needle is inserted at 17 cm, the venous needle is inserted at 26 cm and the venous anastomosis is at 38 cm

Comparing the plots for different Q_G values learns us that the pressure level in the vein decreases with increasing Q_G value.

A more detailed analysis of the pressures is shown in figure 8.5 and allows to present the pressure drop in between the needles, over the VN and over the graft. These results vary if the combination of Q_G and Q_R is altered.

Part of the flow in the graft is deviated at the AN and a second time at the VN because a parallel extracorporeal circuit is connected. The roller pump speed determines the deviated flow rate and influences the pressure drop in between the needles. The tendency is the same for all imposed access flow rates (500, 1000 and 1500 ml/min) and for all pressure drops (systolic, mean and diastolic): i.e. the pressure drop decreases with an increasing Q_R. There even exists a negative mean pressure drop (pressure rise) at $Q_{G,500}$ with $Q_{R,500}$. The higher the access flow rate is, the higher the pressure drop becomes for a constant Q_R. The systolic pressure drop is negative for $Q_{G,500}$ combined with $Q_{R,400}$ and $Q_{R,500}$; the diastolic pressure drop is negative for $Q_{R,500}$ combined with $Q_{G,500}$ and $Q_{G,1000}$.
At the VN, fluid is returned to the vascular access. The pressure drop after the VN varies depending on Q_R. The higher Q_R, the lower the pressure drop after the VN. When the pressure drops are compared for different Q_G values and a fixed Q_R, the highest pressure drop exists for the highest Q_G value. $\Delta p_{sys,VN}$ is negative for $Q_{G,500}$ and $Q_{R,500}$; $\Delta p_{dia,VN}$ is negative for $Q_{R,500}$ whatever Q_G is and for $Q_{R,400}$ for $Q_{G,500}$ and $Q_{G,1000}$; $\Delta p_{mean,VN}$ is negative at $Q_{R,500}$ if combined with $Q_{G,500}$ and $Q_{G,1000}$.
The pressure drop over the whole graft Δp_{graft} is the difference between the pressure drop at the AA and the VA. $\Delta p_{sys,graft}$ is negative for $Q_{G,500}$ and $Q_{R,500}$; $\Delta p_{dia,graft}$ is negative for $Q_{R,300}$ and $Q_{G,500}$ and for $Q_{R,500}$ if combined with $Q_{G,500}$ or $Q_{G,1000}$; $\Delta p_{mean,graft}$ is negative for the combination of $Q_{G,500}$ and $Q_{R,500}$.

The mean venous pressure increases monotonous from 80 mmHg at $Q_{R,0}$ to 95 mmHg at $Q_{R,500}$ for $Q_{G,500}$. For $Q_{G,1000}$, mean venous pressure increases monotonous from 60 mmHg at $Q_{R,0}$ to 78 mmHg at $Q_{R,500}$. At the highest access flow rate, 1500 ml/min, venous pressure is about 15 mmHg higher when the roller pump is switched on compared to zero roller pump flow rate, but there exists no monotonous increase with increasing Q_R.

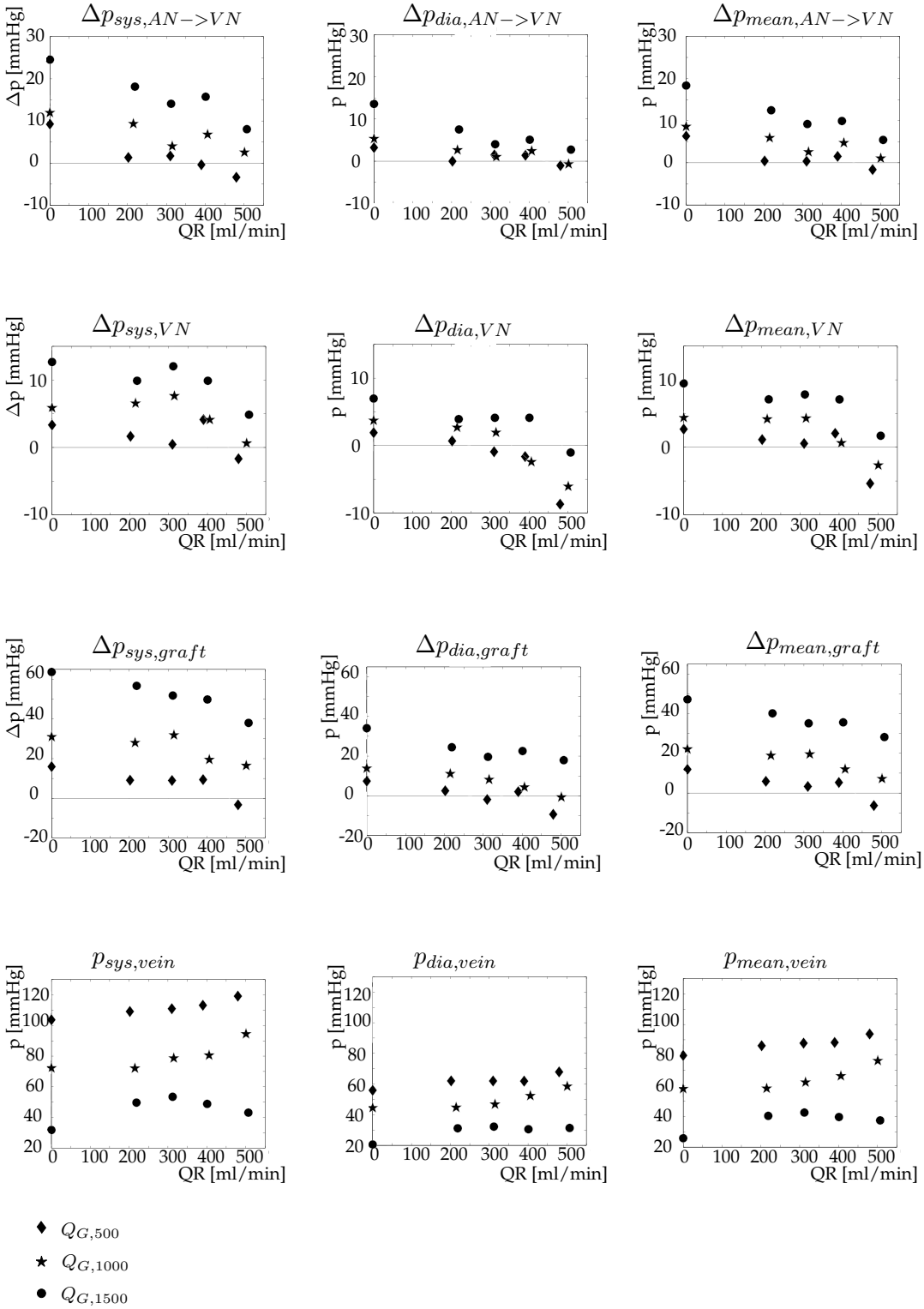

Figure 8.5: Pressure drops: the pressure drop between the needles ($\Delta p_{AN->VN}$) on the first row, the pressure drop after the venous needle (Δp_{VN}) on the second row, the pressure drop over the graft (Δp_{graft}) on the third row. The venous pressure (p_{vein}) in the bottom row.

8.3.2 The information in the velocity signals

Diastolic, mean, and systolic velocity are derived from the ultrasound-doppler images for each combination of Q_R and Q_G. As the diameter of the vein is larger than the diameter of the artery, mean velocity in the vein is lower than mean velocity in the artery. When the graft flow rate increases, the velocities increase. Table 8.2 shows the diastolic (top panel), mean (middle panel) and systolic velocities (bottom panel). The values are reported at the AI, the AA, the VA and the VO for all access flow rates. The range where the velocities are in between is reported and the calculated average is shown. The average diastolic velocity is lower at the AA than at the AI. For the systolic velocity, it is the opposite: it is higher at the AA than at the AI. The inverse is observed at the venous side of the model. The average diastolic velocity at the VA is lower at the VA than at the VO and the average systolic velocity is higher at the VA than at the VO.

8.4 Discussion

The in vitro model is a realistic approximation of a vascular access by means of a PTFE graft on brachial artery in a hemodialysis patient [96]. It has a RD of 4% which is in the range reported by Kosch et al [62]. The pressure wave adjusted at the model inlet has as major characteristics: a mean pressure of 100 mmHg and a pulse pressure of 60 mmHg. This corresponds to the values reported for normotensive patients [62]. The three different flow rates simulate three different clinical cases. The first access flow rate, 500 ml/min, represents the access with risk on thrombosis because of the low flow rate and the high particle residence time [15] [152]. The second flow rate, 1000 ml/min, is a typical flow rate for a well functioning vascular access [15]. The last flow rate, 1500 ml/min, simulates the high flow rate range where no problems appear to perform efficient hemodialysis, but some patients suffer from ischemia, arterial steal or increased cardiac load [15] [31].

The aim of the study is the investigation of the influence of the hemodialysis circuit on the hemodynamics in the vascular access. $Q_{R,0}$ is the control state, it exists in clinic when the access is punctured, but the pump of the dialysis machine is stopped. The five different flow rates in the extracorporeal circuit have a different impact on the hemodynamics in the access.

Diastolic velocity [m/s]

Q_G	500 ml/min		1000 ml/min		1500 ml/min	
	average	range	average	range	average	range
AI	0.59	0.27 - 0.76	2.03	1.96 - 2.09	3.50	3.39 - 3.57
AA	0.58	0.26 - 0.91	1.72	1.25 - 2.08	3.27	2.86 - 3.57
VA	0.35	0.30 - 0.39	0.78	0.71 - 0.92	1.02	0.42 - 1.40
VO	0.37	0.33 - 0.43	0.74	0.60 - 0.92	1.37	1.32 - 1.40

Mean velocity [m/s]

Q_G	500 ml/min		1000 ml/min		1500 ml/min	
	average	range	average	range	average	range
AI	1.31	1.30 - 1.33	2.64	2.60 - 2.66	3.98	3.96 - 3.99
AA	1.30	1.28 - 1.32	2.62	2.60 - 2.66	3.99	3.96 - 4.00
VA	0.59	0.57 - 0.60	1.17	1.14 - 1.20	1.76	1.73 - 1.78
VO	0.59	0.58 - 0.60	1.18	1.16 - 1.19	1.76	1.76 - 1.77

Systolic velocity [m/s]

Q_G	500 ml/min		1000 ml/min		1500 ml/min	
	average	range	average	range	average	range
AI	2.09	1.90 - 2.35	3.26	3.16 - 3.40	4.49	4.22 - 4.69
AA	2.06	1.88 - 2.45	3.50	3.25 - 3.81	4.70	4.43 - 5.12
VA	0.99	0.89 - 1.14	1.70	1.54 - 1.84	2.74	2.27 - 3.78
VO	0.79	0.74 - 0.83	1.59	1.45 - 1.79	2.20	2.10 - 2.37

Δv [m/s]

Q_G	500 ml/min		1000 ml/min		1500 ml/min	
	average	range	average	range	average	range
AI	1.50	1.14 - 1.84	1.22	1.16 - 1.45	0.99	0.66 - 1.25
AA	1.48	0.98 - 2.18	1.79	1.17 - 2.56	1.44	0.86 - 2.26
VA	0.64	0.51 - 0.84	0.92	0.74 - 1.12	1.73	0.88 - 3.36
VO	0.42	0.31 - 0.50	0.85	0.53 - 1.18	0.82	0.70 - 1.05

Table 8.2: Diastolic, mean and systolic velocities, in m/s, at the arterial inlet, arterial anastomosis, venous anastomosis and venous outlet

All measured pressure drops decrease with increasing roller pump flow rate whereas the venous pressure increases due to the supplied energy by the roller pump.
When the mean pressure drop between the needles is considered, it can be remarked that the mean pressure drop between the needles at $Q_{R,0}$ and $Q_{G,500}$ is 6.32 mmHg in contrast to 1.08 mmHg at $Q_{R,500}$ and $Q_{G,1000}$ although the flow rate in between the needles is identical, i.e. 500 ml/min. The same phenomenon can be noticed for $Q_{R,0}$ and $Q_{G,1000}$, the mean pressure drop is here 8.6 mmHg compared to only 5.4 mmHg for $Q_{R,500}$ and $Q_{G,1500}$ although the flow rate is 1000 ml/min in between the needles in both cases. This experience is obvious because energy is supplied to the graft at the venous needle with the flow coming from the artificial kidney and the roller pump.
Two general trends can be observed in figure 8.5. For first: the lower the access flow rate, the lower the pressure drop for a fixed roller pump flow rate. Secondly the pressure drop decreases with an increasing roller pump flow rate for a fixed graft flow rate. The mean pressure drop at $Q_{G,500}$ and $Q_{R,500}$ is negative, indicating a pressure jump over the graft and resulting in a mean venous pressure at the proximal vein that rises above the mean arterial pressure at the arterial anastomosis. If systolic, mean and diastolic pressure drops from AN till VN are negative, the intra-graft pressure at the VN is continuously higher than the intra-graft pressure at the AN. Wat occurs, is the jet pump effect, see appendix.
The lowest absolute venous pressures (systolic, diastolic and mean) are observed at the highest access flow rate: 1500 ml/min. Mean venous pressure is around 40 mmHg, diastolic pressure around 30 mmHg and systolic pressure 50 mmHg. The venous pressure increases with decreasing access flow rate because the corresponding pressure loss over the model is lower at a lower graft flow rate and that pressure loss is subtracted from a fixed level at the AI. At $Q_{G,1000}$ and $Q_{R,200}$, mean venous pressure is 60 mmHg (diastolic venous pressure is 20 mmHg and systolic venous pressure 70 mmHg) and increases to 75 mmHg at $Q_{R,500}$ (diastolic pressure is 50 mmHg and systolic pressure 95 mmHg). At a graft flow rate of 500 ml/min and a roller pump flow rate of 200 ml/min, mean venous pressure is 80 mmHg (diastolic venous pressure is 60 mmHg and systolic pressure is 100 mmHg) and at $Q_{R,500}$, mean venous pressure is increased to 100 mmHg (diastolic venous pressure is 70 mmHg and systolic venous pressure 120 mmHg). These results indicate that the high roller pump flow rates (400-500 ml/min), in combination with low access

flow rates submit the vein to extremely high pressures. The pressure rise in venous pressure is acceptable at the lower roller pump flow rates of 200 and 300 ml/min. The results confirm that a well functioning vascular access, with a flow rate above 600 ml/min [15] [145] is necessary to protect the vein from hypertension. According to the pressure results one would conclude that the highest access flow rate leads to the most advantageous hemodynamics in the graft. The disadvantage of the high access flow rate however is the presence of high wall shear stress values that develop [34] [129] and that are possibly initiators of intimal hyperplasia leading to stenosis development [32].

The venous pressure is high at low access flow rates. If the low flow rate originates from a central vein stenosis, there will exist a pressure drop over that stenosis and the cardiac preload pressure will have decreased due to the pressure loss in the venous traject and the pressure drop over the stenosis [43]. If the low flow rate originates in inflow restrictions e.g. because of a small feeding artery diameter, there exists only the pressure drop in the venous traject. This means that central venous pressure can remain high, cause an increased cardiac preload and reduce the venous drainage that can be the cause of oedema [16] [31]. If a patient suffers from the complications described above, he/she should be referred to provide him/her of a patent graft as soon as possible.

The velocity measurements show a decreased diastolic and an increased systolic velocity at the arterial anastomosis compared to the arterial inlet and at the venous anastomosis compared to the venous outlet. This increased Δv at the anastomosis indicates a disturbed flow pattern and that disturbed flow can be responsible for the vessel wall thrill [86] [87]. No trend with increasing Q_R could be observed in the velocity measurements; systolic, diastolic and mean velocity values are distributed around an average value.

Knowledge of the mean roller pump flow rate and the internal needle diameter make it possible to estimate the mean fluid velocity in the needle. It is 4.15 m/s for a roller pump flow rate of 500 ml/min. The mean graft flow velocity downstream the venous needle at an access flow rate of 500 ml/min is only 0.29 m/s. The jet flowing out of the venous needle has to be decelerated and that energy has to be dissipated. The wall shear stress at the venous needle is 77 Pa and the shear rate 20724 s^{-1} with the assumption of a constant dynamic viscosity of 3.5 mPa.s and

that Poiseuille flow has developed in the needle which is not the case [150]. The calculation can be found in appendix 2. Such high wall shear stresses and shear rates are typically found in stenotic vessels [33]. The acute hemolysis treshold (wall shear stress above 200 Pa [80]) does not occur but leukocyte and platelet activation is plausible [79] [76] [75] [77] [146]. Moreover the graft is a polymeric material where platelet activation increases with increasing blood flow rate [149].

In the near future, this experimental setup will be complemented with a three dimensional computational fluid dynamics (CFD) study that allows to study the flow field in detail in the near environment of the needles and downstream the venous needle. It also will make it possible to calculate the maximum wall shear stress values and the exposure times and compare them to the critical values for red blood cell damage [80].

8.5 Conclusion

In conclusion our experimental results indicate that high roller pump flow rates (400 and 500 ml/min) should be avoided in vascular accesses with a low flow rate because this combination leads to high venous pressures and provokes recirculation. A second drawback of the high roller pump flow rates is the high wall shear stresses introduced in the system allowing leukocyte and platelet activation. This in vitro study offers measurement data to create and validate a CFD study.

8.6 Appendix 1

Figure 8.6 shows a schematic representation of a needle placed in a vascular access graft. The fluid leaves the needle with velocity v_n. The velocity of the fluid that surrounds the needle is v_1. The pressure at the central opening of the needle is p_1. The cylindrical surface of the needle is A_n. The velocity of the fluid more downstream is v_2 and the pressure is p_2. The cylindrical surface of the vascular access graft is A_G. The control volume used to calculate the mass and momentum conservation equation is the gray striped box. The normal on this control volume is $\overrightarrow{n}$.

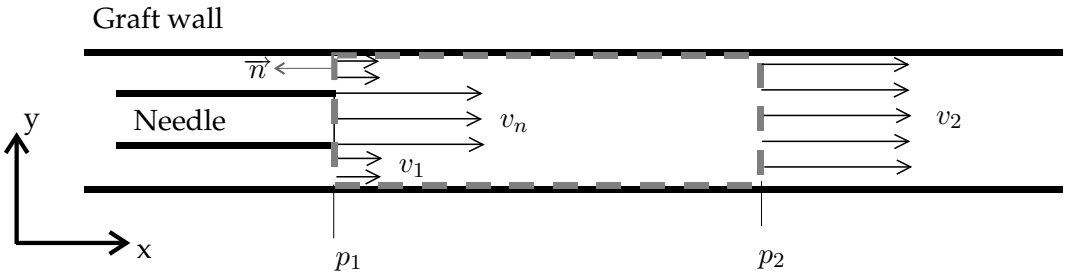

Figure 8.6: Schematic representation of the needle placed in the vascular access graft. The fluid leaves the needle (cilindrical surface A_n) with velocity v_n, and the velocity of the fluid around the needle is v_1. The velocity of the fluid downstream in the graft (cilindrical surface A_G) is v_2. The striped gray box indicates the control volume.

The mass conservation equation gives:

$$\int_S \rho \overrightarrow{v}.\overrightarrow{n}\, dS = 0 \tag{8.2}$$

$$-v_n \rho A_n - v_1 \rho (A_G - A_n) + v_2 \rho A_G = 0 \tag{8.3}$$

$$v_2 = v_1 \frac{A_G - A_n}{A_G} + v_n \frac{A_n}{A_G} \tag{8.4}$$

$$v_2 = v_1 \left(1 - \frac{A_n}{A_G}\right) + v_n \frac{A_n}{A_G} \tag{8.5}$$

The impuls conservation equation is:

$$\frac{\delta}{\delta t} \int_V \rho \overrightarrow{v}\, dV + \int_S \rho \overrightarrow{v}\, \overrightarrow{v}.\overrightarrow{n}\, dS = \overrightarrow{F} \tag{8.6}$$

When only mean velocities and pressures are considered, the first term in the equa-

tion drops out. There exist only velocities in the x direction. Therefore, the impuls conservation equation will be projected on the x axis. This results in:

$$\rho A_n v_n^2 + \rho v_1^2 (A_G - A_n) - \rho v_2^2 A_G = (p_2 - p_1) A_G \tag{8.7}$$

$$\tag{8.8}$$

After substitution of 8.5 in 8.7, the equation for the pressure difference ($\Delta p = p_2 - p_1$) becomes:

$$\Delta p = \rho \frac{A_n}{A} (v_n - v_1)^2 \left(1 - \frac{A_n}{A}\right) \tag{8.9}$$

The venous needle velocity v_n and the velocity of the flow around the needle (v_1) at cross section 1 are related to the blood flow rate through the artificial kidney (Q_r) and the flow rate in between the needles (Q):

$$v_n = \frac{Q_r}{A_n} \tag{8.10}$$

$$v_1 = \frac{Q}{A - A_n} \tag{8.11}$$

The pressure difference ($p_2 - p_1$) calculated with 8.9 for the different Q_r and Q values is presented in figure8.7

Qr [ml/min]	Q [ml/min]	p [mmHg]
0	0 ml/min	
100	0 ml/min	0.58
200	0 ml/min	2.32
300	0 ml/min	5.21
400	0 ml/min	9.27
500	0 ml/min	14.48
0	500 ml/min	
100	500 ml/min	0.14
200	500 ml/min	1.30
300	500 ml/min	3.62
400	500 ml/min	7.10
500	500 ml/min	11.73
0	1000 ml/min	
100	1000 ml/min	0.00
200	1000 ml/min	0.58
300	1000 ml/min	2.32
400	1000 ml/min	5.21
500	1000 ml/min	9.27

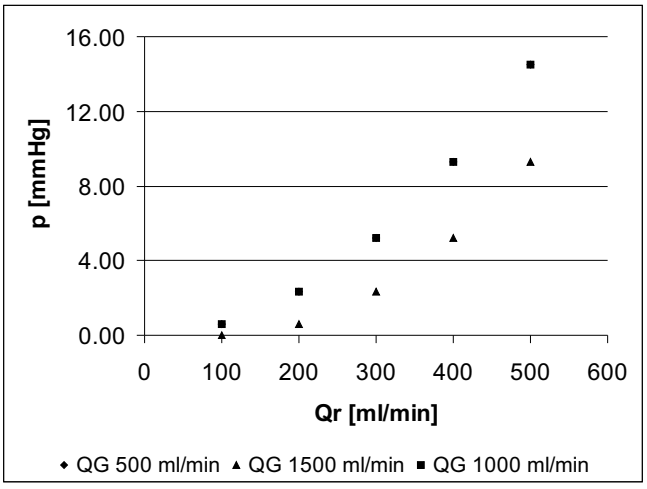

Figure 8.7: The pressure increase due to the jet pump effect of the flow leaving the venous needle

8.7 Appendix 2

The diameter (D) of a 15 Gauge needle, corresponds to an inner needle diameter of 1.60 mm and a flow surface of 2.01mm^2 calculated with the formula:

$$A = \frac{\Pi D^2}{4}$$

For a given mean flow rate (Q) through the needle, we can calculate the mean velocity of the flow in the needle with the formula:

$$v = \frac{Q}{A}$$

For a mean roller pump flow rate of 500 ml/min, we become a mean velocity of 4.15 m/s.
When Poiseuille flow in the needle is assumed, wall shear stress becomes:

$$WSS = \frac{32\mu Q}{\pi D^3}$$

For the mean roller pump flow rate of 500 ml/min and the diameter of 1.60 mm and a dynamic viscosity (μ) of 3.75 mPa.s the result is 77 Pa. The shear rate $\frac{dv}{dy}$ is 20724 s^{-1} and can be calculated as:

$$\frac{dv}{dy} = \frac{WSS}{\mu}$$

Chapter 9

An Improved dialysis needle design

9.1 Introduction

End stage renal disease patients referred to hemodialysis therapy undergo regularly, about three times a week, blood purification sessions. The necessary entry to the blood circulation is gained at the vascular access which is created with an autogenous or non-autogenous fistula or a catheter. Both, the vascular access creation and the hemodialysis sessions, are associated with complications and risks.

The first source of complications and risks is the construction of the vascular access. A surgical intervention is necessary to create in the patient a peripheral blood vessel with a blood flow rate above 500 ml/min that allows blood flow rates of 350 ml/min through the artificial kidney during the hemodialysis session. If an autogenous fistula is constructed, only native vessels are used to construct the vascular access. When only poor native vessels are available, the surgeon's choice often goes to a polytetrafluorethylene (PTFE) graft, which is a body foreign material and that can result in inflammation or allergic reactions.
A complication which is often encountered in hemodialysis vascular accesses, is intimal hyperplasia initiation followed by stenosis development and in the worst case by thrombosis formation.

During the hemodialysis session, the vascular access flow is disturbed by the blood flow towards (at the arterial needle) and from (at the venous needle) the ar-

tificial kidney. To limit the blood damage and vascular access flow disturbance, the needle design of importance. Limited information on needle design is available in literature. A literature survey highlights that (i) the velocity difference between the flow coming out of the venous needle and the flow inside the graft should be limited. Zarate et al. [157] therefore introduced a needle design with flow dividers at the back eyes. (ii) Other studies indicate that the maximal shear stress (SS) should be restricted as it may lead to hemolysis [78] [79] [80]. (iii) A third consideration is the limitation of the infection risk associated with needle punctures. This evokes in vivo tests and is, consequently, out of the scope of this study.

The aim of this work is to design with CFD a novel dialysis needle with an improved flow distribution and a reduced hemolysis risk compared to existing; commercially available needles.

9.2 Methods

9.2.1 The considered geometries

Commercially available needles

Two needle groups are today available on the market: cutting edge needles, already used since years in daily clinical practice, and blunt edge needles, the last years introduced in clinic together with the ”buttonhole” technique [156]. In a first step, the needle geometry of each type, of the same gauge size (15G - inner diameter 1.5 mm), was assessed to compare the hemodynamics inside and around the needles. A 15G sharp edge needle (Dispomed® Geinhausen, Germany) and a 15G blunt edge needle (Nipro, Zaventem, Belgium) were studied under the microscope in order to determine the needle geometry. The major dimensions of both needles are illustrated in figure 9.1. The term ”central opening” refers to the opening at the end of the needle where the ”back eye” concerns the opening in the needle wall. The central opening and back eye design of both needles is different as can be observed in figure 9.1 and table 9.1.

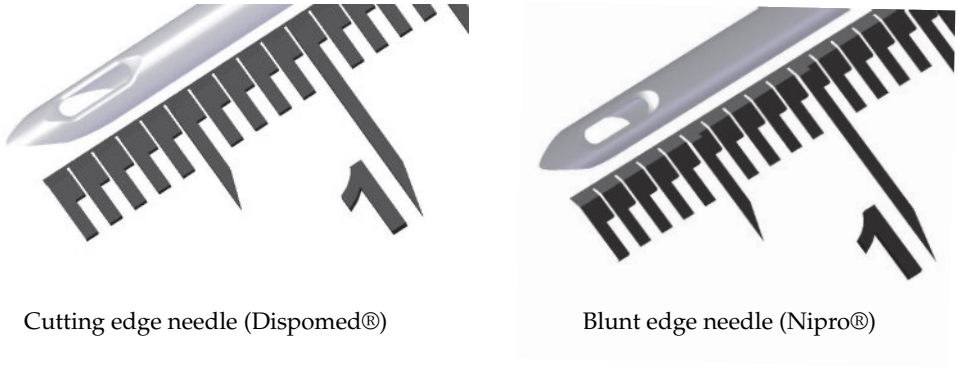

Cutting edge needle (Dispomed®) Blunt edge needle (Nipro®)

Figure 9.1: The dimensions of the cutting and blunt edge needles used in the simulations

Novel dialysis needle

The results of both commercially available needles showed some hemodynamic drawbacks that will be explained later. In an attempt to reduce these drawbacks, simulations were performed on a virtual prototype, cutting needle: prototype 1. This needle, see figure 9.2, has an oval shape at the puncture site that changes into a cylindrical shape at the tube fitting. The smallest inner diameter of the oval is 1.5 mm, like the inner diameter of the 15G needles and the largest inner diameter is 2 mm. The inner diameter of the cylindrical part is 2mm. The design length of the needle is 30 mm. Five different alternatives are designed. The part of the needle wall that is cut out has an egg shape, see figure 9.2, is fixed in the five designs, but the location and the number of back eyes varies. The first needle is the reference needle without any back eye. Next, there are two needles with a back eye placed like the back eyes in the commercially available needles. The difference between both is the distance between the needle tip and the back eye. A fourth needle has two back eyes opposite to the central hole and the last needle has two side eyes. All needles are represented in figure 9.2.
The openings opposite to the central opening will be referred to as “back eyes” and the openings orthogonal to the central opening, will be called “side eyes ”.

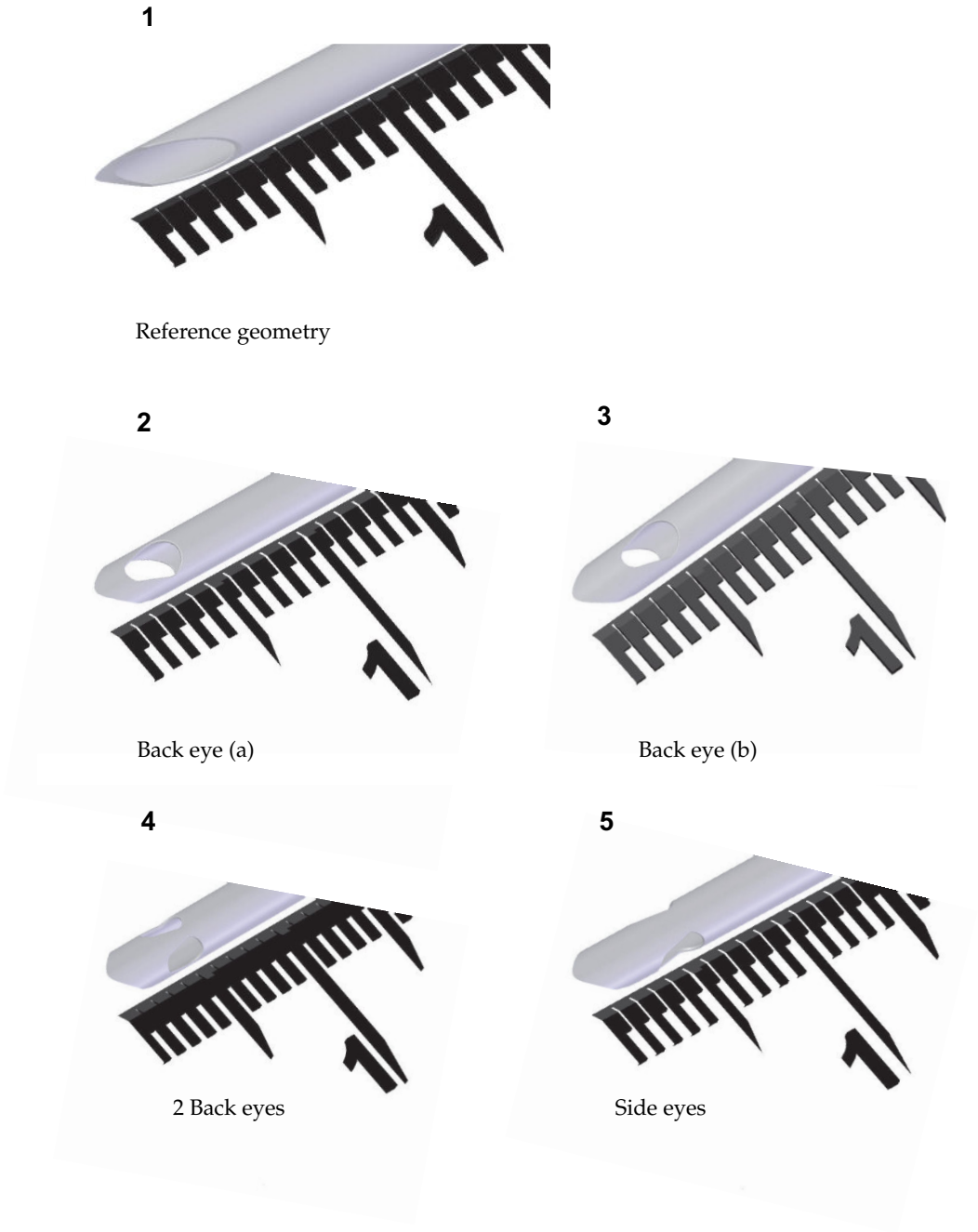

Figure 9.2: The dimensions of the five designs of the prototype 1 needles used in the simulations

The simulations performed with these five needle geometries showed some hemodynamic advantages of the new configuration that are summarized in the results part. The drawback, however, is that several parameters were changed simultaneously in one geometry. Therefore, we disected the study into different substudies, where the impact of changing one parameter at a time was assessed.
First the influence of the diameter is investigated. A 15G needle is compared to a 13G needle, both without back eyes. In a second step, the influence of the side eye position is investigated. The position varied from 5 mm distance between the needle tip and het center of the first hole to 6.5 mm in steps of 0.25 mm. The side eye geometry is identical to the side eye geometry in the prototype 1 needle.
As last, the influence of the side eye geometry is considered. The reference side eye geometry is still the geometry used in the prototype 1 needle. Alternative 1 is based on the largest diameter of the reference geometry and alternative 2 on the smallest diameter, see figure 9.3.

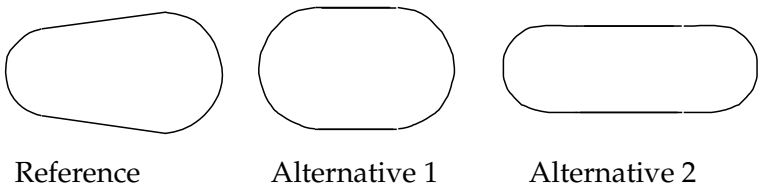

Figure 9.3: The geometry of the alternative side eyes. The reference geometry is identical to the geometry of the side eyes of the VTPrik needle. Alternative 1 is based on the largest diameter of the reference geometry and Alternative 2 on the smallest diameter.

All needles are simulated in the loop graft geometry, previously described in [34]. The needles are placed at exact the same locations as in the in vitro model where this numerical model is validated with [155]. This means that the first needle is placed 10 cm downstream the arterial anastomosis and the venous needle 9 cm downstream the arterial needle. The distance between the venous needle and the venous anastomosis is 12 cm. Both needles are placed so that the blood nicely can flow in and out the needle, without making a 180° turn. The angle between the needle axis and the graft axis is 10° for all needles simulated. The needles tips are 1 cm inside the vascular access. The needle is placed so that the needle tip is close to the upper graft wall. The needles are placed like in the vascular access of a hemodialysis patient. The needle is placed this way in vivo to avoid vessel wall damage. Blood can leave the vascular access through the arterial needle outflow

Neelde type	inner diameter [mm]	outer diameter [mm]	eye geometry	eye position [mm]	cutting/ blunt
Cutting needle	1.5	1.85	oval slot	2.55	cutting
Blunt needle	1.8	1.8	oval slot	2.45	blunt
prototype 1 (reference)	oval (1.5-2)	oval (1.9-2.3)	N/A	N/A	cutting
prototype 1 (back eye a)	oval (1.5-2)	oval (1.9-2.3)	egg shape	2.5	cutting
prototype 1 (back eye b)	oval (1.5-2)	oval (1.9-2.3)	egg shape	3.5	cutting
prototype 1 (side eyes)	oval (1.5-2)	oval (1.9-2.3)	egg shape	5	cutting
prototype 1 (2 back eyes)	oval (1.5-2)	oval (1.9-2.3)	egg shape	4	cutting
13G reference	2	2.3	N/A	N/A	cutting
15G reference	1.5	1.8	N/A	N/A	cutting

Table 9.1: Overview of the dimensions of the different needles.

and is returned to the vascular access via the venous needle inlet.

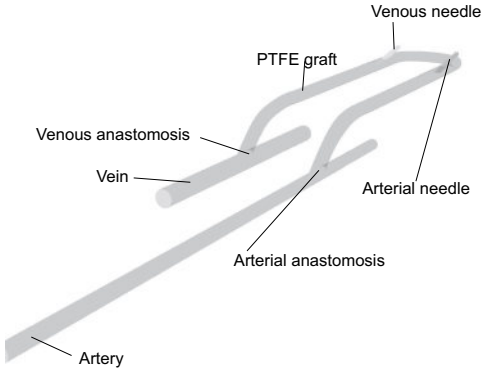

Figure 9.4: The positions of the arterial and venous needle in the graft geometry.

9.2.2 The mesh

The mesh for the computational fluid dynamics (CFD) simulations is made in the software package Gambit 2.0.4 (Fluent, Sheffield, UK).
A disturbed flow pattern can be expected where the arterial needle flow is separated from the graft flow and where the venous needle flow joins the graft flow. The hemodynamics in the direct environment of the needles are of special intrest in this study. Therefore a dense and unstructured mesh is applied in this region. The mesh size of the face meshes is set to 0.05 mm on the central opening and the back eyes. To change gradually to a coarser mesh at a distance of the openings, the inner volume of the needle and the volume surrounding the outside of the needle

are submitted to a size function. The initial volume size is 0.05 mm, the growth factor was set to 1.1 and the maximum size is limited to 0.33 mm.

9.2.3 The preprocessing and postprocessing

The governing equations for the isothermal incompressible unsteady flow are the mass (9.1) and momentum (9.2) conservation equations.

$$\nabla \cdot \overrightarrow{v} = 0 \tag{9.1}$$

$$\frac{\delta \overrightarrow{v}}{\delta t} + (v \cdot \nabla)\overrightarrow{v} = \frac{1}{\rho}(-\nabla p + \nabla \cdot \overline{\overline{SS}}) \tag{9.2}$$

$\overrightarrow{v}$ is the velocity vector, p is the pressure, ρ is the density and $\overline{\overline{SS}}$ is the stress tensor. The governing equations are solved using CFD and the software package Fluent 6.1.18 (Fluent, Sheffield, UK).
Blood is modelled as a non-Newtonian fluid. The dynamic viscosity of blood depends on the strain rate, the hematocrit level and the plasma viscosity. The Quemada viscosity model [7] [8] is programmed in the fluid domain to incorporate this parameter dependent behavior.
All simulations are carried out steady state and the solution was considered converged when the residuals have decreased three decades. The pressure discretization scheme is second order and the momentum discretization scheme second order upwind. The pressure-velocity coupling scheme is SIMPLE.
The boundary condition at the arterial inlet and venous needle inlet is ”velocity inlet”. The boundary conditions set at the sites where blood leaves the vascular access is ”outflow”. The flow rate inside the vascular access is 500 ml/min in all cases simulated. The needle flow rates are set either to 200 (low) or 500 ml/min (high).

9.2.4 Flow distribution and the general hemodynamics

The percentage of flow that is aspirated via the central opening of the arterial needle is compared to the percentage of the flow that is aspirated through the back eyes. Similarly, the percentage of the flow that is returned through the back eyes of the venous needle is compared to the percentage returned through the central

opening.

9.2.5 Hemolysis estimation

This computational fluid dynamics (CFD) study will focus on the one hand on the flow and pressure distribution in needles, and the vascular access, and on red blood cell damage on the other hand.

The hemolysis risk can be verified in in vitro set ups by measuring the free plasma hemoglobin ($dPHb$). Wurzinger et al. [160] performed in vitro experiments and quantified the red blood cell (RBC) damage. The experiments showed that the damage depends on time that the RBC is exposed to a certain shear stress level. Giersiepen et al. [158] performed a two-dimensional regression analysis on the experimental data and expressed a formula to calculate the hemolysis index.

$$HI = 3.62^{-5} t^{0.785} SS^{2.416} \tag{9.3}$$

The Giersiepen equation shows that the hemolysis index is more than quadratically dependent on the shear stress (SS [Pa]) and less than linear dependent on the exposure time (t [s]). Recent experiments have shown that the Giersiepen equation overestimates the HI with one order of magnitude. However, the equation maintains its value as it is a tool to compare different geometries. The Giersiepen equation is the basis of the hemolysis index calculation in this work. The Giersiepen equation is up till now the only quantitative equation available to express the hemolysis index.

When blood passes through an extracorporeal system, the shear stress where the RBCs are exposed to and the exposure time depend on locations where the blood cell passes along their path lines. When blood passes the needle e.g., the RBCs are exposed for only a short period to high shear stresses. When the blood passes the fibers of the artificial kidney in the contrary, it is for a longer period subjected to low shear stress values.
Goubergrits et al. [161] have introduced the principle that the red blood cell damage is irreversible, but damage can be partial, it is not a all or none process.

The procedure to calculate the hemolysis index contains two steps.
The first step, is the calculation of the flow field. The flow field is calculated with

steady boundary conditions.
When the solution is converged, the flow equations are switched off and particle injections are defined on the central opening and the eye(s) of the arterial needle. The particle diameter is set to 6 μm, a representative value for the diameter of red blood cells. Subsequently the solver is switched to the unsteady solver. The interaction between the discrete phase and continuous phase is switched on. Next the time step is chosen so that the particles jump from cell to cell, no cells are skipped. In our simulations, this resulted in a timestep of 0.2 ms. The number of time steps is set so that a particle with the maximal velocity can travel through the whole needle. Then, the inverse of the flow field is patched onto the mesh and particles are released again with the same timestep and for the same number of timesteps. For each particle, the HI is calculated with (9.3). When the hemolysis index reaches 1 for a particle, the HI for that particle is fixed to 1. The final HI for the arterial needle is the average HI value.
The whole procedure is repeated for the venous needle.

9.3 Results

9.3.1 Flow division and hemolysis index

The results for flow division and hemolysis index in the different investigated needles is shown in figures 9.5, 9.6, 9.7 and 9.8.

Cutting versus blunt needle

Flow distribution It can be observed that the flow division in the **venous needles** is comparable: 98.5% of the flow is sent through the central opening of the blunt needle whereas 95% is sent through the central opening of the cutting edge needle. The flow through the back eye is negligible for both needles. This is observed for both blood flow rates through the artificial kidney
When the **arterial needle** is considered, it should be remarked that the majority of the flow still passes through the central opening: 77% for the blunt needle and 58% for the cutting edge needle. Nevertheless, for both needles, the contribution of the back eyes to the flow distribution is significant.

Hemolysis index The HI is higher in the blunt **arterial needle** at $Q_{b,500}$ compared to the cutting arterial needle. The opposite is valid in the arterial needles at $Q_{b,200}$. For the **venous needles**, the same trend can be observed at $Q_{b,200}$ and $Q_{b,500}$: the HI in the cutting edge needle is lower compared to the HI in the blunt needle.

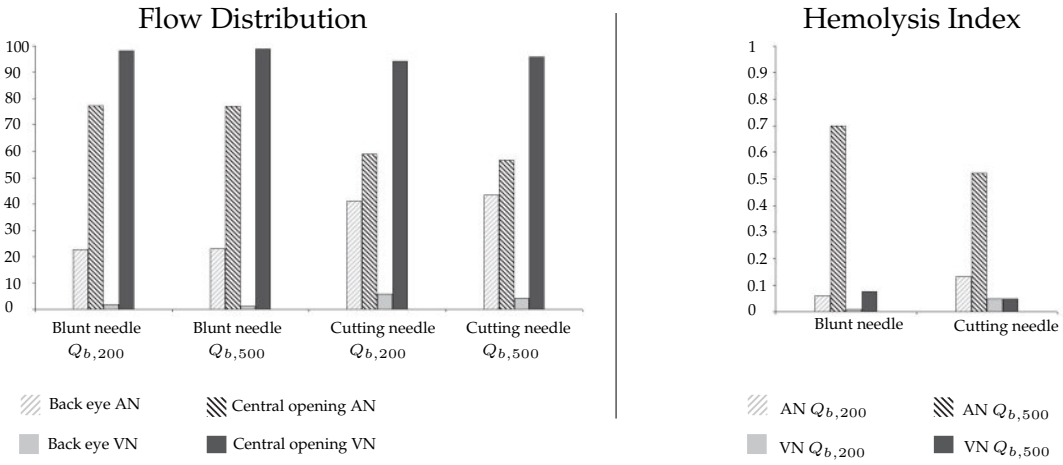

Figure 9.5: The flow distribution and the hemolysis index in the commercially available needles

prototype 1 needle design

Five different geometries are considered: (i) the reference needle without back eyes, (ii) the needle with back eye location a, (iii) the needle with back eye location b, (iv) the needle with 2 side eyes and (v) the needle with two back eyes.

Flow distribution The flow distribution graphs clearly show that the flow distribution in the **arterial needle** strongly depends on the back eye geometry and number. When only one back eye is present, the percentage of the flow going through the back eyes varies between 36 and 54.7%. When two back eyes or two side eyes support the flow through the central opening, the percentage increases: 73% at $Q_{b,200}$ and 83% at $Q_{b,500}$ for the needle with two side eyes and 50% at $Q_{b,200}$ and 65% at $Q_{b,500}$ for the needle with two back eyes.
The back eye(s) or side eyes contribute for less than 10% in the **venous needles** and this is independent from the blood flow rates.

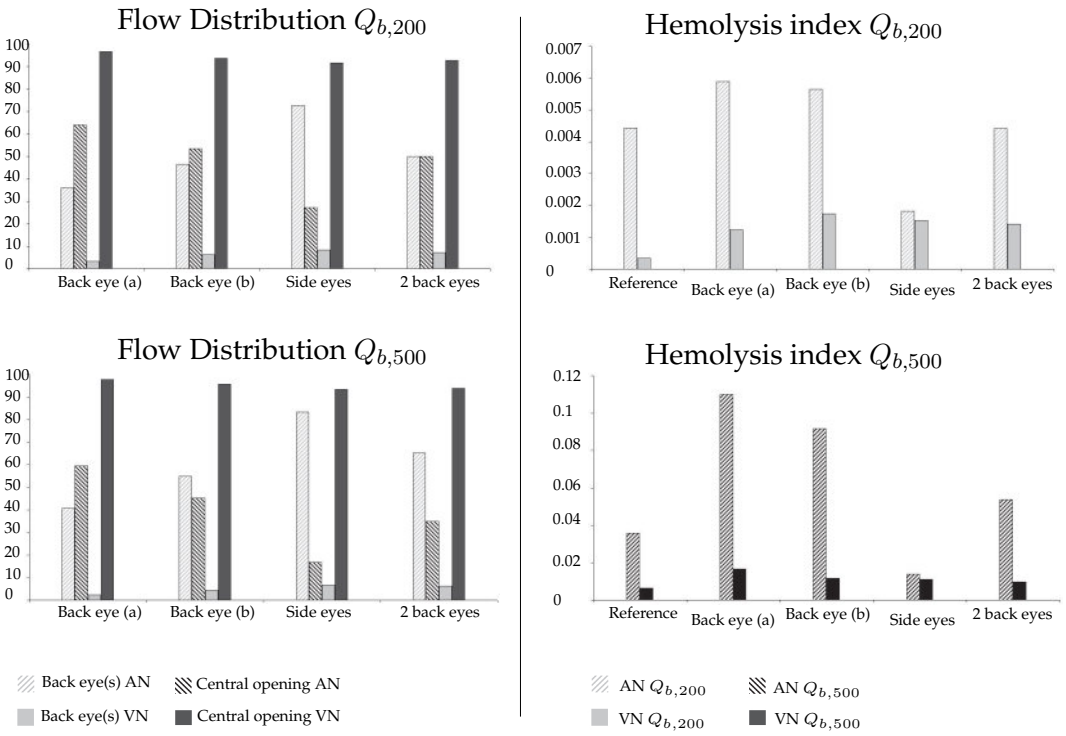

Figure 9.6: The flow distribution and the hemolysis index in the VTPrik needles

Hemolysis index The hemolysis indexes for the arterial and venous needles at $Q_{b,200}$ and $Q_{b,500}$ are shown in the right panels of figure 9.6. The trend is independent from the blood flow rates but the absolute values differ. When the **arterial needle** is considered first, it is clear that the lowest HI is present in the needle with two side eyes. All other needle designs show considerably higher HIs. For the **venous needle**, it is the reference needle that has the lowest HI.

The arterial needle with side eyes shows the lowest hemolysis index of all arterial needles. Therefore, the needle with side eyes will be investigated in the next part of the study.

13G needle with side eyes compared to 15G needle with side eyes and the influence of the side eye position

It was clear from the previous simulations that the flow division is little dependent on the blood flow rate and that the highest hemolysis indexes are encountered

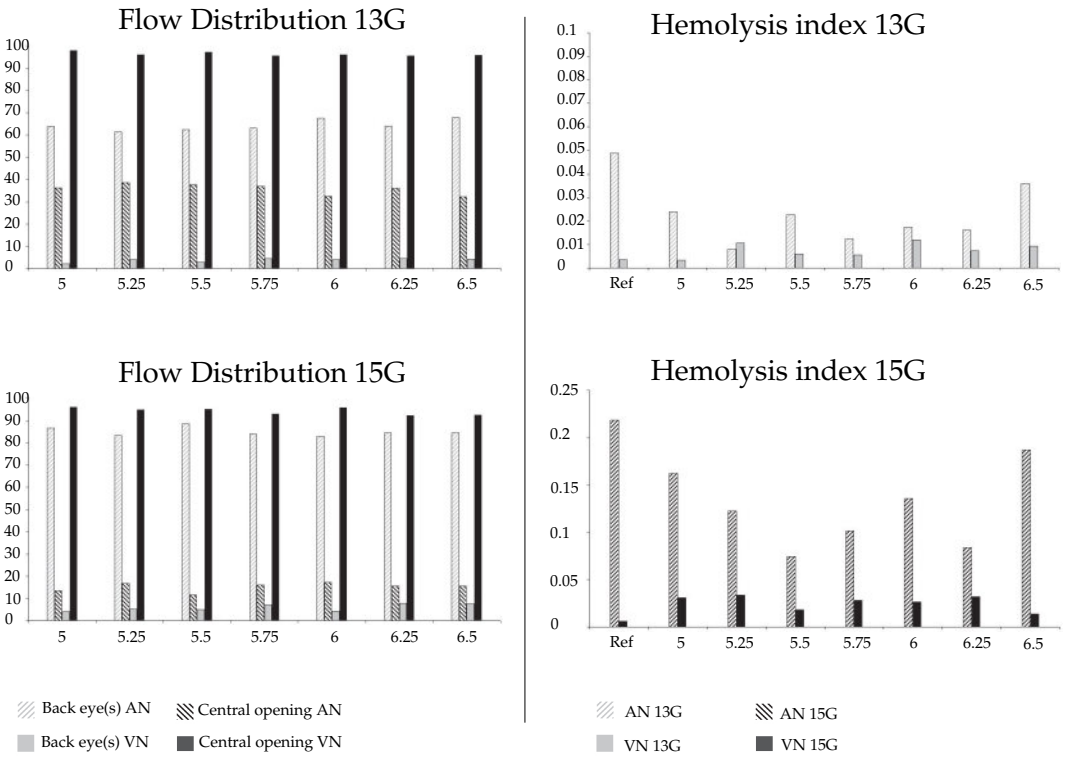

Figure 9.7: The flow distribution and the hemolysis index in the 13G and 15G needles

at $Q_{b,500}$. Therefore the simulations to investigate the influence of the side eye position are only executed for $Q_{b,500}$.

Flow distribution The flow distribution in the arterial 13G needle varies limited depending on the side eye position: between 61.4 and 68% of the flow enters the **arterial 13G needle** through the side eyes. The flow distribution in the **venous 13G needle** also varies limited: between 92.2 and 96.1% of the flow leaves the VN through te central opening.

The absolute values of flow distribution differ in the 15G needle, but the trend is similar: the flow distribution varies only little for two different side eye positions. Between 82.8 and 88.5% of the flow enters the **arterial 15G needle** through the side eyes of the arterial needle and between 92.2 and 96.1% of the flow leaves the **venous 15G needle** through the central opening.

Hemolysis index The HI calculations in both **arterial needles**, the 13G and 15G needle, show that the highest HIs are found in the reference needle and the needle with side eye position at 6.5 mm. The interjacent needle positions show the lowest HIs. The opposite is true for the **venous needles**: the reference needles show the lowest HIs.

The 15G needle has the lowest HI for the needle with side eyes at 5.5 mm. The 13G needle with side eyes at 5.5 mm has not the lowest HI, but notwithstanding a low HI value. Therefore, the side eyes were placed at 5.5 mm from the needle tip in the next substudy.

Influence of the side eye geometry

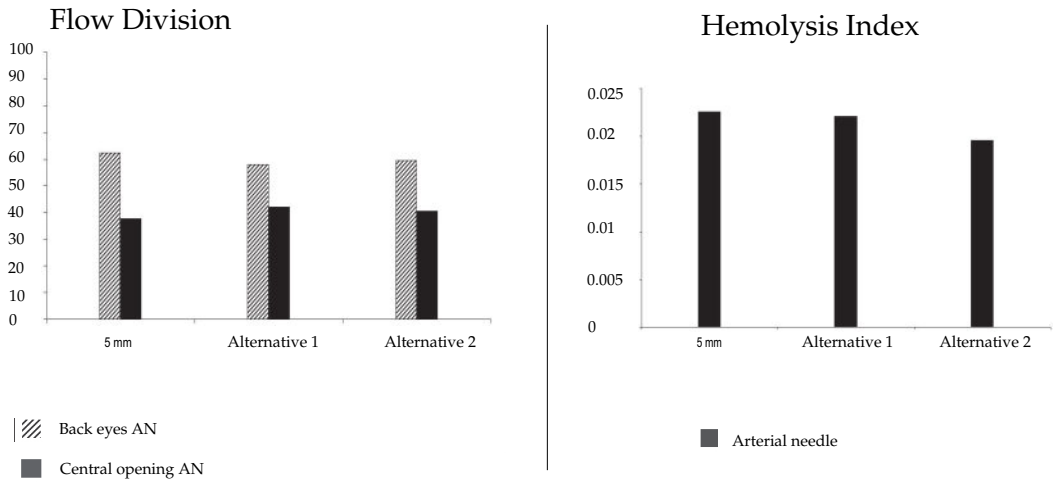

Figure 9.8: The flow distribution and the hemolysis index in the two alternative needle designs with beginning of the side eye at 5.5 mm

It is clear from the previous studies that the **arterial needle** is the needle with the highest HI values and that the HI is considerably lower in the 13G needle compared to a 15G needle. The 13G needle with side eye position at 5.5mm is compared to two alternative side eye designs. All needles are simulated at $Q_{b,500}$. The flow division alters between 58 and 62.4%. The hemolysis index is 0.023 in the AN with side eye at 5.5mm, alternative 1 has a HI of 0.022 and alternative 2 has the lowest HI: 0.020. The results are shown in figure 9.8.

From this study can be concluded that alternative 2 is the optimal side eye geometry.

9.3.2 The intragraft pressure at the venous needle

Two flows merge at the venous needle: the part of the flow that was not aspirated through the arterial needle and the flow that is pumped through the venous needle into the graft causing a pressure rise after the venous needle. Energy from the extracorporeal system is added to the vascular access at the venous needle. The impact of this energy supply is investigated.
Figure 9.9 shows the pressure distribution in a midplane of the venous 13G needle. The pressures shown are limited between 89 and 96 mmHg. The pressure inside the needle 0.5 cm from the central needle opening is 90.6 mmHg (1); the pressure upstream the venous needle is 89 mmHg (2) and the pressure 4.2 cm downstream the venous needle is 95.2 mmHg (3). The latter value indicates the pressure increases downstream the venous needle.

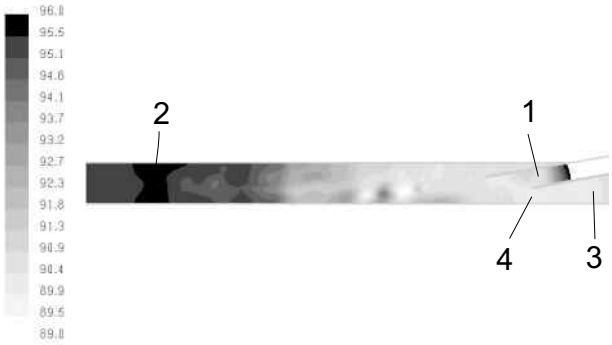

Figure 9.9: The intragraft pressure in a midplane in a cylindrical venous 13G needle

Figure 9.10 shows the corresponding pressure distribution in a midplane in the venous 15G needle. The pressure inside the needle at a distance of 0.5 cm from the central opening is 90.6 mmHg (1). The pressure upstream the venous needle is 90.1 mmHg (2) and the maximal pressure downstream occurs 1 cm after the central opening and amounts 97.5 mmHg (3).

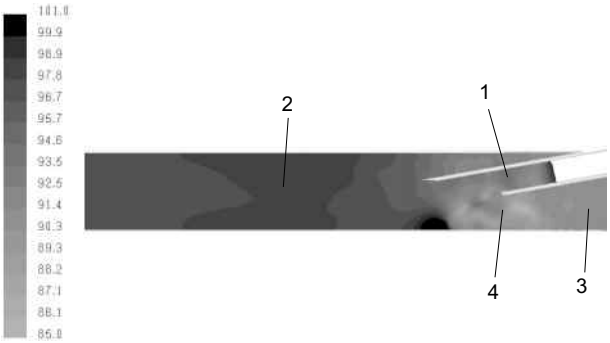

Figure 9.10: The intragraft pressure in a midplane in the cylindrical venous 15G needle

9.4 Discussion

The aim of this study was first the comparison of two commercially available needles concerning the flow division and the hemolysis index. In a second part, new, virtual prototypes of needles are designed and investigated for their performance: flow division and hemolysis index.

The flow distribution and hemolysis index calculated in the commercially available needles is presented in figure 9.5. It is clear that the flow division is dependent on the back eye design in the arterial needle as well as in the venous needle. The flow division in the arterial and venous needle is, however nearly independent of the blood flow rate through the needle.
Despite a nearly identical flow distribution, the hemolysis index differs depending on the needle type, the needle position, and the blood flow rate. The HI increases considerably with an increased flow rate. It can also be observed that the HI in the arterial needles is higher than the HI in the venous needles for both blood flow rates. This means that the flow through the back eyes strongly contributes to the HI as this is the major difference between both needles.

The flow divisions and HIs in the prototype 1 needle are visualized in figure 9.6. It can be observed that the back eye(s) / side eye(s) influence the flow division in the arterial prototype 1 needle. However, these numbers should be interpreted cautiously as the free flow surface in the case of the two back eyes and the two side eyes has increased compared to the single back eyes. Even more, the flow surface in the needle with two side eyes is higher than in the needle with two back eyes.

The needle with the side eyes, which has the highest extra flow surface, aspirates most of the flow through the side eyes. In this needle geometry, the flow division depends on the blood flow rate aspirated.
Nearly all the flow in the venous needle leaves the needle through the central opening just like in the commercially available needles. This is the case for all back eye geometries, which means that only flow dividers would be able to force the flow through the back and side eyes. Flow dividers are introduced by Zarate et al. [157] and force flow through the side and back eyes. On the other hand, there is no important argument to send flow through the back/side eyes of the venous needle. Flow dividers may introduce vortexes and high shear zones inside the needle, especially at blood flow rates of 500 ml/min. Therefore flow dividers were not an option for a new needle design.
The HI in the prototype 1 needle in arterial position has the best hemodynamic outcome with two side eyes for both flow rates. This design combines two advantages. First it has the lowest HI. Secondly, the flow is equally distributed over the three openings: each opening contributes for about 33% to the total flow aspirated. The HI in the venous needle is the lowest in the case of the needle without side eyes.

The simulations described above pointed out that an arterial needle with side eyes has the most beneficial HI and flow division whereas the venous needle without side eyes shows the most beneficial HI.
The drawback of prototype 1 is that it is not easy to fabricate because of its oval shape that gradually increases to a round shape. Therefore, we also simulated cylindrical needles: a 15G and 13G needle with a cilindrical basis. These needles were only simulated with side eyes as the previous simulations showed that this was the optimal configuration. However, the next question that arose was whether the side eye position influences the HI and flow division. This was investigated in the next set of simulations.
The results of the cylindrical 13 and 15G needles with side eyes pointed out that the flow division is nearly independent from the side eye position. The HI however strongly depends on the side eye position. The side eye position at 5.5mm from the needle tip shows an acceptable HI. Therefore, this position is chosen to further optimize the side eye geometry.
In the last set of simulations, the flow surface of the central opening and side eyes is identical, but their geometry is different. The result is that the flow division is nearly identical, but the hemolysis index is the lowest for alternative 2, which

makes this needle the most beneficial arterial needle.
The results concerning the venous needle from the previous set simulations are confirmed: the lowest HI is encountered in the needle without side eyes. It should be concluded that the optimal venous needle is a needle without side or back eyes.

What is remarkable, is the pressure rise that occurs inside the graft downstream the venous needle. There is a pressure rise present because energy is supplied by pumping the flow through the venous needle. This can be calculated with the Bernoulli equation along two stream lines: a first from a point inside the venous needle to the place with the maximum pressure and a second stream line from 1 cm upstream the venous needle to the place with maximum pressure downstream the venous needle. (The complete calculations are added in appendix 1.) The theoretical pressure calculated along the first streamline is 100 mmHg in the 15G needle and 96 mmHg in the 13G needle compared to 97.5 mmHg and 95 mmHg respectively in the CFD simulations. These theoretical calculations approach the CFD calculations very well, but underestimate the pressure losses. The pressure loss along streamline two is negligible; the pressures upstream and downstream both needles is nearly equal. It is clear that the energy supplied by the venous needle causes the pressure rise inside the graft downstream the venous needle.

The major limitation of this study is of course that the results are not validated in vitro with blood. This is the next step to consider. The different needles have to be fabricated and an in vitro set up has to be constructed to measure adequately the flow division and the hemolysis index.

9.5 Conclusion

The results clearly show that in the arterial position a 13G needle with side eyes is the needle with the optimal flow division and lowest hemolysis index. However, the trauma caused by a 13G needle is considerably higher than the trauma caused by a 15G needle. As the 15G needle with side eyes also has the advantage of a low hemolysis index compared to the commercially available needles, but does not cause a considerable trauma, it is advised to test the outcome of 15G needles with side eyes.

Part V

Conclusion and Future work

Chapter 10

Conclusion

A well functioning vascular access is absolutely necessary to perform adequate hemodialysis. The hemodialysis therapy and other renal replacement therapies are explained in chapter 1. A vascular access can be constructed using native vessels or using polytetrafluorethylene graft material. The different vascular accesses are discussed in chapter 3. A typical complication encountered with a graft vascular access is stenosis formation at the venous anastomosis. This stenosis has to be discovered at the time that it starts to limit the flow since thrombosis danger becomes real at low flow rates.

To get insight in the hemodynamics inside a graft vascular access, a physiological relevant in vitro model for a vascular access with a PTFE (polytetrafluorethylene) graft has been created and used to measure pressure and velocity distribution inside the vascular access, chapters 4,6,8. The principal characteristics of this model are that the arterial and venous compliance are respected, that the anastomoses are sutured by a vascular surgeon, and that the pressure and flow waveforms in the model approximate in vivo waveforms reported in literature. An important advantage of in vitro models is that parameters can be altered one by one, something which is definitely impossible in a patient study.

The model is used in three different set-ups. In the first, in detail described in chapter 4, the influence of graft geometry on the hemodynamics, is investigated. A 6 mm graft was compared to a 4-7 mm graft. The major difference between both graft geometries is the pressure drop over the arterial anastomosis, which is higher in the 4-7 graft compared to the pressure drop over the arterial anastomosis of the

6 mm graft. However, as there exists pressure recovery downstream the arterial anastomosis of the 4-7 mm graft, a comparable pressure loss along the graft for both geometries was observed. Both graft models showed similar problems in the vein: the pressure is increased compared to the venous pressure in the normal venous circulation and the flow is still pulsatile in the vein.
In a second study, explained in chapter 6, axial symmetric venous outflow stenoses of different percentages were created in the model and it allowed to investigate the sensitivity of stenosis detection parameters. The newly defined parameter, the pressure ratio appears to be the most promising parameter since this pressure ratio detects all significant stenoses and the stenoses present at a low flow rate. The first available in vivo data, chapter 7, confirm this statement.
A third study assessed the impact of the blood flow through the extracorporeal system, chapter 8. The major outcome was that the pressure inside the vascular access increases with increasing blood flow rate through the extracorporeal system and with a decreasing access flow rate. A well functioning vascular access with an access flow rate above 600 ml/min is absolutely necessary to limit the blood pressure and blood flow rates above 400 ml/min should be avoided in the extracorporeal system.

The second type of studies included in this thesis are the computational fluid dynamic (CFD) studies. The first numerical study, investigated the hemodynamics in a normal functioning vascular access, chapter 5. Wall shear stress values that can cause endothelial damage, platelet and leucocyte activation, and red blood cell damage are observed.
In the second study, chapter 9, we focussed on the hemodialysis needle design, from hemodynamic point of view. Different needles were studied on the flow division and hemolysis index. Two commercially available needles were investigated together with new, virtual designs. It was observed that the back and side eyes strongly influence the flow division and the hemolysis index. The optimal geometry for an arterial needle, the blood withdrawing needle, is a needle with side eyes as the flow is equally divided between the side eyes and the central opening and the hemolysis index is lower than in all other geometries considered. The optimal geometry for a venous needle, the blood returning needle, is a needle without back or side eyes, since the back and side eyes contribute for less than 10% to the total flow and the needles with side and back eyes have a higher hemolysis index compared to the needle without back or side eyes.

This work investigated the hemodynamics in a vascular access by means of a PTFE graft. The vascular access was studied under three different hemodynamic conditions. First, the disadvantages of the 4-7 mm graft were proven. Secondly, a new parameter, the pressure ratio, was formulated to discover significant stenoses. In the last part, the vascular access was assessed under a hemodialysis session, which clarified that an access flow rates of 500 ml/min should be avoided just like blood flow rates of 500 ml/min through the artificial kidney. A proposal for new hemodialysis needles with a reduced hemolysis index is formulated.

Chapter 11

Future prospects

Throughout this whole PhD, both in vivo and in numero, we considered only the under arm. An extension of this work can consist of the development of a model of the complete arm, or even a complete aortic tree with a vascular access in the arm or leg. Such an experimental model could be useful to investigate the potential of the development of steal syndrome or to investigate the effect of a vascular access on the heart.
A further extension, is the development of a compliant in vitro model of a native arterio venous fistula. When these results would be compared to the results of this PhD, the hemodynamic differences between both vascular access types could lead to further insights that explain the different outcome rates for both vascular access types.

The CFD studies included in this thesis show that CFD is complementary to in vitro experiments and offers detailed information about derived parameters like the wall shear stress. The existing models can be extended for fluid structure interaction (FSI) in a first step. This way, the wall movement under the physiologic pressure could be modeled.
When one would have the possibility to include hemodialysis patients into a follow up study, it would be interesting to make a patient-specific model at the access construction. The hemodynamics at this stage can be observed and investigated. When the patient returns a month later to the angiography department, the blood vessels will have remodelled. When a new patient specific model is distilled, the hemodynamics can be computed again. The difference between the hemodynamics in both situations, can probably provide us of factors that initiate vascular remodelling. Especially a long term follow-up study could be very interesting since the

evolution in time of the vessel wall, and the fluid properties could probably clarify stenosis and thrombosis formation, the majority of the reasons of vascular access failure.

Appendix A

Millar pressure transducer, model MPC-500 specifications

Type of sensor	Diffused semiconductor
Type of catheter	polyurethane
Length	70 cm nominal
Size	5F
Pressure Range	-50 to +300 mmHg
Overpressure	-760 to 4000 mmHg
Rated excitation Voltage	2.5 to 7.5 Vdc or Vac, rms. Performance specifications are for 5Vdc
Sensitivity	5μV/V/mmHg, nominal
Temperature Error Band at Zero Pressure	1 mmHg, BSL, room temperature to body temperature 2 mmHg maximum shift, approximately 23° to 38° C
Linearity and Hysteresis (Combined)	$\pm$0.5%, BSL, of full scale
Drift	3 mmHg or less in 24 hours, after zeroing in water
Natural Frequency	50kHz, nominal
Input Impedance	1000 Ω, nominal
Output Impedance	1000 Ω, nominal
Reference Pressure	Atmosphere

DTX plus disposable transducers DT-XX, DT-NN, DT-XO, TNF-R

Pressure range	-30 mmHg to +300 mmHg
Overpressure tolerance	7.755 mmHg
Bridge resistance	Input range: 1.1 to 3.45 Ω
	Output range: 300 Ω (± 30 Ω)
Excitation voltage	Up to 10V DC or AC RMS maximum, up to 5kHz
Maximum inaccuracy due to	The maximum deviation due to the total effects of non-
non-linearity, hysteresis	linearity, hysteresis and sensitivity variation, shall be no
and sensitivity variations	more than 2% of the reading or 1 mmHg, whichever is
	greater, from a straight line through zero and having a
	slope of 5 μV/V/mmHg at 25% and an excitation of 7.5V.
Thermal coefficient of sensitivity	± 0.1% °C
Operating temperature range	+15°C to +40 °C

Bibliography

[1] GREGOIRE, L., *Functionele anatomie van de mens* Spruyt, Eds. Van Mantegem en De Boes b.v., Leiden, 1996

[2] Metry, G., Spittle, M., Rahmati, S., Giller, C., Giller, A., Kaufman, A., Schneditz, D., Manno, E., Brener, Z., Boniece, I., Ronco, F., Ronco, C., Levin, *Online monitoring of cerebral hemodynamics during hemodialysis* American Journal of Kidney Diseases 40 (5): 996-1004 nov 2002

[3] Kiani, M.F., Hudetz, A.G. *A semi-empirical model of apparent blood viscosity as a function of vessel diameter and discharge hematocrit* Biorheology, 28:65-73, 1991

[4] Walawender, W.P., Chen, T.Y., Cala, D.F. *An approximate Casson fluid model for tube flow of blood* Biorheology, 12: 111-119, 1975

[5] Cho, Y.I., Kensey, K.R., *Effects of the non-Newtonian viscosity of blood on flows in a diseased arterial vessel. Part 1: Steady flows* Biorheology, 28: 241-262, 1991

[6] Verdonck, P., Flaud, P., Oddou, C., Dufaux, J., Segers, P., *Blood and vascular tissure rheology* Precourse 10th Conference of the European Society of Biomechanics, Leuven; 1996

[7] Cockelet, G.C., *The rheology and tube flow of blood* In: Handbook of bioengineering, eds. R. Skalak, S. chien, Londen, Mc Green Hill, 1987.

[8] Quemada, D., *General features of blood circulation in narrow vessels* In: Arteries and arterial blood flows, ed. C.M. Rodkiewicz

[9] Canaud, B., My, H., Morena, M., et al., *Dialock: a new vascular access device for extracorporeal renal replacement therapy. Preliminary clinical results.* Nephrology Dialysis Transplantation 14 (3): 692-698; 1999.

[10] J. Megerman, N.W. Levin, T.S. Ing, B. Canaud, H. My, *Hemodialysis (HD) Access with the DialockTM Device* Blood Purif 16:242; 1998

[11] Boorgu, R., Dubrow, A.J., Levin, N.W., et al., *Adjunctive antibiotic/anticoagulant lock therapy in the treatment of bacteremia associated with the use of a subcutaneously implanted hemodialysis access device* ASAIO Journal 46 (6): 767-770; 2000.

[12] Megerman J, Levin NW, Ing TS, et al. *Development of a new approach to vascular access* Artificial Organs 23 (1): 10-14 Jan 1999

[13] Neumann, M.E. *Two new access devices have potential to replace the temporary catheter* Nephrology News and Issues 40, 1999

[14] Malovrh, M. *5th European Basic Multidisciplinary Hemodialysis Access Course.* Brdo pri Kranj, Karger AG, p. 20(4): 442, 2002

[15] *5th European Basic Multidisciplinary Hemodialysis Access Course* Brdo pri Kranj, Karger AG, p. 409-490; 2002

[16] Butler, C. E., and Tilney, N. L., 1996. *Hemodialysis Access Part B - Permanent.* In C. Jacobs, C. M. K., K.M. Koch, J.F. Winchester (Eds.), Replacement of renal function by dialysis. Kluwer Academic Publishers, Dordrecht, 1996, p. 293-304.

[17] Hodges., T.C., Fillinger, M.F., Zwolak, R.M., et al., *Longitudinal comparison of dialysis access methods: Risk factors for failure* Journal of Vascular Surgery 26 (6): 1009-1019 Dec 1997

[18] Schwab, S.J., Oliver, M.J., Suhocki, P., McCann, R. *Hemodialysis arteriovenous access: detection of stenosis and response to treatment by vascular access blood flow.* Kidney International 59:358-362; 2001.

[19] Sands, J.J., Jabyac, P.A., Miranda, C.L., Kapsick, B.J., *Intervention based on monthly monitoring decreases hemodialysis access thrombosis* ASAIO Journal 45:147-150; 1999

[20] Jindal, K.K., Ethier, J.H., Lindsay, R.M., Barre, P.E., Kappel, J.E., Carlisle, E.J., Common, A., *Clinical practice guidelines for vascular access.* Canadian Society of Nephrology, J. Am. Soc. Nephrol. 1999; 10. Suppl 13: S297-S305

[21] Leapman, S.B., Boyle, M., Pescovitz, M.D., et al., *The arteriovenous fistula for hemodialysis access: Gold standard or archaic relic?* American Surgeon 62 (8): 652-656; 1996

[22] Bhandari, S., Wilkinson, A., Sellars, L., *Saphenous-vein forearm grafts and gortex thigh grafts as alternative forms of vascular access* Clinical Nephrology 44 (5): 325-328; 1995.

[23] Himmelfarb, J., Saad, T., *Hemodialysis Vascular Access: Emerging Concepts* Current Opinion in Nephrology and Hypertension, 5:485-491, 1996.

[24] Van Waeleghem, J.P., Elseviers, M.M., Lindley, E.J. *Management of vascular access in Europe.* Part I: A study of centre based policies. EDTNA/ERCA Journal 4: 8-34, 2000.

[25] Orpadt Flanders Survey, Results 2000, http://www.orpadt.be/documenten/ORPADT 2000 ENG.pdf

[26] Kirkman, R.L., *Technique for flow reduction in dialysis access fistulas.* Surgery Gynecology & Obstetrics 172 (3): 231-233; 1991.

[27] Enzler, M.A., Rajmon, T., Lachat, M., et al., *Long-term function of vascular access for hemodialysis* Clinical Transplantation 10 (6): 511-515 Part 1 Dec 1996

[28] Glickman, M. H., Stokes, G. K., Ross, J. R., Schuman, E. D., Sternbergh, W. C., Lindberg, J. S., Money, S. M., Lorber, M. I., *Multicenter evaluation of a polyurethaneurea vascular access graft as compared with the expanded polytetrafluoroethylene vascular access graft in hemodialysis applications* Journal of Vascular Surgery, 34 (3): 465-472; 2001.

[29] Taylor, S.M., Eaves, G.L., Weatherford, D.A., et al., *Results and complications of arteriovenous access dialysis grafts in the lower extremity: A five year review* American Surgeon 62 (3): 188-191; 1996

[30] Turmel-Rodrigues, L., Pengloan, J., Rodrigue, H., et al., *Treatment of failed native arteriovenous fistulae for hemodialysis by interventional radiology* Kidney International 57 (3): 1124-1140; 2000.

[31] Rigg, K. M. , *Complications of Vascular Access.* In J.A. Akoh (Eds.). Dialysis Access, Current Practice. London: Imperial College Press, 2001, p. 131-147.

[32] Lemson, M.S., Intimal hyperplasia in prosthetic vascular access The effect of flow variation and anastomotic geometry on its development University Hospital Maastricht, PhD thesis, 2000.

[33] Kroll, M.H., Hellums, J.D., Mc Intire, L.V., Schafer, A.I., Moake, J.L., *Platelets and shear stress* Blood 88(5):1525-1541, 1996.

[34] Van Tricht, I., De Wachter, D., Tordoir, J., Verdonck, P., *Comparison of the hemodynamics in straight and tapered hemodialysis grafts by means of CFD* J. Biomech., In Press.

[35] Hofstra, L., Bergmans, D., Leunissen, K. M. L., Hoeks, A. P. G., Kitslaar, P., Daemen, M., Tordoir, J. H. M., *Anastomotic intimal hyperplasia in prosthetic arteriovenous fistulas for hemodialysis is associated with initial high flow velocity and not with mismatch in elastic properties*, Journal of the American Society of Nephrology, 6, (6): 1625-1633, 1995.

[36] Tordoir, J. H. M., Debruin, H. G., Hoeneveld, H., Eikelboom, B. C., Kitslaar, P., *Duplex Ultrasound Scanning in the Assessment of Arteriovenous-Fistulas Created for Hemodialysis Access - Comparison with Digital Subtraction Angiography* Journal of Vascular Surgery, 10 (2): 122-128; 1989.

[37] Sivanesan, S., How, T. V., Bakran, A., *Sites of stenosis in AV fistulae for haemodialysis access* Nephrology Dialysis Transplantation, 14 (1): 118-120; 1999.

[38] National Kidney Foundation *K/DOQI Clinical Practice Guidelines for Vascular Access* Am J Kidney Dis, 37: S137-S181, 2001.

[39] Krivitski, N. M., MacGibbon, D., Gleed, R. D., Dobson, A., *Accuracy of dilution techniques for access flow measurement during hemodialysis* American Journal of Kidney Diseases, 31 (3): 502-508; 1998.

[40] Paulson, W. D., *Blood flow surveillance of hemodialysis grafts and the dysfunction hypothesis* Seminars in Dialysis, 14, (3): 175-180; 2001.

[41] Malovrh, M., *5th European Basic Multidisciplinary Hemodialysis Access Course.* Brdo pri Kranj, Karger AG, p. 20(4): 442, 2002

[42] Kleinekofort, W., Kraemer, M., Rode, C., Wizemann, V., *Extracorporeal pressure monitoring and the detection of vascular access stenosis.* International journal of artificial organs 25: 45-50, 2002.

[43] Van Tricht, I., De Wachter, D., Tordoir, J., and Verdonck, P., *Assessment of stenosis in vascular access grafts.* International journal of artificial organs, 28(7):617-622, 2004.

[44] Hill, R., Bagust, A., Bakhai, A., et al., *Coronary artery stents: a rapid systematic review and economic evaluation* Health technology assessment 8 (35): 1+ Sep 2004.

[45] Schaffer, D., *A prospective randomized trial of 6 mm versus 4-7 mm PTFE grafts for hemodialysis access in diabetic patients.* Vascular access for hemodialysis, Precept Press, 91-94, 1997.

[46] Sabanayagam, P., *15-Year experience with tapered (4-7 mm) and straight (6 mm) PTFE angio-access in the ESRD patient* Henry, M.L., and Ferguson, R.M., In Vascular access for hemodialysis, Precept Press, p.91-94, 1997.

[47] Nassar, G.M., Ayus, J.C. *Infectious complications of the hemodialysis access* Kidney International 60:1-13; 2001

[48] Besarab, A. *Intervention for intra-access stenosis* Seminars in Dialysis 14: 401-402; 2001

[49] Schwab, S.,J., Raymond, J.,R., Saeed, M., Newman, G.E., Dennis, P.A., Bollinger, R.R. *Prevention of hemodialysis fistula thrombosis. Early detection of venous stenoses.* Kidney International 36: 701-711: 1989

[50] Depner, T.A., Rizwan, S., Stasi, T.A. *Pressure effects on roller pump blood flow during hemodialysis* ASAIO Transactions 36: M456-M459; 1990

[51] Sands, J. *The role of color-flow Doppler ultrasound in the management of hemodialysis accesses* ASAIO Journal 44:41-43; 1998

[52] Lindsay, R.,M., Bradfield, E., Rothera, C., Kianfar, C., Malek, P., Blake, B.,G. *A comparison of methods for the measurement of hemodialysis access recirculation and access blood flow rate* ASAIO Journal, 44: 62-67; 1998

[53] Lindsay, R.M., Blake, P.G., Malek, P., Posen, G., Martin, B., Bradfield, E., *Hemodialysis access blood flow rates can be measured by a differential conductivity technique and are predictive of access clotting.* American Journal of Kidney Diseases 1997; 30:475-482

[54] Steuer, R.R., Miller, D.R., Zhang, S., Bell, D.A., Leypoldt, J.K. *Noninvasive transcutaneous determination of access blood flow rate.* Kidney International 2001; 60:284-291

[55] Schneditz, D., Wang, E., Levin, N.W., *Validation of haemodialysis recirculation and access blood flow measured by thermodilution.* Nephrology and Dialysis Transplantation 1999; 14:376-383

[56] Neyra, N.R., Ikizler, T.A., May, R.E., Himmelfarb, J., Schulman, G., Shyr, Y., Hakim, R.M. *Change in access blood flow over time predicts vascular access thrombosis.* Kidney International 1998; 54:1714-1719

[57] Wang, E., Schneditz, D., Nepomuceno, C., Lavarias, V., Martin, K., Morris, A.T., Levin, N.W. *Predictive value of access blood flow in detecting access thrombosis.* ASAIO Journal 1998; 44:M555-M558

[58] Paulson, W.D., Ram, S.J., Birk, C.G., Zapczynski, M., Martin, S.R., Work, J. *Accuracy of decrease in blood flow in predicting hemodialysis graft thrombosis.* American Journal of Kidney Diseases 2000; 35:1089-1095

[59] Schwab, S.J., Oliver, M.J., Suhocki, P., McCann, R., *Hemodialysis arteriovenous access: detection of stenosis and response to treatment by vascular access blood flow.* Kidney International 2001;59:358-362

[60] Tonelli, M., Jindal, K., Hirsch, D., Taylor, S., Kane, C., Henbrey, S., *Screening for subclinical stenosis in native vessel arteriovenous fistulae.* Journal American Society Nephrology 2001; 12:1729-1733

[61] McCarley, P., Wingard, R.L., Shyr, Y., Pettus, W., Hakim, R.M., Ikizler, T.A., *Vascular access blood flow monitoring reduces access morbidity and costs.* Kidney International 2001; 60:1164-1172

[62] Kosch, M., Levers, A., Barenbrock, M., Matzkies, F., Schaefer, R. M., Kisters, K., Rahn, K. H., Hausberg, M., *Acute effects of haemodialysis on endothelial function and large artery elasticity* Nephrology Dialysis Transplantation, 16 (8): 1663-1668; 2001.

[63] Verdonck, P., Kleven, A., Verhoeven, R., Angelsen, B., Vandenbogaerde, J. *Computer-controlled in vitro model of the human left heart.* Med Biol Eng Comput 30: 656-9., 1992.

[64] De Wachter, D., De Somer, F., Verdonck, P. *Hemodynamic comparison of two different pediatric aortic cannulas.* Int J Artif Organs 25: 867-74., 2002.

[65] Glagov, S., *Intimal Hyperplasia, Vascular Modeling, and the Restenosis Problem* Circulation 89 (6), 2888-2891, 1994.

[66] Nyberg, S. L., Hughes, C. B., Valenzuela, Y. M., Jenson, B. M., Benda, M. M., McCarthy, J. T., Sterioff, S., Stegall, M. D., *Preliminary experience with a cuffed ePTFE graft for hemodialysis vascular access* ASAIO Journal, 47 (4): 333-337, 2001.

[67] Hofstra, L., Bergmans, D, Hoeks, A. P. G., Kitslaar, P., Leunissen, K. M. L., Tordoir, J. H. M., *Mismatch in Elastic Properties around Anastomoses of Interposition*

Grafts for Hemodialysis Access Journal of the American Society of Nephrology, 5 (5): 1243-1250, 1994.

[68] Prischl, F.C., Kirchgatterer, A., Brandstatter, E., et al., *Parameters of prognostic relevance to the patency of vascular access in hemodialysis patients* Journal of the American Society of Nephrology 6 (6): 1613-1618; 1995.

[69] Bassiouny, H. S., White, S., Glagov, S., Choi, E., Giddens, D. P., and Zarins, C. K., *Anastomotic intimal hyperplasia: mechanical injury or flow induced.* Journal of Vascular Surgery 15: 708-16; discussion 716-7, 1992

[70] Miller, J. H., Foreman, R. K., Ferguson, L., Faris, I., *Interposition Vein Cuff for Anastomosis of Prosthesis to Small Artery*, Australian and New Zealand Journal of Surgery, 54 (3): 283-285, 1984.

[71] Taylor, R. S., Loh, A., McFarland, R. J., Cox, M., Chester, J. F., *Improved Technique for Polytetrafluoroethylene Bypass-Grafting - Long-Term Results Using Anastomotic Vein Patches* British Journal of Surgery, 79 (4): 348-354; 1992.

[72] Gagne, P. J., Martinez, J., DeMassi, R., Gregory, R., Parent, F. N., Gayle, R., Meier, G. H., Philput, C., *The effect of a venous anastomosis Tyrell vein collar on the primary patency of arteriovenous grafts in patients undergoing hemodialysis*, Journal of Vascular Surgery, 32 (6): 1149-1154, 2000.

[73] Salacinski, H. J., Punshon, G., Krijgsman, B., Hamilton, G., Seifalian, A. M., *A hybrid compliant vascular graft seeded with microvascular endothelial cells extracted from human omentum*, Artificial Organs, 25 (12): 974-982; 2001.

[74] Salacinski, H. J., Tiwari, A., Hamilton, G., Seifalian, A. M., *Cellular engineering of vascular bypass grafts: role of chemical coatings for enhancing endothelial cell attachments* Medical and Biological Engineering and Computing, 39 (6): 609-618; 2001.

[75] McIntire, L.V., Martin, R.R., *Mechanical trauma induced PMN leucocyte dysfunction* In: Gross D.R., Hwang N.H.C., eds. The Rhology of Blood vessels and associated tissues. Alphen aan den Rijn: Sijthoff and Noordhoff.

[76] Hellums, J.D., Hardwick, R.A., *Response of platelets to shear stress-a review* In: Gross D.R., Hwang N.H.C., eds. The Rhology of Blood vessels and associated tissues. Alphen aan den Rijn: Sijthoff and Noordhoff, 160-183, 1981.

[77] Nevarill, C.G., Lynch, E.C., Alfrey, C.P., Hellums, J.D., *Erythrocyte damage and destruction induced by shearing stress* Journal Laboratory Clinical Medicine 71:781-790, 1968.

[78] Sutera, S.P., *Flow-induced trauma to blood cells* Circulation Research 41: 2-8, 1977.

[79] Blackshear, P.L., Dorman, F.D., Steinbach, E.J., *Shear, wall interaction and hemolysis* Transactions American Society Artificial International Organs 12:113-120, 1966.

[80] Leverett, L.B., Hellums, J.D., Alfrey, C.P., Lync, E.C., *Red blood cell damage by shear stress* Biophysics Journal 12:257-273; 1972

[81] Salam, T.A., Lumsden, A.B., Suggs, W.D., Ku, D.N., *Low shear stress promotes intimal hyperplasia thickening* Journal of Vascular Investment 2: 12-22, 1996

[82] Fry, D.L., *Acute vascular endothelial changes associated with increased blood velocity gradients* Circulation Research 22: 165-197, 1968

[83] Malek, A. M., Alper, S. L., Izumo, S., *Hemodynamic shear stress and its role in atherosclerosis* Jama-Journal of the American Medical Association, 282 (21): 2035-2042,1999.

[84] Jiang, Z. H., Wu, L. Z., Miller, B. L., Goldman, D. R., Fernandez, C. M., Abouhamze, Z. S., Ozaki, C. K., Berceli, S. A., *A novel vein graft model: adaptation to differential flow environments* American Journal of Physiology-Heart and Circulatory Physiology, 286 (1):H240-H245; 2004.

[85] Dammers, R., Tordoir, J. H. M., Welten, R, Kitslaar, P, Hoeks, A. P. G., *The effect of chronic flow changes on brachial artery diameter and shear stress in arteriovenous fistulas for hemodialysis* International Journal of Artificial Organs, 25 (2): 124-128; 2002.

[86] Fillinger, M. F., Reinitz, E. R., Schwartz, R. A., Resetarits, D. E., Paskanik, A. M., Bruch, D., Bredenberg, C. E., *Graft Geometry and Venous Intimal-Medial Hyperplasia in Arteriovenous Loop Grafts* Journal of Vascular Surgery, 11 (4): 556-566; 1990.

[87] Loth, F., Fischer P.F., Arlan, N., Bertram C.D., Lee, S.E., Royston, T.J., Shaalan, W.E., Bassiouny, H.S., *Transitional Flow at the venous anastomosis of an arteriove-*

nous graft: potential activation of the ERK1/2 mechanotransduction pathway Journal of Biomechanical Engineering - Transactions of the ASME 125: 49-61; 2003.

[88] Hayashi, K., Mori, K., Miyazaki, H., *Biomechanical response of femoral vein to chronic elevation of blood pressure in rabbits* American Journal of Physiology-Heart and Circulatory Physiology, 284 (2): H511-H518; 2003.

[89] Redwood, A. J., Moore, S., Sayadelmi, L., Tennant, M., *Autogenous artery grafts in hypertensive (SHR) rats do not have increased smooth muscle cell hyperplasia in the graft neointima, compared with grafts in normotensive rats* Journal of Anatomy, 195: 407-412; 1999.

[90] Bassiouny, H. S., White, S., Glagov, S., Choi, E., Giddens, D. P., Zarins, C. K., *Anastomotic Intimal Hyperplasia - Mechanical Injury or Flow Induced* Journal of Vascular Surgery, 15 (4): 708-717; 1992.

[91] Sivanesan, S., How, T. V., Black, R. A., Bakran, A., *Flow patterns in the radio-cephalic arteriovenous fistula: an in vitro study* Journal of Biomechanics, 32 (9): 915-925; 1999.

[92] Keynton, R. S., Evancho, M. M., Sims, R. L., Rodway, N. V., Gobin, A., Rittgers, S. E., *Intimal hyperplasia and wall shear in arterial bypass graft distal anastomoses: An in vivo model study* Journal of Biomechanical Engineering-Transactions of the ASME, 123 (5): 464-473; 2001.

[93] Meyerson, S. L., Skelly, C. L., Curi, M. A., Shakur, U. M., Vosicky, J. E., Glagov, S., Schwartz, L. B., *The effects of extremely low shear stress on cellular proliferation and neointimal thickening in the failing bypass graft* Journal of Vascular Surgery, 34 (1): 90-96; 2001.

[94] Jackson, Z. S., Ishibashi, H., Gotlieb, A. L., Langille, B. L., *Effects of anastomotic angle on vascular tissue responses at end-to-side arterial grafts* Journal of Vascular Surgery, 34 (2): 300-307, 2001.

[95] Ojha, M., Cobbold, R. S. C., Johnston, K. W., *Influence of Angle on Wall Shear-Stress Distribution for an End-to-Side Anastomosis* Journal of Vascular Surgery, 19 (6): 1067-1073; 1994.

[96] Van Tricht, I., De Wachter, D., Tordoir, J., Verdonck, P., *Hemodynamics in a compliant In Vitro model of a Straight versus Tapered PTFE Arteriovenous Graft.* Journal Surgical Research 116:297-304, 2004

[97] Fisher, R. K., How, T. V., Carpenter, T., Brennan, J. A., Harris, P. L., *Optimising Miller cuff dimensions. The influence of geometry on anastomotic flow patterns* European Journal of Vascular and Endovascular Surgery, 21 (3):251-260; 2001.

[98] Heise, M., Schmidt, S., Krüger, U., Rückert, R., Rösler, S., Neuhaus, P., Settmacher, U., *Flow pattern and shear stress distribution of distal end-to-side anastomoses. A comparison of the instantaneous velocity fields obtained by particle image velocimetry* Journal of biomechanics, 37 (7): 1043-1051; 2004

[99] Li, X.M., Rittgers, S.E., *Hemodynamic factors at the distal end-to-side anastomosis of a bypass graft with different POS : DOS flow ratios* Journal of Biomedical Engineering - Transactions of the ASME 123(3): 270-276; 2001

[100] Lee, D., Su, J. M., Liang, H. Y., *A numerical simulation of steady flow fields in a bypass tube* Journal of Biomechanics, 34 (11):1407-1416; 2001.

[101] Longest, P. W., Kleinstreuer, C., *Computational haemodynamics analysis and comparison study of arterio-venous grafts* Journal of Medical Engineering & Technology, 24 (3):102-110; 2000.

[102] Rosental, J.J., Bell, D.D., Gaspar, M.R., et al. *Prevention of high flow problems of arteriovenous grafts - development of a new tapered graft* American Journal of Surgery 140 (2): 231-233 1980

[103] Ene-Iordache, B., Mosconi, L., Remuzzi, G., Remuzzi, A., *Computational Fluid Dynamics of a vascular access case for hemodialysis* Journal of Biomedical Engineering - Transactions of the ASME 123(3) 284-292; 2001

[104] Kute, S. H., Vorp, D. A., *The effect of proximal artery flow on the hemodynamics at the distal anastomosis of a vascular bypass graft: Computational study* Journal of Biomechanical Engineering-Transactions of the ASME, 123 (3):277-283; 2001.

[105] Lei, M., Giddens, D. P., Jones, S. A., Loth, F., Bassiouny, H., *Pulsatile flow in an end-to-side vascular graft model: Comparison of computations with experimental data* Journal of Biomechanical Engineering-Transactions of the ASME, 123 (1): 80-87; 2001.

[106] Leuprecht, A., Perktold, K., Prosi, M., Berk, T., Trubel, W., Schima, H. *Numerical study of hemodynamics and wall mechanics in distal end-to-side anastomoses of bypass grafts* Journal of Biomechanics, 35 (2): 225-236; 2002.

[107] Krueger, U., Zanow, J., Scholz, H., *Computational fluid dynamics and vascular access* Artificial Organs, 26 (7): 571-575, 2002.

[108] Long, Q., Xu, X. Y., Ramnarine, K. V., Hoskins, P., *Numerical investigation of physiologically realistic pulsatile flow through arterial stenosis* Journal of Biomechanics, 34 (10): 1229-1242; 2001.

[109] Mittal, R., Simmons, S. P., Udaykumar, H. S., *Application of large-eddy simulation to the study of pulsatile flow in a modeled arterial stenosis* Journal of Biomechanical Engineering-Transactions of the ASME, 123 (4):325-332: 2001.

[110] Tang, D., Yang, J., Yang, C., Ku, D. N., *A nonlinear axisymmetric model with fluid-wall interactions for steady viscous flow in stenotic elastic tubes* Journal of Biomechanical Engineering-Transactions of the ASME, 121 (5):494-501; 1999.

[111] Longest, P. W., Kleinstreuer, C., *Numerical simulation of wall shear stress conditions and platelet localization in realistic end-to-side arterial anastomoses*, Journal of Biomechanical Engineering-Transactions of the ASME, 125 (5): 671-681; 2003.

[112] Miller, P.E, Tolwani, A., Luscy, C.P., et al. *Predictors of adequacy of arteriovenous fistulas in hemodialysis patients* Kidney International 56 (1): 275-280; 1999

[113] Revanur, V.K., Jardine, A.G., Hamilton, D.H., et al., *Outcome for arterio-venous fistula at the elbow for haemodialysis* Clinical Transplantation 14 (4): 318-322 Part 1 Aug 2000

[114] Himmelfarb, J., et al., Hemodialysis vascular access: emerging concepts. Current Opinion Nephrology Hypertension 5: 485-91; 1996.

[115] Rodriguez, J.A., Armadans, L., Ferrer, E., Olmos, A., Codina, S., Bartolom, J., Borrellas, J., Piera, L., *The function of permanent vascular access* Nephrology Dialysis transplantation 402-408(7), 2000.

[116] Elcheroth, J., Depauw, L., Kinnaert, P., *Elbow arteriovenous fistulas for chronic hemodialysis* British journal of surgery 81 (7): 982-984 Jul 1994

[117] Winsett, O.E., Wolma, F.J., *Complications of vascular access for hemodialysis* Southern Medical Journal 78 (5): 513-517; 1985

[118] Bender, M.H.M., Bruyninckx C.M.A., Gerlag, P.G.G., *The brachiocephalic elbow fistula - A useful alternative angioaccess for permanent hemodialysis* Journal of vascular surgery 20 (5): 808-813 Nov 1994.

[119] Hibberd, A.D., *Brachiobasilic fistulat with autogenous basilic vein - surgical technique and pilot-study* Australian and New Zealand Journal of Surgery 61 (8): 631-635; 1991

[120] Tordoir, J.H., *Long-term follow-up of the polytetrafluoroethylene (PTFE) prosthesis as an arteriovenous fistula for haemodialysis* European Journal Vascular Surgery, 2 (1), p. 3-7; 1988

[121] Heintjes, R.J., Eikelboom, B.C., Steijling, J.J.F., et al., *The results of denatured homologous vein grafts as conduits for secondary hemodialysisaccess surgery.* European Journal of Vascular and Endovascular Surgery 9 (1): 58-63; 1995

[122] Bosman, P.J., Blankestijn, P.J., van der Graaf, Y., et al. *A comparison between PTFE and denatured homologous vein grafts for haemodialysis access: a prospective randomised multicentre trial* European journal of vascular and endovascular surgery 16 (2): 126-132; 1998.

[123] Eltayar,A., Szendro, G., *The Value of Ultrasonic Imaging in Defining the Anatomy for Vascular Access.* In J.A. Akoh, N. S. H. (Eds.). Dialysis Access, Current Practice. London: Imperial College Press, 2001, p. 131-147.

[124] Al-kutoubi, A. Radiology of Access. In J.A. Akoh, N. S. H. (Eds.). Dialysis Access, Current Practice. London: Imperial College Press, 2001, p. 131-147.

[125] Segers, P., and Verdonck, P. Principles of Vascular Physiology In P. Lanzer and E. J. Topol, E. H. S. (Eds.). Panvascular Medicine. Integrated clinical management., 2002, p. 116-137.

[126] Sumpio, B. E., Banes, A. J., Levin, L. G., and Johnson, G., Jr. Mechanical stress stimulates aortic endothelial cells to proliferate. Journal of Vascular Surgery 6: 252-6., 1987.

[127] Wladis, A. R., Mesh, C. L., White, J., Zenni, G. C., Fischer, D. B., and Arbaugh, J. J. Improving longevity of prosthetic dialysis grafts in patients with disadvantaged venous outflow. Journal of Vascular Surgery 32: 997-1005., 2000.

[128] Dammers, R., Planken, R. N., Pouls, K. P., Van Det, R. J., Burger, H., Van Der Sande, F. M., and Tordoir, J. H. *Evaluation of 4-mm to 7-mm versus 6-mm prosthetic brachial-antecubital forearm loop access for hemodialysis: results of a randomized multicenter clinical trial.* Journal of Vascular Surgery 37: 143-8, 2003

[129] Kleinstreuer, C., Hyun, S., Buchanan, J.R., Longest, P.W., Archie, J.P., Truskey G.A., 2000 *Hemodynamic parameters and early intimal thickening in branching blood vessels.* Critical Reviews in Biomedical Engineering, 24: 102-110

[130] Leuprecht, A., Perktold, K., Prosi, M., et al. Numerical study of hemodynamics and wall mechanics in distal end-to-side anastomoses of bypass grafts Journal of Biomechanics 35 (2): 225-236 Feb 2002

[131] Krueger, U., Zanow, J., and Scholze, H., 2000. *Comparison of Two Different Arteriovenous Anastomotic Forms By Numerical 3D Simulation of Blood Flow* Journal of Angiology 9: 226-31.

[132] Lorthois, S., Lagree, P. Y., Marc-Vergnes, J. P., and Cassot, F., 2000. *Maximal wall shear stress in arterial stenoses: application to the internal carotid arteries.* Journal of Biomechanical Engineering 122: 661-6.

[133] Madras, P. N., Ward, C. A., Johnson, W. R., and Singh, P. I., 1981. *Anastomotic hyperplasia.* Surgery 90: 922-3.

[134] Ojha, M., Cobbold, R. S., and Johnston, K. W., 1993 *Hemodynamics of a side-to-end proximal arterial anastomosis model.* Journal of Vascular Surgery 17: 646-55.

[135] Raptis, S., and Miller, J. H., 1995. *Influence of a vein cuff on polytetrafluoroethylene grafts for primary femoropopliteal bypass.* Br J Surg 82: 487-91.

[136] Rus, R., Ponikvar, R., Kenda, R., Buturovic-Ponikvar J., 2003. *Efffect of Local Physical Training on the Forearm Arteries and Veins in Patients with End-Stage Renal Disease* Blood Purification 21: 389-394.

[137] Vanholder, R., 1992 *Biocompatibility Issues in Hemodialysis* Clinical Materials 10: 87-133

[138] Dumars, M.C., Thompson, W.E., Bluth, E.I., Lindberg, J.S., Yoselevitz, M., Merritt, C.R.B., *Management of Suspected Hemodialysis Graft Dysfunction: Usefulness of Diagnostic US* Radiology 222(1): 103-107, 2002

[139] Ahya, S.N., Windus, D.W., Vesely, T.M. *Flow in hemodialysis grafts after angioplasty: Do radiologic criteria predict success?* Kidney International 59: 1974-1978, 2001

[140] Ayarragaray, J.E.F. *Surgical treatment of hemodialysis-related central venous stenosis or occlusion: Another option to maintain vascular access.* Journal of Vascular Surgery 37: 1043-6, 2003

[141] Atray, N.K., Paulson, W.D., *Blood Flow Surveillance of Hemodialysis Grafts: Insights from Two Case Reports.* Seminars in Dialysis 15: 370-374, 2002.

[142] Ziegler, T., Silacci, P., Harrison, V.J., Hayoz, D., *Nitric Oxide Synthase Expression in Endothelial Cells Exposed to Mechanical Forces.* Hypertension 32:351-355, 1998.

[143] Zhao, S., Suciu, A., Ziegler, T., Moore, J.E., Brki, E., Meister, J-J., Brunner, H.R., *Synergistic Effects of Fluid Shear Stress and Cyclic Circumferential Stretch on Vascular Endothelial Cell Morphology and Cytoskeleton.* Arteriosclerosis, Thrombosis and Vascular Biology 15:1781-1786, 1995.

[144] Casey, P.J., Dattilo, J.B., Dai, G., Albert, J.A., Tsukurov, O.I., Orkin, R.W., Gertler, J.P., Abbott, W.M. *The effect of combined arterial hemodynamics on saphenous venous endothelial nitric oxide production.* Journal of Vascular Surgery 33:1199-1205, 2001.

[145] National Kidney Foundation. K/DOQI Clinical Practice Guidelines for Hemodialysis Adequacy, 2000. American Journal of Kidney Diseases 37:S7-S64, 2001 (suppl 1)

[146] Wootton, D.M., Ku, D.N., *Fluid mechanics of vascular systems, diseases, and thromboses* Annual Revisions Biomedical Engineering 01:299-329, 1999.

[147] Chiu, J.-J., Chen, L.-J., Chen, C.-N., Lee, P.-L., Lee, C.-I. *A model for studying the effect of shear stress on interactions between vascular endothelial cells and smooth muscle cells* Journal of Biomechanics 37:531-539, 2004

[148] Giersiepen, M., Wurzinger, L.J., Opitz, R., Reul, H. *Estimation of shear stress-related blood damage in heart-valve prostheses- in vitro comparison of 25 aortic valves* International journal of artificial organs 13(5):300-306, 1990.

[149] Rhodes, N.P., Kumary, T.V., Williams, D.F., *Influence of wall shear rate on parameters of blood compatibility of intravascular catheters* Biomaterials 17 (20):1995-2002, 1996.

[150] De Wachter, D.S., Verdonck, P.R. Verhoeven, R.F., Hombrouckx, R.O., *Red cell injury assessed in a numeric model of a peripheral dialysis needle* ASAIO Journal 42 (5): M524-M529, 1996.

[151] Grigioni, M., Daniele, C., Morbiducci, U., D'Avenio, G., *The power-law mathematical model for blood damage prediction: analytical developments and physical inconsistencies* Artificial Organs 28(5): 467-475, 2004

[152] Longest, P. W., Kleinstreuer, C., *Comparison of Blood Particle Deposition Models for Non-parallel Flow Domains*, Journal of Biomechanics, Vol. 36:421-430, 2003.

[153] Depner, T.A., Rizwan, S. Stasi, T.A., *Pressure effects on roller pump blood flow during hemodialysis*, ASAIO transactions, Vol 36(3):456-9, 1990.

[154] Polaschegg, H.D., *Pressure drops in cannulas for hemodialysis*, The International Journal of Artificial Organs Vol 24(9):614-623, 2001.

[155] Van Tricht, I., De Wachter, D., Tordoir, J., and Verdonck, P., *Experimental analysis of punctured vascular access grafts.* ASAIO journal, In press, 2005.

[156] Twardowski, Z.J., *Constant Site (Buttonhole) Method of Needle Insertion for Hemodialysis*. Dialysis and Transplantation 24:559-560-576 (evidence level: C) 1995.

[157] Zarate, *AR New needle for two needle hemodialysis* ASAIO Journal 44 (5): M549-M554 Sep-Oct 1998

[158] Giersiepen, M., *Ermittlung von Strmungsprofilen und schubspannungen an Herzklappenprothesen mit Hilfe der LDA in pulsatiler Strmung.* Doctoral Thesis. RWTH Aachen, 1988.

[159] Schgner,P., R., Reul,F., Rau,H., *Recent findings on flow induced blood damage : critical shear stresses and exposure times obtained with a high shear Couette-system*, Artificial Organs, 23(7) p.680.,1999

[160] Wurzinger,L.,J., Opitz, R., Eckstein, H., *Mechanical blood trauma: an overview* Angeiologie, 38:81-97, 1986.

[161] Goubergrits, L., Affeld, K. *Numerical estimation of blood damage in artificial organs* Artificial Organs 28 (5): 499-507 May 2004